

**DE-DUPLICATION OF PERSON'S IDENTITY USING  
MULTI-MODAL BIOMETRICS**

*A THESIS*

*submitted by*

**N. PATTABHI RAMAIAH**

*for the award of the degree*

*of*

**DOCTOR OF PHILOSOPHY**



**DEPARTMENT OF COMPUTER SCIENCE AND ENGINEERING  
INDIAN INSTITUTE OF TECHNOLOGY HYDERABAD**

**APRIL 2015**

## THESIS CERTIFICATE

This is to certify that the thesis entitled **De-duplication of Person's Identity using Multi-modal Biometrics** submitted by **N. Pattabhi Ramaiah** to the Indian Institute of Technology, Hyderabad for the award of the degree of Doctor of Philosophy is a bonafide record of research work carried out by him under my supervision. The contents of this thesis, in full or in parts, have not been submitted to any other Institute or University for the award of any degree or diploma.

Hyderabad - 502 205

Date:

Dr. C. Krishna Mohan

Dept. of Computer Science and Engg.

## ACKNOWLEDGMENTS

I would like to express my sincere gratitude to Dr. C. Krishna Mohan for providing me with the opportunity to do my research work under his guidance. His emphasis on steady and committed effort has motivated me during the course of the research work. I have immensely benefited from the excellent research environment that he has created and nurtured.

I am extremely grateful to our director, Prof. U.B. Desai, for providing excellent computing facilities and such a nice atmosphere for doing my research work. I am extremely thankful to my doctoral committee members Dr. Naveen, Dr. Sobhanbabu, Dr. Sri Rama Murthy, Dr. Balasubrahmanian and my doctoral committee chairman Dr. M. V. Pandurangarao. My special thanks to Dr. C. S. Sastry for his guidance and encouragement.

My special thanks to A. Tirupathi Rao, M. Srinivas, V. Nageswarao, Ramu Naidu and my classmates for their support, motivation and help at critical moments during my project work. I would like to take this opportunity to thank my beloved parents and my wife who have been moral boosters to me and who encouraged me to take up this course and supported me throughout this course with their love and affection.

I would like to thank my teachers, grand parents, parents, and all family members for making me what I am today. I express my heartfelt appreciation and gratitude to my wife Srilatha for her steadfast support, patience and understanding. Our little daughter Naomika provided me with precious moments of joy which have been welcome distractions from research. Finally, I thank everyone who helped me directly or indirectly during my stay at IIT Hyderabad.

*N. Pattabhi Ramaiah*

## ABSTRACT

**Keywords:** *multi-modal biometrics; fingerprints; iris; iris fibers; face; signature; de-duplication; de-noising; support vector machines; principle component analysis; online dictionary learning; slap fingerprint segmentation; iris classification; kernel transformation learning; cross-sensor fingerprint recognition.*

The objective of this work is to explore approaches to create unique identities by the de-duplication process using multi-modal biometrics. Various government sectors in the world provide different services and welfare schemes for the benefit of the people in the society using an identity number. A unique identity (UID) number assigned for every person would obviate the need for a person to produce multiple documentary proofs of his/her identity for availing any government/private services. In the process of creating unique identity of a person, there is a possibility of duplicate identities as the same person might want to get multiple identities in order to get extra benefits from the Government. These duplicate identities can be eliminated by the de-duplication process using multi-modal biometrics, namely, iris, fingerprint, face and signature. De-duplication is the process of removing instances of multiple enrollments of the same person using the person's biometric data. As the number of people enrolled into the biometric system runs into billions, the time complexity increases in the de-duplication process. In this thesis, three different case studies are presented to address the performance issues of de-duplication process in order to create unique identity of a person.

In the first de-duplication case study, Government of Andhrapradesh undertook the de-duplication of ration cards using 52 million people iris codes over 6.26 quadrillion iris matches performed to remove duplicate enrollments in 61 days which is not a scalable solution. In this thesis, we propose an approach for classification of iris images based

on sparse representation of Gabor features using dictionary learning for large-scale de-duplication applications. Also, an iris adjudication process is illustrated by comparing the matched iris-pair images side-by-side to make the decision on the identification score using color coding. Iris classification and adjudication framework is proposed in iris de-duplication architecture to speed-up the identification process and reduce the identification errors.

In the second de-duplication application, Government of Orissa collected a total of 1.8 million slap fingerprint images of 0.6 million citizens as part of targeted public distribution system (TPDS) process. The slap fingerprint images had some noisy data due to some external factors which affect the calibration process of the fingerprint device. While doing the segmentation of these slap fingerprints, some of the fingerprint images are improperly segmented because of the noise present in the data and as a result there is a reduction in the performance of de-duplication process. A de-noising approach is proposed to remove the noise present in the data using binarization of slap fingerprint image and region labeling of desired regions with 8-adjacency neighborhood. A new algorithm is proposed using feature transformation learning in kernel space in order to improve the accuracy of cross-sensor fingerprint matching. The kernel learning uses the distance kernel matrix for optimization using similar and dissimilar class constraints. These constraints reduces the sensor mismatch problem when the matching is performed for cross-sensor in the transformed domain. Also, a semi-automated latent fingerprint identification is proposed to markup fingerprint landmarks manually using the image enhancement filters which will further improve the identification performance.

In the third de-duplication scenario, Government of Andhrapradesh has issued around 22 million ration cards in which there are few ration cards created in an unauthorized manner in order to mislead the benefits of beneficiaries. We propose a method for de-duplication of face photographs based on color histograms. Also, the issue of degraded face recognition with non-uniform illumination conditions is addressed in face photograph de-duplication, especially in outdoor environment. A new method is

proposed for face recognition to address the issue of non-uniform illumination using convolutional neural networks (CNN). The symmetry of facial information is exploited to improve the performance of the face recognition system by considering the horizontal reflections of facial images.

Also, the thesis addresses some issues related with biometric data acquisition and storage while creating a persons' identity in the E-Society. The best practices for biometric data acquisition and identity creation is presented using multi-modal biometrics fingerprints, iris, face and signature. In order to store the signature biometric on a smart card, a novel algorithm is proposed for reducing the size of data.

In summary, this thesis proposes new methods for the de-duplication of person's identity at various stages using multi-modal biometrics. In iris de-duplication process, an approach for iris classification and iris adjudication process is proposed using on-line dictionary learning. The methods explored in the fingerprint de-duplication process are de-noising fingerprint images for accurate fingerprint segmentation, improvement in the fingerprint matching performance using kernel transformation learning and a semi-automated latent fingerprint identification system. In face/photograph de-duplication process, an illumination invariant face recognition system is proposed using convolutional neural networks (CNN). And also, an approach for photograph de-duplication is proposed in targeted public distribution system. Finally, the thesis presents an e-Society application in the context of multi-modal biometrics.

# TABLE OF CONTENTS

Thesis certificate	i
Acknowledgments	ii
Abstract	iii
List of tables	x
List of figures	xii
Abbreviations	0
<b>1 INTRODUCTION TO DE-DUPLICATION OF BIOMETRICS</b>	<b>1</b>
1.1 Biometric recognition system . . . . .	3
1.1.1 Biometric identification . . . . .	3
1.1.2 Biometric verification . . . . .	4
1.1.3 De-duplication of biometrics . . . . .	4
1.2 Multi-modal biometrics . . . . .	4
1.2.1 Face . . . . .	5
1.2.2 Signature . . . . .	5
1.2.3 Fingerprint . . . . .	6
1.2.4 Iris . . . . .	6
1.2.5 Performance evaluation of biometrics . . . . .	7
1.3 Issues addressed in this thesis . . . . .	9
1.4 Organization of the thesis . . . . .	10
<b>2 OVERVIEW OF APPROACHES FOR DE-DUPLICATION OF BIOMETRICS</b>	<b>11</b>
2.1 Iris recognition system . . . . .	11
2.1.1 Early history of iris biometrics . . . . .	12

2.1.2	Iris segmentation . . . . .	15
2.1.3	Iris texture analysis and representation . . . . .	15
2.1.4	Matching iris representations . . . . .	16
2.1.5	Issues addressed in iris recognition system . . . . .	17
2.2	Fingerprint recognition system . . . . .	18
2.2.1	Issues addressed in fingerprint recognition system . . . . .	21
2.3	Face recognition system . . . . .	22
2.3.1	Issues addressed in face recognition system . . . . .	24
2.4	Summary . . . . .	24
<b>3 IRIS CLASSIFICATION BASED ON SPARSE REPRESENTATIONS USING DICTIONARY LEARNING FOR LARGE-SCALE IRIS DE-DUPLICATION APPLICATIONS</b>		<b>25</b>
3.1	Iris classification for large-scale de-duplication applications . . . . .	26
3.2	Architecture of iris de-duplication system . . . . .	26
3.2.1	Enrollment using a centralized iris de-duplication system . . . . .	27
3.2.2	Enrollment using a de-centralized iris de-duplication system . . . . .	27
3.3	Sparse representation and dictionary learning . . . . .	31
3.4	Proposed iris classification and adjudication framework . . . . .	33
3.5	Experimental results . . . . .	36
3.6	Summary . . . . .	43
<b>4 DE-NOISING SLAP FINGERPRINT DATA FOR ACCURATE FINGERPRINT SEGMENTATION IN LARGE-SCALE DE-DUPLICATION APPLICATIONS</b>		<b>45</b>
4.1	Fingerprint de-duplication system . . . . .	46
4.2	De-duplication complexity of fingerprint data . . . . .	47
4.2.1	Enrollment using a centralized fingerprint de-duplication system . . . . .	48
4.2.2	Enrollment using a decentralized fingerprint de-duplication system . . . . .	48
4.3	Noise removal method for slap fingerprint image segmentation . . . . .	50
4.3.1	Binarization of slap image . . . . .	51



4.3.2	Foreground and background segmentation of slap image . . . . .	51
4.3.3	Resampling and region labeling of slap image with 8-adjacency .	53
4.3.4	Reconstruction of the original data for the larger labeled regions	53
4.4	Cross-sensor fingerprint recognition using kernel learning . . . . .	54
4.5	Experimental results . . . . .	56
4.6	Summary . . . . .	62
<b>5</b>	<b>ENHANCEMENTS TO LATENT FINGERPRINT IDENTIFICATION USING ISO 19794-2 FINGERPRINT TEMPLATES</b>	<b>63</b>
5.1	Latent fingerprint identification in forensics . . . . .	63
5.2	Automated latent fingerprint identification . . . . .	66
5.2.1	Fingerprint enhancement . . . . .	66
5.2.2	Normalization, binarization and thinning . . . . .	67
5.2.3	Feature extraction . . . . .	68
5.2.4	Spurious minutia removal . . . . .	68
5.2.5	Matching . . . . .	69
5.3	Semi-automated latent fingerprint identification . . . . .	70
5.3.1	Image acquisition . . . . .	71
5.3.2	Image markup and matching . . . . .	72
5.3.3	Result review/adjudication . . . . .	72
5.3.4	Evidence exhibit/reporting . . . . .	72
5.4	Experimental results . . . . .	73
5.5	Summary . . . . .	76
<b>6</b>	<b>DEDUPLICATION USING PHOTOGRAPH AND FACE IMAGES</b>	<b>78</b>
6.1	Photograph de-duplication for public distribution system . . . . .	79
6.1.1	CBIR technique using color histogram refinement . . . . .	80
6.1.2	Extraction of features from photograph images . . . . .	81
6.1.3	$k$ -means clustering algorithm . . . . .	82
6.1.4	De-duplication process of photographs . . . . .	83

6.2	Face recognition in de-duplication process . . . . .	84
6.2.1	Illumination invariant facial recognition using convolutional neural network . . . . .	85
6.3	Experimental results . . . . .	86
6.4	Summary . . . . .	94
<b>7</b>	<b>UNIQUE IDENTITY CREATION USING MULTIMODAL BIOMETRICS FOR E-SOCIETY APPLICATIONS</b>	<b>95</b>
7.1	Unique identity creation using compressed biometric data . . . . .	96
7.1.1	Best practices for biometric enrollments . . . . .	97
7.1.2	Proposed compression algorithm for signature biometrics . . . . .	101
7.2	Biometrics in e-Governance using hand-held fingerprint units . . . . .	101
7.2.1	Aadhaar authentication . . . . .	102
7.2.2	Fingerprint authentication approach using PoS units . . . . .	103
7.3	Experimental results . . . . .	104
7.4	Summary . . . . .	106
<b>8</b>	<b>CONCLUSIONS AND FUTURE WORK</b>	<b>107</b>
8.1	Contributions of the work . . . . .	108
8.2	Directions for future research . . . . .	109
	<b>Appendix A</b>	<b>111</b>
	<b>Appendix B</b>	<b>114</b>
	<b>References</b>	<b>117</b>

## LIST OF TABLES

1.1	Metrics used to evaluate a biometric [1] . . . . .	8
3.1	Complexity of a centralized iris de-duplication system . . . . .	28
3.2	Complexity of a de-centralized iris de-duplication system . . . . .	29
3.3	Iris classes defined based on $k$ -means clustering and PCA . . . . .	38
3.4	Iris classes based on the iris fibers Stream, Flower and Jewel-Shaker . .	40
3.5	Classification performance (in %) on test data set for dictionary size = 60 . . . . .	41
3.6	Classification performance (in %) on test data set for dictionary size = 90 . . . . .	41
3.7	Classification performance (in %) on test data set for dictionary size = 120 . . . . .	41
3.8	Classification performance on validation data set for dictionary sizes 60, 90 and 120 . . . . .	42
3.9	Confusion matrix for both test data and validation iris data sets . . . .	42
4.1	Complexity of centralized fingerprint de-duplication system . . . . .	49
4.2	Complexity of de-centralized fingerprint de-duplication system . . . . .	50
4.3	Fingerprint segmentation statistics . . . . .	56
4.4	NFIQ scores for segmented fingerprints . . . . .	57
4.5	Equal error rates (EER) of cross-sensor fingerprint recognition using kernel adaptation . . . . .	61
5.1	ISO/IEC 19794-2 template data information . . . . .	70
5.2	Results of latent fingerprint matching . . . . .	74
5.3	Comparison of rank-1 identification rate . . . . .	75

6.1 De-duplication results of photograph images . . . . . 88

6.2 Five sets of Extended Yale Database B . . . . . 90

6.3 Misclassification error (%) of the proposed approach for the five sets . . 91

6.4 Classification performance (%) of the proposed approach on the en-  
hanced facial data . . . . . 92

6.5 Comparison of classification (%) performance with existing approaches 93

7.1 The standard biometric image dimensions . . . . . 105

## LIST OF FIGURES

1.1	Multi-biometrics: Face, fingerprint, iris, retina, palmprint and hand geometry are physiological characteristics. Gait and signature are some of the behavioral characteristics. . . . .	2
1.2	Biometric recognition system. . . . .	3
2.1	Sample iris image . . . . .	12
2.2	Major steps in iris biometrics processing. . . . .	14
2.3	Major steps in fingerprint recognition system. . . . .	18
3.1	Iris de-duplication architecture . . . . .	31
3.2	Iris classes: (a) stream, (b) flower and (c) jewel-shaker structures. . .	33
3.3	Iris fibers: (a) stream, (b) flower, (c) jewel and (d) shaker. . . . .	33
3.4	Iris image segmentation . . . . .	36
3.5	Normalized iris image . . . . .	36
3.6	Experimental results for the classification approaches <i>SVM-4Class-PCA-Kmeans</i> and <i>ODL-4Class-PCA-Kmeans</i> for the three iris databases namely, CASIA1, IITD and UPOL . . . . .	39
3.7	Experimental results for all the proposed classification approaches on UPOL iris database . . . . .	40
3.9	Iris adjudication: side-by-side comparison of genuine iris matches with hamming distances (a) 0.21, (b) 0.19, (c) 0.16, (d) 0.15, (e) 0.19 . .	42
3.8	Classification accuracy for three different dictionary sizes 60, 90 and 120	43
3.10	Iris adjudication: side-by-side comparison of impostor iris matches with hamming distances (a) 0.48, (b) 0.46, (c) 0.43, (d) 0.51, (e) 0.37 . .	43
4.1	Noisy slap fingerprint image . . . . .	50

4.2	Histogram of noisy slap image . . . . .	52
4.3	Illustration of sequence of steps of de-noising slap fingerprints for accurate slap fingerprint segmentation: (a) slap with high noise, (b) slap with low noise, (c,d,e,f) are segmented fingers of the slap with high noise, (g,h,i,j) are segmented fingers of the slap with low noise, (k) foreground-background separation of high noisy slap, (l) foreground-background separation of low noisy slap. . . . .	58
4.4	Illustration of sequence of steps of de-noising slap fingerprints for accurate slap fingerprint segmentation: (a) noise-free slap of high noise, (b) noise-free slap of low noise, (c,d,e,f) are segmented fingers of noise-free slap of high noise, and (g,h,i,j) are segmented fingers of noise-free slap of low noise. . . . .	59
4.5	Levels of fingerprint image NFIQ scores for the entire dataset - before noise removal process . . . . .	60
4.6	Levels of fingerprint image NFIQ scores for the entire dataset - after noise removal process . . . . .	60
4.7	De-duplication statistics of targeted public distribution system . . . . .	60
5.1	Chance prints: (a) visible prints, (b) semi-visible prints or plastic prints, (c) latent prints . . . . .	64
5.2	Different fingerprint types: (a) rolled (b) plain and (c) latent prints . . . . .	65
5.3	Fingerprint image enhancement . . . . .	67
5.4	Steps in latent fingerprint image enhancement and feature extraction: (a) sample latent print, (b) image normalization, (c) de-noising image, (d) image binarization, (e) image thinning, (f) feature extraction. . . . .	69
5.5	Rolled fingerprint image with the corresponding quality image . . . . .	70
5.6	Evidence exhibit of a particular matched fingerprint pair . . . . .	73
5.7	CMC curves for different quality latent prints (good, bad, and ugly) . . . . .	75

5.8	Finger markup filters: (a) sample latent print from NIST SD-27, (b) region of interest marking, (c) enhance image with color filters, (d) brightness and contrast enhancements, (e) Sobel filter applied with gradient direction $0^0$ , (f) Sobel filter applied with gradient direction $90^0$ , (g) Sobel filter applied with gradient direction $180^0$ , (h) Sobel filter applied with gradient direction $270^0$ . . . . .	76
5.9	Finger markup filters: (a) emboss filter applied with gradient direction $0^0$ , (b) emboss filter applied with gradient direction $90^0$ , (c) emboss filter applied with gradient direction $180^0$ , (d) emboss filter applied with gradient direction $270^0$ , (e) lighting filter applied with gradient direction $0^0$ , (f) lighting filter applied with gradient direction $90^0$ , (g) lighting filter applied with gradient direction $180^0$ , (h) lighting filter applied with gradient direction $270^0$ . . . . .	77
6.1	Family photograph of a household ration card . . . . .	80
6.2	Decomposition of images into frequency bands by wavelet transforms . . . . .	82
6.3	Architecture of convolutional neural network . . . . .	86
6.4	Duplicate household ration cards . . . . .	89
6.5	Typical distribution of Extended Yale Face dataset B facial images across the five sets (only 6 instances per subset are shown) . . . . .	90
6.6	Classification performance (%) on five sets of Extended Yale Face dataset B . . . . .	91
6.7	Classification performance (%) including the horizontally reflected facial images on five sets of Extended Yale Face dataset B . . . . .	92
6.8	Comparison of classification (%) performance with existing methods . . . . .	94
7.1	Enrollment station with biometric sensors . . . . .	98
7.2	4-4-2 Fingerprints . . . . .	99
7.3	Iris images . . . . .	99
7.4	Face photograph . . . . .	100

7.5	Signature . . . . .	100
7.6	Signature image compression . . . . .	102
B.1	Illustration of the idea of support vectors and an optimal hyperplane for linearly separable patterns. . . . .	115



## ABBREVIATIONS

FAR	- False Accept Rate
FRR	- False Reject Rate
EER	- Equal Error Rate
FER	- Failure to Enroll Rate
ROC	- Receiver Operating Characteristic
HD	- Hamming Distance
ED	- Euclidean Distance
JPEG	- Joint Photographic Experts Group
JP2	- JPEG 2000
ISO	- International Organization for Standardization
NIST	- National Institute of Standards and Technology
NFIQ	- NIST Fingerprint Image Quality
WSQ	- Wavelet Scalar Quantization
PCA	- Principal Component Analysis
ICA	- Independent Component Analysis
CCV	- Color Coherence Vector
NLPCA	- Nonlinear Principal Component Analysis
HMM	- Hidden Markov Model
TPDS	- Targeted Public Distribution System
CBIR	- Content Based Image Retrieval

# CHAPTER 1

## INTRODUCTION TO DE-DUPLICATION OF BIOMETRICS

Government of India provides different services and welfare schemes for the benefit of the people in the society. Some of these services include issuance of birth certificate, voter identity card, driving license, and passport etc. Also, welfare schemes like targeted public distribution system (TPDS), national rural employment guarantee system (NREGS), health insurance, old age pensions etc. for the economic and social upliftment of the people. A unique identity (UID) number assigned for every citizen would obviate the need for a person to produce multiple documentary proofs of his/her identity for availing any Government service, or private services like opening of a bank account. The unique identity (UID) number would remain a permanent identifier right from birth to death of every citizen in the country. UID would enable Government to ensure that benefits under various welfare programmes reach the intended beneficiaries, prevent cornering of benefits by a few section of people and minimize frauds. UIDs are also expected to be of help in law and order enforcement, effective implementation of the public distribution system, define social welfare entitlements, financial inclusion and improve overall efficiency of the government administration. The biometrics play a key role in providing unique identity of a person. Recent survey on biometrics market indicates that the funding for the Government biometric based projects such as, national ID Program, biometric drivers license, biometric passports & visas, is expected to be about 21.9 Billion US\$ by 2020.



**Fig. 1.1:** Multi-biometrics: Face, fingerprint, iris, retina, palmprint and hand geometry are physiological characteristics. Gait and signature are some of the behavioral characteristics.

There are different biometrics such as iris, fingerprints, face, hand geometry, signature, voice patterns etc... which are being used by the industry all over the world for an extensive array of highly secure identification and personal verification solutions. Fig. 1.1 illustrates two different categories of biometrics. One category of biometrics related to physiological characteristics which include face, fingerprint, iris, retina,

palm-print and hand geometry. The other type of biometrics have the behavioral characteristics which include gait and signature. Each biometric has their own advantages and disadvantages which should be considered before designing/developing a biometric recognition system.

## 1.1 BIOMETRIC RECOGNITION SYSTEM

Biometric recognition system can be used to accomplish either identification or verification, and the selection and implementation of the technology and related procedures are closely tied to this objective. In general, different processing steps involved in biometric recognition system are explained in Fig. 1.2.

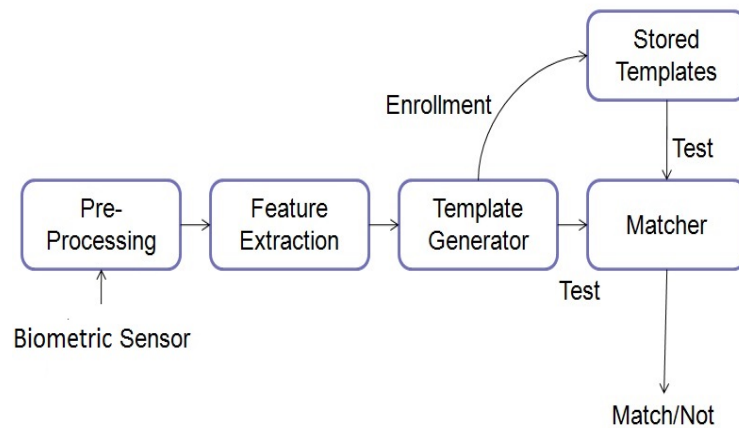


Fig. 1.2: Biometric recognition system.

### 1.1.1 Biometric identification

Biometric identification means the comparison of a test biometric sample against a database of previously enrolled biometric samples. It can be represented as the relation 1:many or 1:n comparisons.

### **1.1.2 Biometric verification**

Biometric verification means the validating a test biometric sample against previously enrolled biometric sample of the same individual. It can be represented as the relation 1:1 comparison. Almost all the biometric authentication systems use the biometric verification.

### **1.1.3 De-duplication of biometrics**

De-duplication is the process of removing instances of multiple enrollments of the same person using the person's biometric data. During de-duplication, matching the biometrics of a person is done against the biometrics of other persons to ensure that the same person is not enrolled more than once. This will ensure that each person will have a unique identity. The de-duplication process can be both online as well as offline, where the online de-duplication process is called as centralized de-duplication and the offline process is called as de-centralized de-duplication.

## **1.2 MULTI-MODAL BIOMETRICS**

Multimodal biometrics means combining two or more biometric modalities in the development of a single biometric identification system. Biometric recognition systems based solely on uni-modal biometrics which can not meet the desired biometric performance requirements in large-scale biometric applications due to the problems such as noisy biometric information, failure to enroll rate, spoof attacks, unacceptable error rates and environmental conditions. These biometrics have their own advantages and applications to which they are effective.

The main reason for adopting multi-modal biometric is to introduce certainty in the biometric recognition process, minimal effort for de-duplication process, real time identification and reduced spoof biometric spoof attacks.

Advantages of using multi-modal biometrics are:

- Even though the cost of the enrollment process using multi-modal biometrics increases about 5 - 10% marginally higher when compared with a single/dual biometric enrollment, the total cost of the biometric solution using multi-modal biometrics will be reduced significantly due to the reduced cost of de-duplication during biometric enrollments.
- The failure to enroll (FTE) rate is high for single individual biometrics (due to scars, aging or illegible in case of fingerprints).

The biometrics used in this thesis are explained briefly as follows:

### **1.2.1 Face**

The face can be considered as the most convenient biometric to acquire without user cooperation for recognizing the people. Face recognition [2] has gained much attention from the research groups of pattern recognition and machine learning since the early 1990s. Face recognition is a difficult task due to the issues with illumination variance which affects the identification rate. Facial recognition system can not distinguish between identical twins. Facial recognition uses 9 geometric points for recognizing a person with false acceptance rate of 1%.

### **1.2.2 Signature**

Signature [3] is a behavioral biometric. It can be collected in two different ways. First one is the off-line mode, where the users write their signature on paper and then capture it using an optical scanner or camera. The other one is the on-line mode, where the users write their signatures on digital signature tablets. Signature recognition has a false accept rate of 1 in 5000.

### **1.2.3 Fingerprint**

A fingerprint consists of ridges and valleys on the surface of the finger. The uniqueness of a fingerprint can be determined by the minutiae points. Minutiae points are the local ridge features which are identified by a ridge bifurcation or a ridge ending. Fingerprint is a physical biometric which is mainly used in forensic analysis as well as civilian identification. Fingerprints play an important role in forensic analysis for criminal identification using the clues collected from the crime scene. Fingerprint-based identification has been known and used for a very long time. The fingerprint impressions which are left on the articles by the offenders at the crime scene are called as chance prints. There are three ways of forming the chance prints, namely, visible prints, semi-visible prints and latent prints. The visible prints are the fingerprints which are collected and covered with ink, blood, dust, paint, etc. Semi-visible prints, also known as plastic prints are the fingerprints which are collected by applying some pressure on the surface such as soap, wax, melted candle, etc. The latent prints are the fingerprints which are collected by leaving the finger impressions formed with sweat from fingers. The latent prints have the poor quality of ridge impressions and partial fingerprint area. First two cases need no further development for analysis and identification of suspects as the ridge information is clear for identification, where as latent fingerprints need developments and enhancements to identify the suspects. The advantages of fingerprints are cost effectiveness at the time of fingerprint authentication systems which uses low cost fingerprint scanners.

### **1.2.4 Iris**

The iris is an annular region between pupil and sclera. The sclera means the white region which combines the tissue and blood vessels near iris. The pupil region is the darker region which is located at the center of eye and its size depends on the specular reflections. The iris consists of texture information like furrows, ridges, and pigment spots. The iris biometric is stable in the lifetime of a person. The texture information

of iris do not change with external environmental factors. Even the left eye of a person is unique when compared to right eye of the same person. One of the most important advantages of using iris as a biometric is the lower effort, lesser infrastructure required for de-duplication.

Almost all of the currently deployed iris recognition systems use the data acquired at near infra-red (NIR) wavelengths. These systems are believed to be more accurate among all the existing biometric recognition systems. There have been recent efforts to develop visible wavelength based iris recognition techniques in order to eliminate the NIR radiation hazards and the limitations of existing iris recognition systems. In this context, the iris pigmentation plays an important role while acquiring images under visible wavelengths. The concentration of melanin pigment is more in dark colored iris which can be acquired with greater texture details under near infra-red illumination. The color of iris can be determined by considering the variable proportions of the two molecules, namely, eumelanin (brown/black) and pheomelanin (red/yellow). The appearance of dark colored iris is not very clear under visible illumination since it has more eumelanin molecules which absorbs the visible illumination deeply. In order to ensure enhanced texture details under visible wavelengths, the power of visible illumination should be increased which can be uncomfortable to the users. Also, the external environmental illumination can add more noise to the visible iris images in terms of shadows, specular and diffuse reflections. These factors should be considered before selecting an image acquisition setup especially under visible wavelengths.

### **1.2.5 Performance evaluation of biometrics**

A comparative study of the performance of multiple biometrics done by the centre for mathematics and scientific computing, national physical laboratory (NPL) of UK is given in the Table 1.1, in terms of different error rates, namely, false acceptance rate (FAR), false rejection rate (FRR), equal error rate (EER) and failure to enroll rate (FER). A true acceptance (TA) means when the system verifies, an identity claim, and



the claim is true. A false acceptance (FA) means when the system verifies an identity claim, but the claim is false. A true rejection (TR) occurs when the system does not verify an identity claim and the claim is false. A false rejection (FR) occurs when the system does not verify an identity claim, but the claim is true.

**Table 1.1:** Metrics used to evaluate a biometric [1]

Biometric	FAR	FRR (%)	FER (%)	Scalability	Stability
Iris	1:1.2 million	0.1 - 0.2	0.5	1: all search	Very stable
Fingerprint	1:100000	2.0 - 3.0	1.0 - 2.0	1: 1 match	Changes
Facial recognition	1:100	10	0.0	1:1 match	Changes
Signature	1:5000	15 - 25	0.0	1:1 match	Changes

Biometric recognition system is not 100% accurate due to the trade-offs between the error rates. Based on the requirement of the applications like, high security, forensics or civilian, the thresholds on error rates should be fixed properly. The matching accuracy for the biometric recognition system can be evaluated using the performance measures, namely, equal error rate (EER), receiver operating characteristic (ROC) curve, cumulative match characteristic (CMC) curve and the decidability index (DI).

The equal error rate (EER) is where the false rejection rate equals the false acceptance rate. The ROC curve plots the genuine acceptance rate on the  $Y$ -axis and the false acceptance rate on the  $X$ -axis, or, alternatively, the false rejection rate on the  $Y$ -axis and the false acceptance rate on the  $X$ -axis. The point on the ROC curve indicates the equal-error rate (EER). The CMC curve plots the percentage of correctly identified on the  $Y$ -axis and the cumulative rank considered as a correct match on the  $X$ -axis. The decidability index ( $d'$ ) can be defined as

$$d' = \frac{|\mu_A - \mu_I|}{\sqrt{\frac{1}{2}(\sigma_A^2 + \sigma_I^2)}}, \quad (1.1)$$

where  $\mu_A$  and  $\mu_I$  are the means of authentic and impostor distance score distributions, respectively, and  $\sigma_A$  and  $\sigma_I$  are the standard deviations of the two distributions, respectively.

### 1.3 ISSUES ADDRESSED IN THIS THESIS

Though biometric systems are successfully implemented in large-scale applications like Aadhaar and e-KTP, there are two main factors contribute to the complexity of biometric recognition system, namely, matching accuracy and scalability of the system as explained in the following subsections. These two issues are addressed in this thesis in the context of large-scale de-duplication applications.

**Accuracy:** An ideal biometric system should always provide the correct identity decision when a biometric sample is presented. However, a biometric system seldom encounters a sample of a user's biometric trait that is exactly the same as the template. This results in a number of errors as discussed in section 1.2.5 and there by limits the system accuracy. The main factor affecting the accuracy of a biometric system is noisy biometric data.

**Scalability:** In the case of a biometric verification system, the size of the database (i.e. number of enrolled users in the system) is not an issue because each authentication attempt basically involves matching the query with a single template. In the case of large scale identification systems where  $N$  identities are enrolled in the system, sequentially comparing the query with all the  $N$  templates is not an effective solution due to two reasons. Firstly, the throughput of the system would be small if the value of  $N$  is quite large. For example, if the size of the database is 1 million and if each match requires an average of 100 microseconds, then the throughput of the system will be less than 1 per minute. Furthermore, the large number of identities also affects the false match rate of the system adversely. Hence, there is a need to efficiently scale the system. This is usually achieved by a process known as filtering or indexing where the database is pruned based on extrinsic (e.g., gender, ethnicity, age, etc.) or intrinsic (e.g., fingerprint pattern class) factors and the search is restricted to a smaller fraction of the database that is likely to contain the true identity of the user.

## 1.4 ORGANIZATION OF THE THESIS

An overview of the existing approaches in biometric recognition system is presented in Chapter 2. Some research issues are identified in the de-duplication process of biometric recognition system which are addressed in this thesis. In Chapter 3, an approach to classification of iris images is proposed based on sparse representation of Gabor features using dictionary learning for large-scale de-duplication applications. Also, an iris adjudication process is illustrated by comparing the matched iris-pair images side-by-side to make the decision on the identification score using color coding. A de-noising approach was proposed in Chapter 4 for accurate slap fingerprint segmentation to improve the accuracy of fingerprint de-duplication. Also, a cross-sensor fingerprint recognition is proposed using kernel transformation learning. In Chapter 5, a semi-automated latent fingerprint identification is proposed to markup fingerprint landmarks manually using the image enhancement filters which will further improve the identification performance. A new method is proposed in Chapter 6, for face recognition to address the issue of non-uniform illumination using convolutional neural networks (CNN). A new approach for photograph de-duplication was proposed using color histograms to eliminate the duplicate ration cards in targeted public distribution system. In Chapter 7, the best practices for biometric data acquisition and identity creation were presented using multi-modal biometrics (fingerprints, iris, face and signature) in order to minimize the data storage on a smart card. Chapter 8 summarizes the research work carried out as part of this thesis, highlights the contributions of the work and discusses directions for future work.

## CHAPTER 2

# OVERVIEW OF APPROACHES FOR DE-DUPLICATION OF BIOMETRICS

De-duplication can be defined as the process of removing duplicate identities of a person using multi-modal biometrics, namely iris, fingerprints and face. During de-duplication, matching the biometrics of a person can be done against the biometrics of other persons to ensure that the same person is not enrolled more than once. This will ensure that each person will have a unique identity. This chapter reviews some of the existing approaches of biometric recognition systems used in the de-duplication process. Different steps involved in iris recognition system and the related work is briefly described in Section 2.1. In Section 2.2, the existing approaches for all the components of fingerprint recognition system are reviewed. Early work in facial recognition system is presented in Section 2.3. Some research issues arising out of the review of existing methods are identified, which are addressed in this thesis.

### 2.1 IRIS RECOGNITION SYSTEM

The iris is an annular region between pupil and sclera [4] as shown in Fig. 2.1. The sclera means the white region which combines the tissue and blood vessels near iris. The pupil region is the darker region which is located at the center of eye and its size depends on the specular reflections. The iris consists of texture information like furrows, ridges, and pigment spots. The iris biometric is stable in the lifetime of a person. The texture information of iris do not change with external environmental factors. Even the left eye of a person is unique when compared to right eye of the

same person. [5].

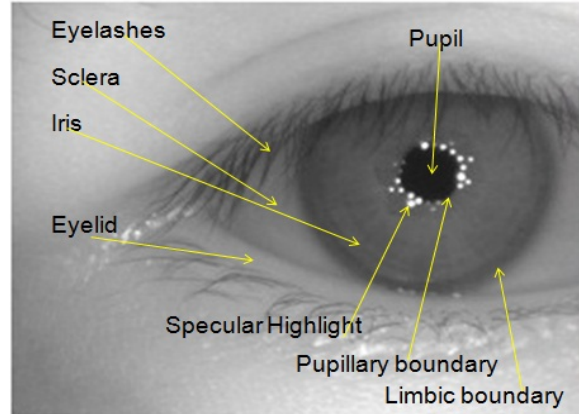


**Fig. 2.1:** Sample iris image

### 2.1.1 Early history of iris biometrics

**Flom and Safirs concept patent:** The automatic iris recognition system is well known in recent days, however this idea exists over 100 years old. Flom and Safir [6] have taken a patent for the concept of automatic iris recognition system in 1987. In 1992, Johnston [7] have investigated that the iris biometrics can be used in iris identification and verification systems, but the results are not published.

**Daugman's approach:** Daugman's work [8], [9] is very significant in the early history of iris biometrics. Daugman's 1994 patent [10] gives the operational details of iris recognition system. Now, the Daugman's approach is the standard reference model in the field of iris biometrics. Almost all existing commercial iris biometric technologies use Daugman's work because of the patents taken by Flom Safir and Daugman. Daugman's patent states that the system acquires through a video camera a digitized image of an eye of the human to be identified. A deformable template was specified by a set of parameters and allowed knowledge about the expected shape of an eye to guide the detection process [11]. The pupillary and limbic boundaries [12] of an iris image are

approximated as circles using three parameters: the radius  $r$ , and the coordinates of the center of the circle,  $x_0$  and  $y_0$ . The integrodifferential operator [9] used for iris segmentation is:

$$\max_{r, x_0, y_0} G_\sigma(r) * \frac{\partial}{\partial r} \int \frac{I(x, y)}{2\pi r} ds, \quad (2.1)$$

where  $G_\sigma(r)$  is a smoothing function and  $I(x, y)$  is the image of the eye.

Even though the pupillary and limbic boundaries are considered as circular, in few cases the boundaries are not circular. Daugman proposed an alternative segmentation approach in [13] to address this issue and also to eliminate the noisy iris region occluded by eyelids or eyelashes. All iris images are of not in same size due to the problems like, the distance between camera and iris and the illumination can cause the iris dilations or contractions. In order to solve this problem, the extraction of iris region is transformed into a normalized iris image where every pixel is defined by two coordinates, namely, radial angle ranges from 0 to 360 and radial coordinate that ranges from 0 to 1. The iris contractions and dilations stretches iris linearly. The pupillary boundary appears on the bottom of the normalized image where as the limbic boundary appears on the top of the image. The rotation of iris region is considered in the matching phase of iris recognition system. Daugman uses 2-D Gabor filters to extract the texture information from the normalized iris image [10].

The texture information is analyzed and represented as iris template and is matched against the stored iris templates. In large scale iris recognition systems, the comparison between two iris images should be very fast. So, Daugman selected the quantization of filter phase response into pair of binary bits in the iris texture representation. The complex coefficient was transformed into a two bit binary code where the first bit equals to one if the real part of the complex coefficient was  $+ve$ , otherwise it equals to zero and the second bit equals to one if the imaginary part of the complex coefficient was  $+ve$ , otherwise it equals to zero. After analyzing the iris texture, the resultant binary information was represented as a binary iris code of size 256 bytes (2048 bit). These

binary codes can be compared using bitwise operations in efficient manner. Daugman defined a normalized Hamming distance which calculates the fraction of bits disagree in both the binary iris codes. The rotation invariance was achieved by shifting the binary iris code for different orientations in the angular coordinate. The minimum value of normalized Hamming distance was considered as the final matching score between two iris codes. These steps are summerized into different modules of an iris biometrics system as shown in Fig. 2.2.

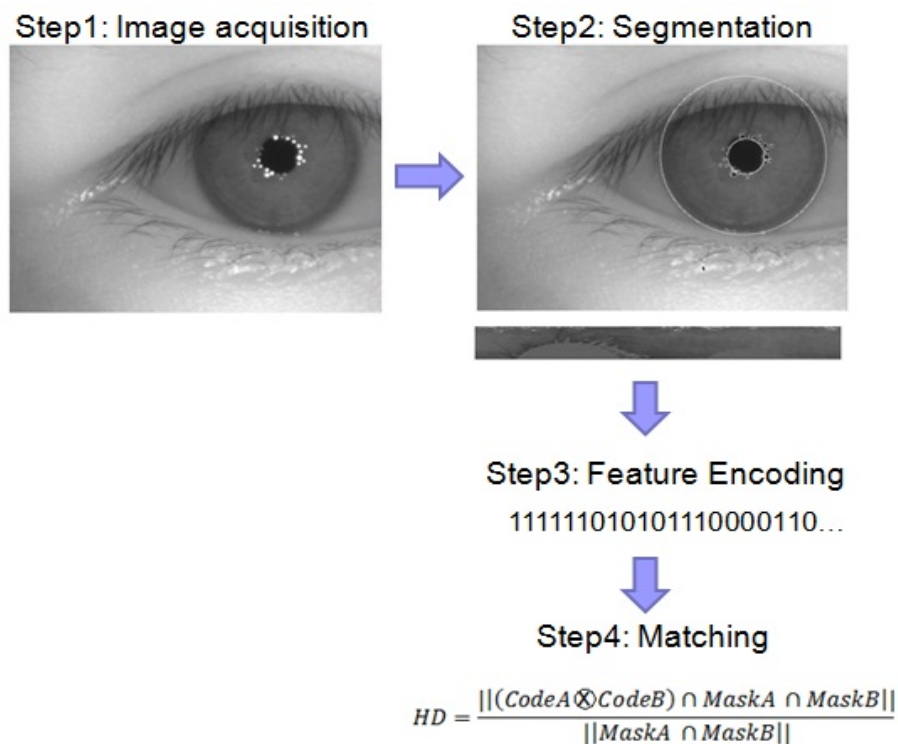


**Fig. 2.2:** Major steps in iris biometrics processing.

**Wildes' approach:** Wildes [14] developed an iris biometric recognition system at Sarnoff Labs. The approach is technically different from Daugman's iris recognition system. The iris image acquisition in Daugman's approach uses "an LED-based light source with a standard video camera," where as Wildes' approach uses "a diffuse source and polarization in conjunction with a low light level camera." The iris boundary

detection in Daugman's algorithm uses an integro-differential operator which responds at maximum to circular boundary. By contrast, Wildes' algorithm computes the binary edge map and a Hough transform to detect iris circular boundary. Daugman's approach uses the normalized Hamming distance to compute the dissimilarity measure between two iris codes, where as Wildes' approach uses a Laplacian of Gaussian filter at multiple scales to produce a template and computes the normalized correlation as a similarity measure.

### **2.1.2 Iris segmentation**

As mentioned earlier, Daugman's approach to iris segmentation uses an integro-differential operator, and Wildes [14] uses a method involving edge detection and a Hough transform. Different variations of the Hough transform and edge detection approach have been used by many researchers. Most of the iris segmentation research have been carried out by improving the Wildes' iris segmentation approach. Huang et al. [15] suggested the modification of first finding the iris boundaries in a rescaled image to reduce computational complexity. Liu et al. [16] assumed the pupillary and limbic boundaries as two concentric circles and applied Canny edge detection and a Hough transforms. Sung et al. [17] use histogram equalization and high-pass filtering in order to detect the collarette boundary apart from the traditional methods for finding the iris boundaries.

### **2.1.3 Iris texture analysis and representation**

Many approaches have been suggested for iris texture analysis and representation. Sun et al. [18] proposed an approach for iris feature extraction using a Gaussian filter. The gradient vector field of an iris image is convolved with a Gaussian filter, yielding a local orientation at each pixel in the unwrapped template. Similar ideas were presented in [19] from the same research group. A dyadic wavelet transform of a sequence of 1-D intensity signals around the inner part of the iris is used by Ma et al. [20] to



create binary iris code. Similar work is described in [21]. Chenhong and Zhaoyang [22] and Chou et al. [23] proposed iris feature extraction using Laplacian-of-Gaussian filter which finds "blobs" in the image that are relatively darker than surrounding regions. Yao et al. [24] presented the feature extraction using modified log-Gabor filters because the log-Gabor filters are "strictly bandpass filters where as the Gabor filters are not." They have mentioned that Gabor filter would represent the high frequency components in natural images. Monro et al. [25] use the discrete cosine transform for feature extraction. They apply the DCT to overlapping rectangular image patches rotated 45 degrees from the radial axis.

#### **2.1.4 Matching iris representations**

In biometrics, it has been found that using multiple samples for enrollment and comparing the probe to multiple gallery samples will result in improved performance [26–28]. Several papers show that this is also true for iris recognition. Du [29] performs experiments using one, two, and three images to enroll a given iris. The resulting rank-one recognition rates are 98.5%, 99.5%, and 99.8%, respectively. Liu and Xie [30] present an algorithm that uses direct linear discriminant analysis (DLDA). Algorithms that use multiple training samples to enroll an image must decide how to combine the scores from multiple comparisons. In 2003, Ma et al. [31] suggested analyzing multiple images and keeping the best-quality image. In their 2004 paper [20], it is stated that when matching the input feature vector with the three templates of a class, the average of the three scores is taken as the final matching distance. Krichen et al. [32] represent each subject in the gallery with three images so that for each client and for each test image, the minimum value of its similarity measure to the three references images of the client is considered, which is more appropriate when there are large "outlier" type errors in the scores rather than considering the average of similarity scores in [20].

Almost all of the currently deployed iris recognition systems use the data acquired at near infra-red (NIR) wavelengths. These systems are believed to be more accurate

among all the existing biometric recognition systems. There have been recent efforts to develop visible wavelength based iris recognition techniques in order to eliminate the NIR radiation hazards and limitations of existing iris recognition systems. In this context, the iris pigmentation plays an important role while acquiring images under visible wavelengths. The concentration of melanin pigment is more in dark colored iris which can be acquired with greater texture details under near infra-red illumination. The color of iris can be determined by considering the variable proportions of the two molecules, namely, eumelanin (brown/black) and pheomelanin (red/yellow). The appearance of dark colored iris is not very clear under visible illumination since it has more eumelanin molecules which absorb the visible illumination deeply. In order to ensure enhanced texture details under visible wavelengths, the power of visible illumination should be increased which can be uncomfortable to the users. Also, the external environmental illumination can add more noise to the visible iris images in terms of shadows, specular and diffuse reflections. These factors should be considered before selecting an image acquisition setup especially under visible wavelengths.

### **2.1.5 Issues addressed in iris recognition system**

Government of Andhrapradesh [33] undertook the de-duplication of ration cards using 52 million people iris codes in order to ensure that the benefits under various welfare programs reach the intended beneficiaries, prevent cornering of benefits by a few sections of people and minimize frauds. There are over 6.26 quadrillion (6,262,668,889,152,840) iris matches performed in de-centralized manner to remove duplicate enrollments in 61 days with high-end blade servers equipment which is not a scalable solution. The scalability issue of iris de-duplication process is addressed in the context of targeted public distribution system (TPDS) in order to reduce the search time drastically thereby providing the scalable iris de-duplication solutions. We propose an approach for classification of iris images based on sparse representation of Gabor features using dictionary learning for large-scale de-duplication applications. Also, an iris adjudica-

tion process is illustrated by comparing the matched iris-pair images side-by-side to make the decision on the identification score using color coding. Iris classification and adjudication framework is proposed in iris de-duplication architecture to speed-up the identification process and reduce the identification errors.

## 2.2 FINGERPRINT RECOGNITION SYSTEM

Fingerprint recognition is a complex pattern recognition problem since it is difficult to design accurate matching algorithms which extracts minutia features, especially in poor quality fingerprint images. The steps involved in fingerprint recognition system are illustrated in Fig. 2.3.

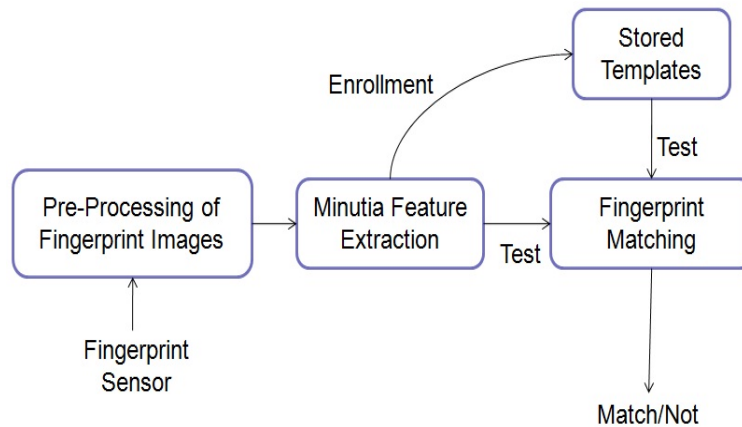


**Fig. 2.3:** Major steps in fingerprint recognition system.

A fingerprint [34] consists of ridges and valleys on the surface of the finger. The uniqueness of a fingerprint can be determined by the minutiae points. Minutiae points are the local ridge features which are identified by a ridge bifurcation or a ridge ending. One way of acquiring fingerprints is to capture the slap fingerprint. Slap fingerprints are taken by pressing four fingers simultaneously onto a slap fingerprint scanner. In general, the capturing process will take place in the fashion of 4-4-2 fingers, means capture left four fingers at one time, followed by all right four fingers and then fol-

lowed by two thumb fingers. The captured slap fingerprints go for the slap fingerprint segmentation [35] which splits the individual fingers from the slap image. The left four fingers slap can be segmented as in the sequence of left little (LL), left ring (LR), left middle (LM) and left index (LI). The right four fingers slap can be segmented as in the sequence of right index (RI), right middle (RM), right ring (RR) and right little (RL). The two thumb fingers can be segmented as left thumb (LT) and right thumb (RT). The finger positions are the position codes defined in Table 12 of ANSI/NIST-ITL 1-2007 [36].

The methods described in [37] - [38], use different filtering techniques to enhance the significant details of single fingerprint images. Fingerprint segmentation using block-wise grey-level variance or local histogram of ridge orientations are described in [39]. In some techniques the Gabor filters are used to divide fingerprint into foreground and background. The United States Patent 7072496 [40] presented the segmentation algorithm using edge detection and convex hull calculation by segmenting the image into different disconnected regions. In 2004, NIST organized a contest called slap fingerprint evaluation 2004 (SlapSeg04) [35]. Thirteen segmentation algorithms were evaluated within the contest. One algorithm which is accessible publicly is the NIST's own algorithm called NIST fingerprint segmentation algorithm (NFSEG) [41]. The other twelve algorithms are the intellectual property of different companies. NFSEG algorithm first pre-process the slap input images and then binarises. In 2008, NIST again conducted the contest called slap fingerprint segmentation evaluation II (SlapSegII). The difference between the two contests is the metrics used for successful slap fingerprint segmentation. SlapSeg04 [42] used the fingerprint matching algorithm to determine the accuracy of slap fingerprint segmentation. SlapSegII used the ground truth data which has hand marked segmentation boxes as baseline using NFSEG algorithm.

Manvjeet Kaur [43] have introduced the methods combined to create minutia extractor and minutia matcher. Mana Tarjo-man [44] introduced structural approach to fingerprint classification by using the directional image of fingerprints instead of

singularities. Singularities detection is used to increase the accuracies. Lie Wei [45] Proposed a method for rapid singularities searching algorithm which used delta field Poincar index and a rapid classification algorithm to classify the fingerprint into five classes. The detection algorithm searches the direction field which the larger direction changes to get the singular points. Singular point detection is used to improve the accuracy. Alessandra Lumini and Loris Nanni [46] developed a method for minutia based fingerprint and its approach to the problem as two-class pattern recognition. The obtained feature vector by minutia matching is classified into genuine or imposter by Support Vector Machine resulting remarkable performance improvement.

Anil K Jain [47] proposed latent fingerprint matching based on Local minutia matching and Global minutia matching computed matched pair based similarity measure to compute the similarity between latent and rolled/plain fingers. Linag Li [48] have proposed improved cross matching algorithm for the fingerprint images captured from different sensors technology optical, capacitive and thermal sensors shown the results with multiple sensors. Some researchers proposed fingerprint identification techniques using a gray level watershed method to find out the ridges present on a fingerprint image by directly scanned fingerprints are inked impressions.

The majority of the algorithms developed for automated fingerprint matching are based on minutiae [49], [50] and [51]. Several recent studies on fingerprint matching have focused on the use of local minutiae descriptors [52], [49], [53], [54]. Some algorithms combine ridge orientation with minutiae information either at feature level by including ridge orientation information in local minutiae descriptors [55], [56] or at score level by combining scores from minutiae matching and global orientation field matching [56], [57]. The latent matching accuracy is improved by using the features which are located manually from the latents' [58], [59], [60], [61]. However, marking extended features (orientation field, ridge skeleton, etc.) in poor quality latents' is very time-consuming and might be only feasible in rare cases. However, only a small portion of latents can be correctly identified using this approach. There have also been some studies on fusion of multiple matchers [62] or multiple latent prints [50]. NIST has

been conducting a multi-phase project on evaluation of latent finger-print technologies (ELFT) to evaluate latent feature extraction and matching techniques [63]. Jain et. al. have proposed a latent matcher for automatic identification of suspects by using the extended features, namely, singularity, ridge quality map, and ridge flow map [47], [64]. The latent fingerprint image quality is measured by spectral image validation and verification (SIVV)-based metric [65] and the latent fingerprint image quality (LFIQ) metric based on triangulation of minutiae points [66].

### **2.2.1 Issues addressed in fingerprint recognition system**

Government of Orissa collected a total of 1.8 million (approximately) slap fingerprint images of 0.6 million (approximately) citizens as part of targeted public distribution system (TPDS) process. The fingerprint device which is used to collect the slap fingerprint images has inbuilt real time feedback on the quality of the slap fingerprints being captured. However, the slap fingerprint images have some noisy data due to some external factors which affect the calibration process of the fingerprint device. While doing the segmentation of slap fingerprints, some of the fingerprint images are improperly segmented because of the noise present in the data and as a result the de-duplication accuracy was reduced. The issue of de-duplication accuracy is addressed in this thesis. A de-noising approach is proposed to remove the noise present in the data using binarization of slap fingerprint image and region labeling of desired regions with 8-adjacency neighborhood.

Also, due to the increasing demand for fingerprint biometrics, new fingerprint scanners are being deployed for scanning fingerprint images and the old fingerprint scanners are being frequently upgraded. The user enrollment is very expensive and time-consuming especially in large scale de-duplication applications. However, upgrading with new fingerprint scanners for cross-sensor matching where the test fingerprint data is verified with the data enrolled with different fingerprint scanner often lead to reduced fingerprint matching performance. The issue of cross-sensor fingerprint

matching performance degradation is also addressed in this thesis. In order to improve the accuracy of cross-sensor fingerprint matching, a new algorithm is proposed using feature transformation learning in kernel space. The kernel learning uses the distance kernel matrix for optimization using similar and dissimilar class constraints. These constraints reduces the sensor mismatch problem when the matching performed for cross-sensor in the transformed domain. Also, a semi-automated latent fingerprint identification is proposed to markup fingerprint landmarks manually using the image enhancement filters which will further improve the identification performance.

### **2.3 FACE RECOGNITION SYSTEM**

Face recognition [67] has gained much attention from the research groups of pattern recognition and machine learning since the early 1990s. Face recognition is a difficult task due to the issues with illumination variance which affects the identification rate [68]. A fuzzy Fisher-face approach was proposed for face recognition [69] using Fisher discriminant analysis and principle component analysis. Face recognition is used in applications like access control and surveillance [2]. A new framework for face recognition and feature extraction is proposed with kernel fisher discriminant analysis and fisher linear discriminant analysis [70]. Wiskott et. al. [71] proposed face recognition algorithm by using labeled elastic bunch graphs matching based on Gabor wavelet transform. A face verification algorithm was proposed [72] for training a very large and unknown data of different categories.

Variations in ambient lighting produces significant degradation in face recognition performance [2]. Thermal infrared (thermal IR) has been used in facial recognition systems with some success against the ambient illumination. Near infrared (NIR) has the potential to overcome the problems associated with visible [73] and thermal IR face recognition which is more robust against illumination variations and face detection [74]. NIR is useful for face detection as the bright eye effect [75] allows the eyes to be localized and skin reflectance properties at just above and below 1.4 microns which

highlights the face regions clearly [74]. Over the last decade, convolutional neural networks [76] is widely used for various computer vision tasks [77].

The modeling of face images under varying illumination can be based on a statistical model or physical model. For statistical modelling, no assumption concerning the surface property is needed. Statistical analysis techniques, such as PCA (Eigen face) and LDA (Fisher face), are applied to the training set which contains faces under different illuminations to achieve a subspace which covers the variation of possible illumination. In physical modeling, the model of the process of image formation is based on the assumption of certain object surface reflectance properties such as Lambertian reflectance.

Belhumeur et al. [78] explored an illumination invariant face recognition using a method of 3D linear subspace. Three or more images are taken from the same face using different lighting conditions which construct 3D basis in the method of 3D linear subspace. The face recognition can be done by comparing the test face image with each linear subspace of all the gallery face images belonging to all the identities. A new method called Fisher linear discriminant [78] is proposed in order to maximize the intra-class scatter and inter-class scatter of all the face images and to improve the face recognition performance. Belhumeur and Kriegman [79] presented that the convex illumination cone can be formed using an object which is having a convex and Lambertian surface illuminated at same and different viewpoints simultaneously. The dimensions for this kind of illumination cone is the number of different surface normals.

Pan et al. [80] proposed a new approach for face recognition using hyper-spectral face images. Gao and Leung [81] presented a face recognition algorithm using line edge map. Lee et al. [82] gives a novel approach for face recognition using face images acquired with a configuration of nine directions of light sources. Chen et al. [83] proposed an illumination invariant face recognition by proving the discriminative functions are not illumination invariant even for Lambertian objects. Zhao and Chellappa [84] proposed a novel approach for illumination invariant face recognition using the symmetric properties of shape from shading.



### **2.3.1 Issues addressed in face recognition system**

Face is one of the most widely used biometric in security systems. Despite its wide usage, face recognition is not a fully solved problem due to the challenges associated with varying illumination conditions. Government of Andhrapradesh has issued around 22 million ration cards in which there are few ration cards created in an unauthorized manner in order to mislead the benefits of beneficiaries. The issue related to de-duplication of face photograph images is also addressed in this thesis. We propose a method for de-duplication of face photographs based on color histograms.

The illumination while capturing the face photographs plays an important role especially in out-door environment in the process of unique identity creation using de-duplication process. The issue of illumination invariant face recognition is addressed in this thesis. A new method is proposed for face recognition to address the issue of non-uniform illumination using convolutional neural networks (CNN). The symmetry of facial information is exploited to improve the performance of the face recognition system by considering the horizontal reflections of facial images.

## **2.4 SUMMARY**

This chapter reviewed some of the existing approaches to biometric recognition system, namely, iris recognition system, fingerprint recognition system and face recognition system. Different steps involved in iris recognition system and the related work is briefly described. Also, the existing approaches for all the components of fingerprint and face recognition systems are reviewed. Some research issues arising out of the review of existing methods are identified, which are addressed in this thesis.

## CHAPTER 3

# IRIS CLASSIFICATION BASED ON SPARSE REPRESENTATIONS USING DICTIONARY LEARNING FOR LARGE-SCALE IRIS DE-DUPLICATION APPLICATIONS

Various government sectors in the world provide different services and welfare schemes for the benefit of the people in the society. For instance, Government of India provides different services and welfare schemes for the benefit of the people in the society. Some of these services include issuance of birth certificate, voter identity card, driving license, and passport etc. Also, welfare schemes like targeted public distribution system (TPDS), national rural employment guarantee system (NREGS), health insurance, old age pensions etc. for the economic and social upliftment of the people. A unique identity (UID) number assigned for every citizen would obviate the need for a person to produce multiple documentary proofs of his/her identity for availing any Government service, or private services like opening of a bank account.

De-duplication of biometrics plays a key role in providing unique identity of a person. De-duplication is the process of removing instances of multiple enrollments by the same person using the person's biometric data. As the number of people enrolled into the biometric system runs into billions, the time complexity increases in the de-duplication process while creating a unique identity for every individual. There is a need for biometric de-duplication architecture which is scalable in large-scale databases.

This chapter is organized as follows: Introduction for iris classification is explained

in Section 3.1. Section 3.2 describes the motivation for the proposed iris classification approach by illustrating the complexity involved in de-duplication of large scale iris databases. Section 3.3 gives the details of sparse representation and on-line dictionary learning. In Section 3.4, the proposed iris classification and adjudication framework is presented. Experimental results of the proposed classification and adjudication framework are given in Section 3.5.

### **3.1 IRIS CLASSIFICATION FOR LARGE-SCALE DE-DUPLICATION APPLICATIONS**

De-duplication of iris biometrics is not scalable while creating a unique identity for every individual among the large population. The scalability issues can be addressed using the iris classification approach in order to speed up the de-duplication process. Few researchers already explored iris classification techniques based on hierarchical visual codebook [85], block-wise texture analysis [86] and color information [87]. So far, there are no approaches for classification of iris images based on the pre-defined iris classes in the existing work. In this chapter, we propose an iris classification based on sparse representation of Gabor features using on-line dictionary learning (ODL). Three different iris classes based on iris fiber structures, namely, stream, flower, jewel and shaker, are used for faster retrieval of identities in large-scale de-duplication applications.

### **3.2 ARCHITECTURE OF IRIS DE-DUPLICATION SYSTEM**

During de-duplication process, matching the biometrics of a person is done against the biometrics of other persons to ensure that the same person is not enrolled more than once. This will ensure that each person will have a unique identity. The de-duplication complexity is demonstrated using two different enrollment scenarios, namely, enrollment using a centralized manner and enrollment using a decentralized manner which

are discussed in the following subsections.

### **3.2.1 Enrollment using a centralized iris de-duplication system**

The enrollment in a centralized iris de-duplication system matches the irises of a person against the irises of all the existing enrolled persons. If there is match found, the person will not be enrolled into the system. In order to illustrate the time complexity of the centralized iris de-duplication system, an example considered for 200 million already enrolled persons where a new person waiting for the enrollment. Also, there is an assumption that the system uses 10 blade servers with a total iris comparison capacity of 200 million per second. The number of iris matches performed for different iris images and the time taken for the matching process is shown in the Table 3.1.

In the first scenario, the time taken for matching a single iris against the corresponding iris of the previously enrolled persons is 1 second and the number of matches are 200 million. In the second scenario, the 2 irises of persons are matched against the respective irises of all the previously enrolled persons and observed that the time complexity and comparisons are increased 2 times. In the third scenario, the comparisons are done in a cross comparison manner which means all the 2 irises are matched against all the irises of all the previously enrolled persons. It is observed that the number of comparisons and the time taken for matching are increased to 4 times.

### **3.2.2 Enrollment using a de-centralized iris de-duplication system**

In the case of enrollment using a decentralized manner, the biometrics of persons captured during a certain period have to be matched against the unique identity enrollment database of all the previously enrolled persons. The matching has to be done by aggregating the data from each of the decentralized enrollment stations and matching against the de-duplicated biometrics of all the previously enrolled persons. To illustrate the complexity of a decentralized de-duplication system, let us consider a case where 200 million persons have already been enrolled, and data of 1 million

**Table 3.1:** Complexity of a centralized iris de-duplication system

	Scenario	Number of Matches (millions)	Time (seconds)
1	If 1 iris (say left iris) is matched against all left eyes of previously enrolled persons	200	1
2	If 2 irises are matched against the respective irises of all the previously enrolled persons	400	2
3	If 2 irises are matched against 2 irises of all the previously enrolled persons	800	4

persons has been aggregated from the enrollment stations. The data of the 1 million persons will have to be matched against the 200 million persons to avoid multiple enrollments. Also, it is assumed that there are 10 blade servers with a total matching capacity of 200 million per second. The number of iris matches across different irises to be performed and the time taken for matching the irises is shown in the Table 3.2.

In the first scenario, the time taken for matching a single iris against the corresponding iris of the previously enrolled persons is 11.57 days and the number of matches are 200 trillion. In the second scenario, the 2 irises of person are matched against the respective irises of all the previously enrolled persons and observed that the time complexity and comparisons are increased around 2 times. In the third scenario, the comparisons are done in a cross comparison manner which means all the 2 irises are matched against all the irises of all the previously enrolled persons. It can be observed that the time complexity and the comparisons are increased around 4 times.

**Motivation behind this work:** The state government of Andhrapradesh [33] in India undertake the responsibility to identify the eligible households/beneficiaries and issue a ration card which enables them to avail the prescribed quantity of food grains and/or other commodities. Households can get the government benefits based on their

**Table 3.2:** Complexity of a de-centralized iris de-duplication system

	Scenario	Number of Matches (trillions)	Time (days)
1	If 1 iris (say left iris) is matched against all left eyes of previously enrolled persons	200	11.57
2	If 2 irises are matched against the respective irises of all the previously enrolled persons	400	23.15
3	If 2 irises are matched against 2 irises of all the previously enrolled persons	800	46.30

annual income as part of the targeted public distribution system (TPDS). Identification of eligible beneficiaries and ensuring delivery of food grains and other commodities to them effectively and efficiently is the main goal of TPDS. The government sectors in India also incur a huge expenditure on food subsidy to meet the difference between the economic cost of food grains and the issue price fixed for TPDS. A study done by *planning commission of India* (2005) has indicated that about 58% of the subsidized food grain allocated by the central government to the states/union territories does not reach the beneficiaries because of identification errors and non transparent operations in the implementation of TPDS.

Government of Andhrapradesh [33] undertook the de-duplication of ration cards using 52 million people iris codes, in order to ensure that the benefits under various welfare programs reach the intended beneficiaries, prevent cornering of benefits by a few sections of people and minimize frauds. There are over 6.26 quadrillion (6,262,668,889,152,840) iris matches performed in de-centralized manner to remove duplicate enrollments in 61 days with high-end blade servers equipment which is not a scalable solution. This is the motivation for the proposed classification approach which reduces the search time drastically and provide the scalable de-duplication solutions.

The proposed de-duplication architecture is shown in Fig. 3.1. In the processing

stage, an iris image is segmented and normalized. Then iris templates are extracted using Gabor filters. The de-duplication engine or iris matcher improves the speed of de-duplication by adding multiple blade servers. All the enrolled iris templates are loaded into each blade server and the iris templates are compared in "1 : all" manner in  $N$  blade servers simultaneously. For example, if there are  $N$  query iris templates to be processed, then each query iris template goes to a blade server for de-duplication. If there are more than  $N$  query images, the delta of the iris templates keep on waiting in a queue till any of the blade servers are free. Increasing the blade servers is not an optimal solution, especially in large-scale iris databases. There should be another layer for iris classification to reduce the search space in the de-duplication engine. So, we propose an iris classification based on sparse representation of Gabor features using on-line dictionary learning (ODL). Also, an iris adjudication process is done by comparing the matched iris-pair images side-by-side to know the confidence-level on the matching score based on color coding.

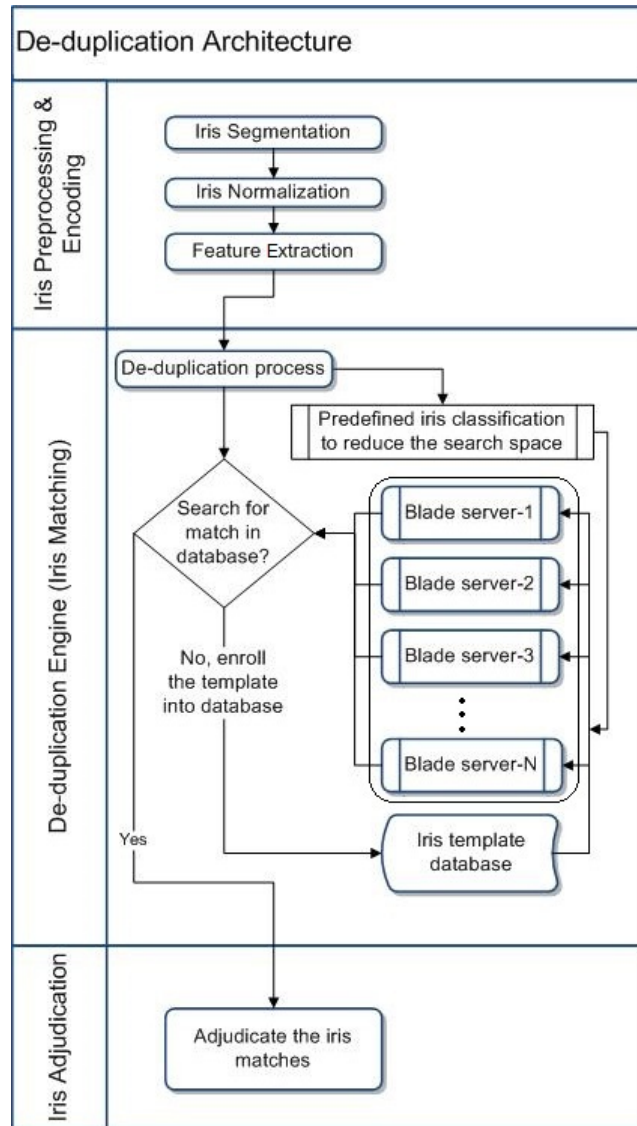


**Fig. 3.1:** Iris de-duplication architecture

### 3.3 SPARSE REPRESENTATION AND DICTIONARY LEARNING

Sparse representation has received a lot of attention from researchers in signal and image processing. Sparse coding involves the representation of an image as a linear combination of some atoms in a dictionary [88]. It is a powerful tool for efficiently representing data in non-traditional ways. This is mainly due to the fact that signals and images of interest tend to enjoy the property of being sparse in some dictionary. These



dictionaries are often learned directly from the training data. Several algorithms like on-line dictionary learning (ODL) [89],  $K$ -SVD [90] and method of optimal directions (MOD) [91] have been developed to process training data. Sparse representation is used to match the input query image with the appropriate class. Etemand and Chelappa [92] proposed a linear discriminant analysis (LDA) based selection and feature extraction algorithm for classification using wavelet packets. In [93], a method for simultaneously learning a set of dictionaries that optimally represent each cluster is proposed. This approach was later extended by adding a block incoherence term in their optimization problem to improve the accuracy of sparse coding. Recently, similar algorithms for simultaneous sparse signal representation have also been proposed [94], [95]. An on-line dictionary learning based on sparse representation is used for classification of images. For a given  $N$  number of classes, we design  $N$  dictionaries to represent the classes. Each image associated with a dictionary provides the best sparsest representation. For every image in the given set of images  $\{y_i\}_{i=1}^n$ , on-line dictionary learning is used to seek the dictionary  $D$  that has the sparsest representation for the image. We define  $l(\hat{\mathbf{D}}, \hat{\Phi})$  as the optimal value of the  $l_1$ -lasso sparse coding problem [96]. This is accomplished by solving the following optimization problem:

$$l(\hat{\mathbf{D}}, \hat{\Phi}) = \arg \min_{\mathbf{D}, \Phi} \frac{1}{N} \sum_{i=1}^N \frac{1}{2} \|\mathbf{Y}_i - \mathbf{D}\Phi_i\|_2^2 \text{ subject to } \|\Phi_i\|_1 \leq \lambda, \quad (3.1)$$

where  $Y$  is the matrix whose columns are  $y_i$  and  $\lambda$  is the sparsity parameter.  $D$  denotes the learned dictionary,  $\Phi$  represents the sparse representation vectors,  $N$  denotes the number of classes and  $Y$  represents the training database. The online dictionary learning algorithm alternates between sparse coding and dictionary update steps. Several efficient pursuit algorithms have been proposed in the literature for sparse coding [91], [97]. The simplest one is the  $l_1$ -lasso algorithm [96]. Main advantage with on-line dictionary learning algorithm is its computational speed as it uses  $l_1$ -lasso algorithm for sparse representation. In sparse coding step, dictionary  $D$  is fixed and representation vectors  $\Phi_i$  are identified for each example  $y_i$ . Then, the dictionary is updated atom by atom in an efficient way.

### 3.4 PROPOSED IRIS CLASSIFICATION AND ADJUDICATION FRAMEWORK

The proposed iris classification approach uses three different classes of iris images [98], namely, stream, flower, and jewel-shaker as illustrated in Fig. 3.2. The iris structure can be determined by the arrangement of white fibers radiating from the pupil. In stream iris structure, these fibers are arranged in regular and uniform fashion. The arrangement of fibers is irregular in the flower iris structure. In jewel iris structure, the fibers have some dots. The shaker iris structure have both the characteristics of flower and jewel iris structures. The arrangement of iris fibers are illustrated in Fig. 3.3.

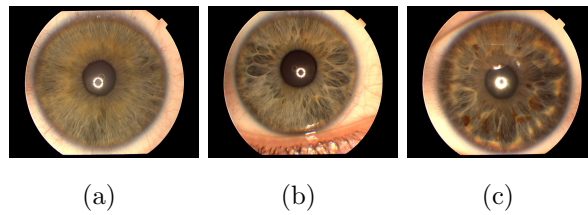


**Fig. 3.2:** Iris classes: (a) stream, (b) flower and (c) jewel-shaker structures.

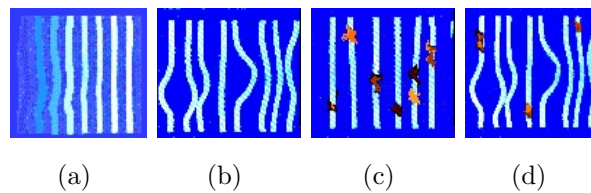


**Fig. 3.3:** Iris fibers: (a) stream, (b) flower, (c) jewel and (d) shaker.

The following are the steps involved in the proposed iris classification and adjudication framework:

**Step 1:** *Iris segmentation and normalization* : The pupillary and limbic boundaries

[12] of an iris image are approximated as circles using three parameters: the radius  $r$ , and the coordinates of the center of the circle,  $x_0$  and  $y_0$ . The integrodifferential operator [9] used for iris segmentation is:

$$\max(r, x_0, y_0) G_\sigma(r) * \frac{\partial}{\partial r} \int_{r, x_0, y_0} \frac{I(x, y)}{2\pi r} ds, \quad (3.2)$$

where  $G_\sigma(r)$  is a smoothing function and  $I(x, y)$  is the image of the eye.

After applying the operator, the resultant segmented iris image is as shown in Fig. 3.4. The segmented iris image is then converted to a dimensionless polar coordinate system based on the Daugman Rubber Sheet model [9] as shown in Fig. 3.5.

**Step 2:** *Feature extraction* [12]: The feature vector of size  $240 \times 20$  is extracted from the normalized iris image of size  $120 \times 20$ . The resultant feature vector is converted to a single column vector by column major ordering. From each class, the training iris images are selected to express as a linear weighted sum of the feature vectors in a dictionary belonging to three different classes of iris.

**Step 3:** *Iris classification using ODL*: An on-line dictionary learning (ODL) algorithm is used to classify the iris data into three different classes to reduce the search space. The weights associated with feature vectors in the dictionary are evaluated using ODL algorithm, which is a solution to  $l_1$  optimization for over-determined system of equations. The feature vectors which belong to a particular iris class carry significant weights which are maximum of non-zero values.

The class  $C = [C_1, \dots, C_N]$  consists of training samples collected directly from the image of interest. In the proposed sparsity model, images belonging to the same class are assumed to lie approximately in a low dimensional subspace. Let  $N$  be the training classes, the  $p^{\text{th}}$  class has  $K_p$  training images  $\{y_i^N\} \ i=1, \dots, K_p$  and  $b$  be an image belonging to the  $p^{\text{th}}$  class which is represented as a linear

combination of these training samples:

$$b = \mathbf{D}^p \Phi^p, \quad (3.3)$$

where  $\mathbf{D}^p$  is a dictionary of size  $m \times K^p$ , whose columns are the training samples in the  $p^{\text{th}}$  class and  $\Phi^p$  is a sparse vector.

The following are the steps involved in the proposed classification method:

1. *Dictionary construction:* Construct the dictionary for each class of training images using on-line dictionary learning algorithm [89]. Then, the dictionaries  $D = [D_1, \dots, D_N]$  are computed using the equation:

$$(\hat{\mathbf{D}}_i, \hat{\Phi}_i) = \arg \min_{\mathbf{D}_i, \Phi_i} \frac{1}{N} \sum_{i=1}^N \frac{1}{2} \|\mathbf{C}_i - \mathbf{D}_i \Phi_i\|_2^2 + \lambda \|\Phi_i\|_1,$$

$$\text{satisfying } \mathbf{C}_i = \hat{\mathbf{D}}_i \hat{\Phi}_i, \quad i = 1, 2, \dots, N.$$

2. *Classification:* In this classification process, the sparse vector  $\Phi$  for given test image is found in the test dataset  $B = [b_1, \dots, b_t]$ . Using the dictionaries of training samples  $D = [D_1, \dots, D_N]$ , the sparse representation  $\Phi$  satisfying  $D\Phi=B$  is obtained by solving the following optimization problem:

$$\Phi^j = \arg \min_{\Phi} \frac{1}{2} \|\mathbf{b}_j - \mathbf{D}\Phi_j\|_2^2; \quad (3.4)$$

$$\text{subject to } \|\Phi_j\|_1 \leq T_1, \text{ and } \hat{i} = \arg \min_i \|\mathbf{b}_j - \mathbf{D}\delta_i(\Phi^j)\|_2^2, \quad \mathbf{j} = 1, \dots, t.$$

where  $\delta_i$  is a characteristic function that selects the coefficients. Then  $b_j$  is assigned to  $C_i$  associated with the  $i^{\text{th}}$  dictionary. It means, finding the sparsest dictionary for a given test data using  $l_1$ -lasso algorithm. Then, test data is assigned to the class associated with this sparsest dictionary.

**Step 4:** *Iris adjudication:* The matched iris pairs are compared using the adjudication process to illustrate the match-ability of iris images based on the similarity of iris

regions marked with three different colors, namely, green, yellow and red. The green, yellow and red colors indicate good, poor and bad match, respectively. The normalized iris image is divided into different regions and the confidence-level of matching for each region is verified and assigned a color code using the dissimilarity measurement.

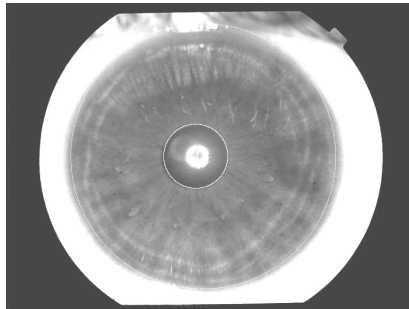


**Fig. 3.4:** Iris image segmentation



**Fig. 3.5:** Normalized iris image

### 3.5 EXPERIMENTAL RESULTS

To enable the effective test of the proposed classification strategy, three standard iris image databases are used, namely, CASIA1 database [99], IITD iris database [100], [101], and UPOL iris database [102], [103], [104].

The CASIA database is by far the most widely used for iris biometric purposes. However, its images incorporate few types of noise, related with eyelid and eyelash obstruction. The database consists of 108 subjects, three instances of left iris and four instances of right iris are collected from each subject. So, there is a total of 756 iris images in the database, all are having the image dimensions  $320 \times 280$  gray-scale images. For testing, 216 iris images are used and the remaining iris images are used for training.

The IITD iris database consists of 224 subjects' data, both left and right iris images. There are 10 instances for each iris image. So, there is a total of 2,232 iris images in the database, all are having the image dimensions  $320 \times 280$  gray-scale images.

The UPOL [104] iris data is collected from 64 subjects, with three samples each of left and right eyes from each subject resulting in a total of 384 iris images. Each iris image is of 24 bit RGB color space with a high resolution image size,  $768 \times 576$ . The images were captured using the optical device (TOPCON TRC50IA) which is connected to a Sony DXC-950p 3CCD camera.

Experiments are performed using the following iris classification approaches:

Approach-1: SVM-4Class-PCA-Kmeans

Approach-2: ODL-4Class-PCA-Kmeans

Approach-3: SVM-3Class-IrisFibers

Approach-4: ODL-3Class-IrisFibers

The results of the above approaches are compared and explained as follows to demonstrate the efficacy of the proposed classification approach in the iris de-duplication architecture.

**Approach-1. SVM-4Class-PCA-Kmeans classification:** This classification approach uses the support vector machine (SVM) as a classifier. The classes are defined by applying the  $k$ -means clustering on the iris feature vectors whose dimensions are reduced to a size by considering the 100 principle components using principle component analysis (PCA). This approach is applied on three standard iris databases, where  $\frac{2}{3}$  rd of the each database is used for training and remaining data is used for testing.

**Approach-2. ODL-4Class-PCA-Kmeans classification:** In this classification approach, the sparsity-based on-line dictionary learning (ODL) is used as a classifier. The  $k$ -means clustering is applied to define the classes on the iris feature vectors whose

dimensions are reduced by considering the 100 principle components using PCA. This approach is applied on three standard iris databases, where  $\frac{2}{3}$   $rd$  of the each database is used for training and remaining data is used for testing.

**Approach-3. SVM-3Class-IrisFibers classification:** This classification approach uses SVM as a classifier. The classes are defined by manual labeling of three iris categories [98] using the iris fiber structures. This approach is applied on UPOL standard iris database, where  $\frac{2}{3}$   $rd$  of the database is used for training and remaining data is used for testing.

**Approach-4. ODL-3Class-IrisFibers classification:** Sparsity-based on-line dictionary learning (ODL) is used in this iris classification approach. This classification approach is used in the proposed iris de-duplication framework. The classes are defined by manual labeling of three iris categories using the iris fiber structures. The experiments are conducted on UPOL standard iris database, where  $\frac{2}{3}$   $rd$  of the database is used for training and remaining data is used for testing.

**Experiment-1** In iris classification approaches 1 and 2, the experiments are conducted using the three databases, namely, CASIA1, IITD and UPOL iris databases with template sizes  $120 \times 20$ . Four classes are identified using  $k$ -means clustering algorithm using the correlation-based distance metric. Table 3.5 describes the details of the number of images in each class and in three different databases.

**Table 3.3:** Iris classes defined based on  $k$ -means clustering and PCA

# of Images in	CASIA1	IITD	UPOL
Class-1	196	525	81
Class-2	203	500	114
Class-3	196	595	69
Class-4	161	580	120

The experimental results are illustrated as shown in Fig. 3.6. It is observed that the *ODL-4Class-PCA-Kmeans* classification approach gives better classification performance due to the effectiveness of sparsity.

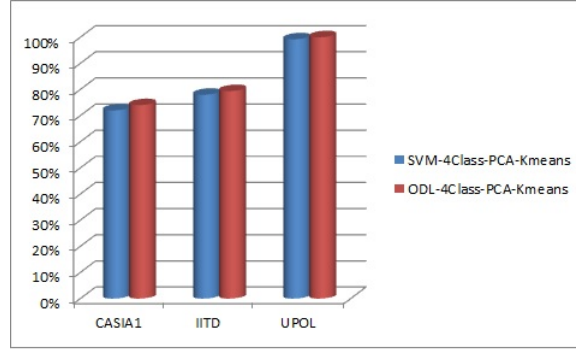


**Fig. 3.6:** Experimental results for the classification approaches *SVM-4Class-PCA-Kmeans* and *ODL-4Class-PCA-Kmeans* for the three iris databases namely, CASIA1, IITD and UPOL

**Experiment-2** In iris classification approaches 3 and 4, the experiments are conducted using the UPOL iris database with template sizes  $240 \times 20$ . Three classes are manually identified in these proposed iris classification approaches using the iris patterns stream, flower and jewel-shaker as shown in Table 3.5. In this experiment, the other two databases are excluded as it was difficult to mark the class labels due to the less clarity to manually identify the iris fiber structures.

The experimental results for the UPOL database are compared using SVM and ODL and illustrated as shown in Fig. 3.7. It is observed that the classification accuracy is better in the ODL-related classification approaches.

**Detailed analysis on the proposed classification approach : ODL-3Class-IrisFibers** In order to evaluate the performance of proposed classification approach using on-line dictionary learning, the database is split into three sets: training set, testing set and validation set. The distribution of all the three sets are taken in such a way that the 2 samples of each iris image is allotted to the training set and validation set, and the remaining iris sample is given to the test set. The training set consists of



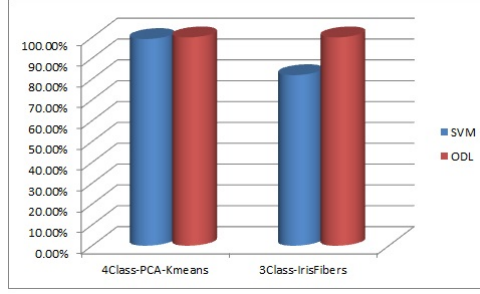


**Fig. 3.7:** Experimental results for all the proposed classification approaches on UPOL iris database

**Table 3.4:** Iris classes based on the iris fibers Stream, Flower and Jewel-Shaker

Class	# of images (%)	Subject Ids
Class-1 (Stream)	192 (50%)	001,006,007,008,011, 013,014,016,018,019, 020,021,023,024,026, 027,028,033,041,042, 044,045,050,051,052, 053,058,059,060,061, 062,064
Class-2 (Flower)	102 (26.56%)	002,009,010,015,017, 022,031,036,037,040, 043,047,048,049,054, 056,063
Class-3 (Jewel-Shaker)	90 (23.44%)	003,004,005,012,025, 029,030,032,034,035, 038,039,046,055,057

224 images where 112 images are from Class-1 (Stream), 60 images are from Class-2 (Flower) and 52 images are from Class-3 (Jewel-Shaker). The number of test images selected from Class-1, Class-2 and Class-3 are 64, 34 and 30, respectively. A set of 32 iris images is assigned to validation set where 16 images belong to Class-1, 8 images belong to Class-2 and 8 images belong to Class-3.

The experiments were conducted in three different ways of choosing test sets (systematically selecting first, second or third samples of each iris) where the performance is almost similar. The classification performance is shown in Tables 3.5, 3.5 and 3.5,

for the test data set with different dictionary sizes 60, 90 and 120, respectively.

**Table 3.5:** Classification performance (in %) on test data set for dictionary size = 60

Class	Residual Parameter		
	0.5	<b>0.05</b>	0.005
Class-1 (Stream)	90.5	<b>97</b>	93.83
Class-2 (Flower)	91.18	<b>94.12</b>	88.2
Class-3 (Jewel-Shaker)	100	<b>100</b>	100

**Table 3.6:** Classification performance (in %) on test data set for dictionary size = 90

Class	Residual Parameter		
	0.5	<b>0.05</b>	0.005
Class-1 (Stream)	95	<b>100</b>	98.5
Class-2 (Flower)	94.12	<b>100</b>	97.06
Class-3 (Jewel-Shaker)	100	<b>100</b>	100

**Table 3.7:** Classification performance (in %) on test data set for dictionary size = 120

Class	Residual Parameter		
	0.5	<b>0.05</b>	0.005
Class-1 (Stream)	95	<b>100</b>	98.5
Class-2 (Flower)	91.18	<b>100</b>	96.06
Class-3 (Jewel-Shaker)	100	<b>100</b>	100

In Table 3.5, the classification accuracy for the validation data set is given. It is observed that 100% classification accuracy is achieved for the dictionary sizes, 90 and 120 with residual error value 0.05 as shown in Fig. 3.8. The confusion matrix for both test data and validation data sets are shown in Table 3.5.

The adjudication results for genuine iris matches are illustrated in Fig. 3.9 and for the impostor iris matches are given in Fig. 3.10. The normalized images shown

**Table 3.8:** Classification performance on validation data set for dictionary sizes 60, 90 and 120

Class	Dictionary Sizes		
	60	<b>90</b>	120
Class-1 (Stream)	91.66	<b>100</b>	100
Class-2 (Flower)	100	<b>100</b>	100
Class-3 (Jewel-Shaker)	100	<b>100</b>	100

**Table 3.9:** Confusion matrix for both test data and validation iris data sets

Class	Testing set			Validation set		
	C1	C2	C3	C1	C2	C3
C1	64	0	0	16	0	0
C2	0	34	0	0	8	0
C3	0	0	30	0	0	8

on these figures are taken from CASIA database for better illustration of adjudication process.

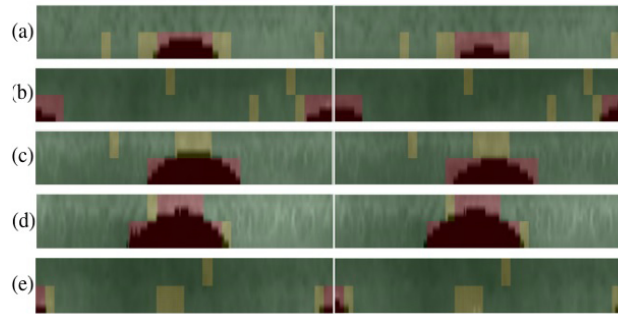


**Fig. 3.9:** Iris adjudication: side-by-side comparison of genuine iris matches with hamming distances (a) 0.21, (b) 0.19, (c) 0.16, (d) 0.15, (e) 0.19

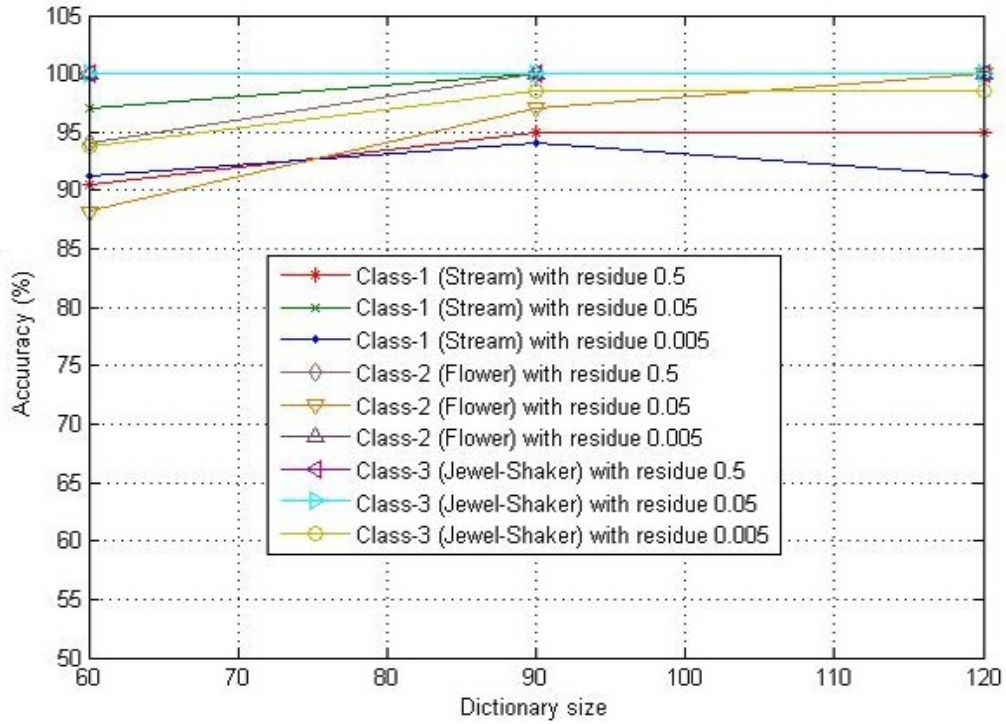


**Fig. 3.8:** Classification accuracy for three different dictionary sizes 60, 90 and 120

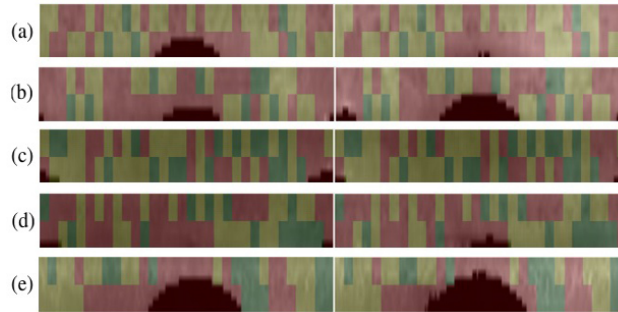


**Fig. 3.10:** Iris adjudication: side-by-side comparison of impostor iris matches with hamming distances (a) 0.48, (b) 0.46, (c) 0.43, (d) 0.51, (e) 0.37

### 3.6 SUMMARY

In this chapter, an iris classification is proposed based on sparse representation of Gabor features using on-line dictionary learning (ODL) for large-scale de-duplication applications. Three different iris classes based on iris fiber structures, namely, stream,

flower, jewel and shaker, are used for faster retrieval of identities. Also, an iris adjudication process is illustrated by comparing the matched iris-pair images side-by-side to make the decision on the identification score using color coding. The efficacy of the proposed classification approach is demonstrated on the standard iris database, UPOL, and it is achieved 100% classification accuracy with dictionary size 90 and residual error 0.05. It is evident that the proposed iris de-duplication architecture can improve the performance of de-duplication process in real time applications.

## CHAPTER 4

# DE-NOISING SLAP FINGERPRINT DATA FOR ACCURATE FINGERPRINT SEGMENTATION IN LARGE-SCALE DE-DUPLICATION APPLICATIONS

This chapter focuses on the accuracy of fingerprint de-duplication in de-centralized architecture. Fingerprint images can have some noisy data while capturing them using slap fingerprint scanners. This noise causes improper slap fingerprint segmentation. The de-duplication requires the plain quality fingerprints. While doing the segmentation of slap fingerprints, some of the fingerprint images might be improperly segmented because of the noise present in the data. As a result, the de-duplication accuracy will be decreased. In this chapter, an attempt is made to remove the noise present in the data using binarization of slap fingerprint image, and region labeling of desired regions with 8-adjacency neighborhood. The distinct feature of this technique is to remove the noise present in the data for accurate slap fingerprint segmentation as well as improve the de-duplication accuracy.

Also, due to the increasing demand for fingerprint biometrics, new fingerprint scanners are being deployed for scanning fingerprint images and the old fingerprint scanners are being frequently upgraded. The user enrollment is very expensive and time-consuming especially in large scale de-duplication applications. However, upgrading with new fingerprint scanners for cross-sensor matching where the test fingerprint data is verified with the data enrolled with different fingerprint scanner often lead to reduced fingerprint matching performance. In this chapter, a new sensor adaptation algorithm is proposed for fingerprint biometrics using kernel transformation learning

in order to improve the fingerprint matching performance.

This chapter is organized as follows: Introduction for fingerprint de-duplication system is explained in Section 4.1. Section 4.2 describes the motivation for the proposed fingerprint matching and de-noising algorithms by illustrating the complexity involved in de-duplication of large scale fingerprint databases. Section 4.3 gives the details of noise removal method for slap fingerprint image segmentation. In Section 4.4, the proposed sensor adaptation algorithm in kernel space is presented. Experimental results of the proposed fingerprint matching and de-noising algorithms are given in Section 4.5.

#### 4.1 FINGERPRINT DE-DUPLICATION SYSTEM

The de-duplication process of fingerprint images is presented in the context of targeted public distribution system (TPDS). The TPDS is a mechanism for ensuring access and availability of food grains and other essential commodities at subsidized prices to the households. Identification of eligible beneficiaries and ensuring delivery commodities to them effectively and efficiently is the basic challenge for TPDS. The major goal of the TPDS process to find the duplicate identities by using fingerprint de-duplication.

A fingerprint [34] consists of ridges and valleys on the surface of the finger. The uniqueness of a fingerprint can be determined by the minutiae points. Minutiae points are the local ridge features which are identified by a ridge bifurcation or a ridge ending. One way of acquiring fingerprints is to capture the slap fingerprint. Slap fingerprints are taken by pressing four fingers simultaneously onto a slap fingerprint scanner. In general, the capturing process will take place in the fashion of 4-4-2 fingers, means capture left four fingers at one time, followed by all right four fingers and then followed by two thumb fingers. The captured slap fingerprints go for the slap fingerprint segmentation [35] which splits the individual fingers from the slap image. The left four fingers slap can be segmented as in the sequence of left little (LL), left ring (LR), left middle (LM) and left index (LI). The right four fingers slap can be segmented as in the

sequence of right index (RI), right middle (RM), right ring (RR) and right little (RL). The two thumb fingers can be segmented as left thumb (LT) and right thumb (RT). The finger positions are the position codes defined in Table 12 of ANSI/NIST-ITL 1-2007 [36].

As part of the targeted public distribution system in India, a total of 1.8 million (approximately) slap fingerprint images of 0.6 million (approximately) citizens are collected to provide the household cards. To capture slap fingerprint images, TP-LSMULTI-4100 fingerprint scanner is used. This device has inbuilt real time feedback on the quality of the slap fingerprints being captured. However, the slap fingerprint images have some noisy data due to some external factors which affect the calibration process of the fingerprint device. All the captured slap fingerprints undergo slap fingerprint segmentation which is given by a third party vendor. In the process of slap fingerprint segmentation, 22% of the total slap fingerprint images are improperly segmented because of noise present in the data. Moreover, the noise present in the slap fingerprint images are segmented as individual fingers instead of splitting the actual finger.

## **4.2 DE-DUPLICATION COMPLEXITY OF FINGERPRINT DATA**

De-duplication is the processing of the biometric data of citizens to remove instances of multiple enrollments by the same citizen. During de-duplication, matching the biometrics of a citizen is done against the biometrics of other citizens to ensure that the same person is not enrolled more than once. This will ensure that each person will have a unique identity. De-duplication will be a necessary component in the targeted public distribution system. De-duplication complexity is discussed in the context of the two different enrollment scenarios which are given below.



#### **4.2.1 Enrollment using a centralized fingerprint de-duplication system**

The enrollment in a centralized fingerprint de-duplication system matches the fingerprints of a person against the fingerprints of all the existing enrolled persons. If there is match found, the person will not be enrolled into the system. In order to illustrate the time complexity of the centralized fingerprint de-duplication system, an example considered for 200 million already enrolled persons where a new person waiting for the enrollment. Also, there is an assumption that the system uses 10 blade servers with a total fingerprint comparison capacity of 5 million per second. The number of fingerprint matches performed for different fingerprint images and the time taken for the matching process is shown in the Table 4.1.

In the first scenario, the time taken for matching a single fingerprint against the corresponding fingerprint of the previously enrolled persons is 40 seconds and the number of matches are 200 million. In the second scenario, the 10 fingerprints of citizen are matched against the respective fingerprints of all the previously enrolled citizens. It is observed that the time complexity of de-duplication and the number of comparisons are increased 10 times. In the third scenario, the comparisons are done in a cross comparison manner where all the 10 fingerprints are matched against all the fingerprints of all the previously enrolled citizens. It is observed that the time complexity of de-duplication and the number of comparisons are increased 100 times.

#### **4.2.2 Enrollment using a decentralized fingerprint de-duplication system**

In the case of enrollment using a decentralized manner, the biometrics of citizens captured during a certain period have to be matched against the unique identity enrollment database of all the previously enrolled citizens. The matching has to be done by aggregating the data from each of the decentralized enrollment stations and matching against the de-duplicated biometrics of all the previously enrolled citizens. To illustrate the complexity of a decentralized de-duplication system, let us consider a case where 200 million citizens have already been enrolled, and data of 1 million

**Table 4.1:** Complexity of centralized fingerprint de-duplication system

	Scenario	Number of Matches (millions)	Time taken (seconds)
1	If 1 finger (say left thumb) is matched against all left thumbs of previously enrolled persons	200	40
2	If all 10 fingers are matched against the respective fingers of all the previously enrolled persons	2000	400
3	If all the 10 fingers are matched against all the fingers of all the previously enrolled persons	20000	4000

citizens has been aggregated from the enrollment stations. The data of the 1 million citizens will have to be matched against the 200 million citizens to avoid multiple enrollments. The assumption to assess the de-duplication complexity, we assume 10 blade servers with a total matching capacity of 5 million per second. The number of fingerprint matches across different fingerprints to be performed and the time taken for matching the fingerprints is shown in the Table 4.2.

In the first scenario, the time taken for matching a single fingerprint against the corresponding fingerprint of the previously enrolled persons is 463 days and the number of matches are 200 trillion. In the second scenario, the 10 fingerprints of citizen are matched against the respective fingerprints of all the previously enrolled citizens. It is observed that the time complexity of de-duplication and the number of comparisons are increased 10 times. In the third scenario, the comparisons are done in a cross comparison manner where all the 10 fingerprints are matched against all the fingerprints of all the previously enrolled citizens. It is observed the time complexity of de-duplication and the number of comparisons are increased 100 times.

**Table 4.2:** Complexity of de-centralized fingerprint de-duplication system

	Scenario	Number of Matches (trillions)	Time taken (days)
1	If 1 finger (say left thumb) is matched against all left thumbs of previously enrolled persons	200	463
2	If all 10 fingers are matched against the respective fingers of all the previously enrolled persons	2000	4630
3	If all the 10 fingers are matched against all the fingers of all the previously enrolled persons	20000	46300

### 4.3 NOISE REMOVAL METHOD FOR SLAP FINGERPRINT IMAGE SEGMENTATION

The noise removal method uses the noisy slap images. Fig. 4.1 represents the sample noisy four-finger slap image which has the dimensions of 500dpi resolution and 1600×1500 image size. Generally, images are two-dimensional arrays of bytes which represent pixels. Each pixel has a grey-scale value which is ranging from 0 to 255. The low grey-scale values represent darker shades and the high grey-scale values represent lighter shades.

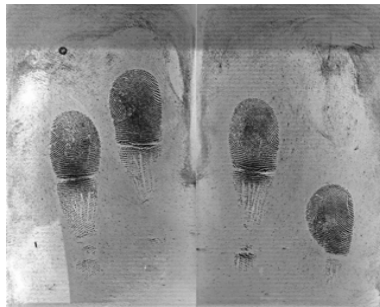


**Fig. 4.1:** Noisy slap fingerprint image

The approach to noise removal process is as follows:

1. Binarization of slap image.
2. Foreground and background segmentation of slap image.
3. Resampling and region labeling of slap image with 8-adjacency neighborhood.
4. Reconstruction of the original data for the larger labeled regions of the slap image.

In the following subsections, each of the above steps is explained in detail:

#### **4.3.1 Binarization of slap image**

Image binarization is a method of replacing the pixel grey-scale values with a '0' if the pixel grey-scale value is less than the threshold value and replace the pixel grey-scale value with a '255' if the pixel grey-scale value is greater than or equal to the threshold value. Most of the noise which is formed due to the device calibration problem has grey-scale values ranging from 50 to 255. These grey-scale values are replaced with 255 in a way which is similar to binarization. The histogram of the noisy slap fingerprint image is illustrated as shown in Fig. 4.2 This process of binarization is applied in two different phases: in the phase-I, the noise is medium and in phase-II, the noise is high. In the phase-I, the threshold is fixed as 100 (empirically) and the binarization process is carried out on the left over 22% of the slap fingerprint images in targeted public distribution system. In the phase-2, the remaining slap fingerprints images which could not be segmented in phase-I are treated as high noise slap fingerprint images. The threshold value for phase-II is fixed as 50 (empirically) and the binarization process is carried out on the remaining slap fingerprint images in phase-1. Experimental results are discussed in Section 4.5.

#### **4.3.2 Foreground and background segmentation of slap image**

In a fingerprint image, the background regions have a very low grey-scale variance value, whereas the foreground regions have a very high variance. In [38], a method

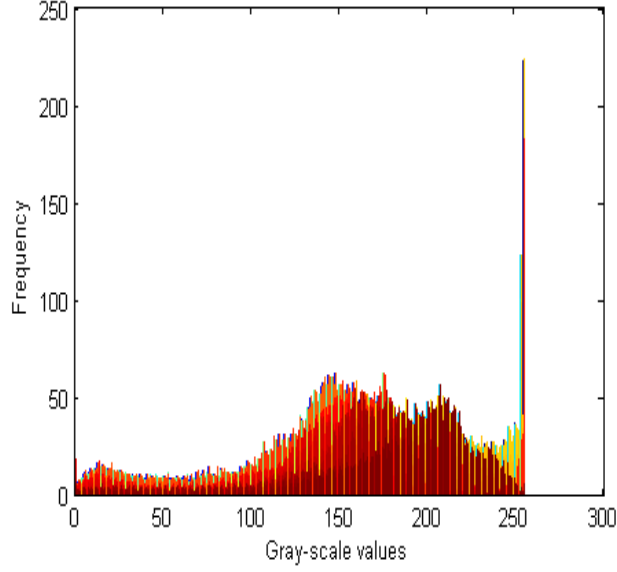


**Fig. 4.2:** Histogram of noisy slap image

based on variance threshold is used to perform the segmentation of foreground and background on the binarized slap fingerprint. In this method, the slap image is divided into blocks and the grey-scale variance is calculated for each block in the image. If the variance is less than the global threshold, then the block belongs to the background region; otherwise, it is assigned to be part of the foreground. The grey-level variance for a block of size  $W \times W$  is defined as:

$$V(k) = \left[ \frac{1}{W^2} \right] \sum_{r=0}^{W-1} \sum_{c=0}^{W-1} (I(r, c) - M(k))^2, \quad (4.1)$$

where  $V(k)$  is the variance for block  $k$ ,  $I(r, c)$  is the grey-level value at pixel  $(r, c)$ , and  $M(k)$  is the mean grey-level value for the block  $k$ . The resultant images are processed using a block size of  $16 \times 16$  and a variance threshold of 100 which gave better performance when compared to other thresholds.

### 4.3.3 Resampling and region labeling of slap image with 8-adjacency

The resultant slap image after separation of foreground and background is resampled to  $160 \times 150$  size to reduce the time complexity. The region labeling process starts with the resampled slap fingerprint image. A region in an image is called connected if any pixel in the region can be reached by moving from one neighboring pixel to the next. The pixels  $p$  and  $q$  are 8-adjacency [105] if  $q$  is in the set  $N_8(p)$ , where  $N_8(p) = \{N(p-1, q-1), N(p-1, q), N(p-1, q+1), N(p, q-1), N(p, q), N(p, q+1), N(p+1, q-1), N(p+1, q), N(p+1, q+1)\}$  and  $N(p, q)$  is the seed point or central pixel. The resultant images are scanned until a foreground pixel is found. An unlabeled foreground pixel is marked with a new label and its position is pushed on to a stack. While the stack is not empty, the pixels on the stack are marked with the label and the neighbor pixels are pushed on to the stack. When the stack is empty, the search continues for the next seed point for the region labeling process. Here, the starting label value is 1 and incremented for each and every next seed point. At the same time, one dimensional array of label count is calculated where the index of the array represents label number.

### 4.3.4 Reconstruction of the original data for the larger labeled regions

In the process of binarization, the slap image will lose some genuine data. In order to get the original data, select the labeled regions which have the count threshold greater than 15000 pixels (empirically) from the one dimensional array of label counts array. The threshold value is fixed empirically. The slap image is scanned until the larger region is found. Then, replace all the pixel values in the region identified by the same label value with the corresponding pixel value from the original image.

The proposed de-noising approach removes the noise present in the fingerprint data for accurate slap fingerprint segmentation as well as improve the fingerprint matching performance thereby the de-duplication accuracy. There are fingerprint matching performance issues while upgrading the fingerprint scanners with new ones for matching

cross-sensor fingerprint images. A framework is proposed to improve the fingerprint matching performance for cross-sensor adaptation using kernel learning which is discussed in next section.

#### 4.4 CROSS-SENSOR FINGERPRINT RECOGNITION USING KERNEL LEARNING

There is huge demand for fingerprint biometrics in civilian identity applications. The need for scanner upgradation and new scanners is essentially required to acquire quality fingerprints time-to-time. However, scanner upgradation might lead to performance degradation while comparing cross-sensor fingerprint images. A framework is proposed to improve the matching performance for cross-sensor adaptation [106] in two different phases. In the first phase, few training samples are selected from three different fingerprint scanners. These samples are used to learn the adaptation parameters from optimized kernel matrix using the initial kernel matrix calculated with similarity measures of all selected samples. A convex optimization problem is formulated to minimize the logDet divergence [107] between the initial kernel matrix and adapted kernel matrix. The sensor adaptation parameters are calculated by imposing the distance preserving constraints [108] and application-specific constraints. The distance constraints are chosen as 20<sup>th</sup> percentile of similar class distances and 85<sup>th</sup> percentile of dissimilar class distances. In the second phase, these parameters are incorporated while fingerprint matching in transformed domain. The steps involved in this framework are explained below:

**Step 1:** Initially, a similarity measurement matrix  $S$  is computed for all the training fingerprint images  $\mathbb{T} = \{I_1, I_2, \dots, I_N\}$  chosen equally from three different sensors.  $S(I_i, I_j)$  represents the  $(i, j)^{th}$  element in matrix  $S$  and it is the similarity measure between the fingerprint templates  $I_i$  and  $I_j$ .

**Step 2:** The similarity matrix is iteratively updated until convergence using kernel learning. For this, a convex optimization problem is formulated as,

$$K^A = \arg \min \zeta_l(K, S), \forall T \quad (4.2)$$

subject to the constraints  $C \geq d_u$ , for similar classes, and  $C \leq d_l$ , for dissimilar classes, where  $K^A$  is the adapted kernel matrix,  $\zeta_l$  is the logDet divergence,  $C = \zeta_e(\phi(I_i), \phi(I_i)) + \zeta_e(\phi(I_j), \phi(I_j)) - 2\zeta_e(\phi(I_i), \phi(I_j))$ ,  $d_u$  is the upper limit of same class distances and  $d_l$  is the lower limit of different class distances.  $\phi(I_i)$  represents the transformed fingerprint template of  $I_i$  and  $\zeta_e$  is the Euclidean distance between the transformed fingerprint templates.

**Step 3:** The adaptation parameters are calculated using the following formula:

$$\Sigma = (S)^{-1}(K^A - S)(S)^{-1}, \quad (4.3)$$

where each element in  $\Sigma$  is represented by  $\sigma_{ij}$  which have the contribution of  $(i, j)^{th}$  constraint imposed on kernel matrix  $K^A$ .

**Step 4:** These adaptation parameters are used for adapting the cross-sensor fingerprint properties (means, adaptation among the sensor-1, sensor-2 and sensor-3) in testing phase.

$$K^A(I_{s1}, I_{s2}) = S(I_{s1}, I_{s2}) + \sum_{ij} \sigma_{ij} S(I_{s1}, I_i) S(I_j, I_{s2}), \quad (4.4)$$

where  $I_{s1}$  is the probe fingerprint template selected from sensor-1 and  $I_{s2}$  is the gallery fingerprint template selected from other sensors.

**Step 5:** Now fingerprint matching can be done in the transformed domain using the following formula:

$$\zeta_e(\phi^A(I_i), \phi^A(I_j)) = K^A(I_{s1}, I_{s1}) + K^A(I_{s2}, I_{s2}) - 2K^A(I_{s1}, I_{s2}), \quad (4.5)$$

where  $\zeta_e$  is the squared Euclidean distance between the transformed fingerprint templates. If the distance is less than a fixed threshold, it can be treated as a match, otherwise it is a non-match.



## 4.5 EXPERIMENTAL RESULTS

The slap fingerprint database which is collected as part of the targeted public distribution system (TPDS) is used for the experiments. This database consists of 1.8 million slap fingerprint images. The image size is  $1600 \times 1500$  with resolution of  $500dpi$ . It is observed that the correct segmentation rate *before noise removal process* is 78%, and *after noise removal process*, the correct segmentation rate is 89% in phase-I and it is 99% in phase-II. These results are presented in Table 4.3.

**Table 4.3:** Fingerprint segmentation statistics

	Segmentation Accuracy (%)
Before noise removal process	78
After noise removal process (phase-I)	89
After noise removal process (phase-II)	99

The images shown in Figs 4.3(a), 4.3(c), 4.3(d), 4.3(e), 4.3(f), 4.3(k), 4.4(a), 4.4(c), 4.4(d), 4.4(e) and 4.4(f) belong to Slap-Group-1 and Figs 4.3(b), 4.3(g), 4.3(h), 4.3(i), 4.3(j), 4.3(l), 4.4(b), 4.4(g), 4.4(h), 4.4(i) and 4.4(j) belong to Slap-Group-2. It is observed that in the Slap-Group-1, Fig 4.3(a) represents the slap with high noise. Figs 4.3(c), 4.3(d), 4.3(e) and 4.3(f) are the segmented fingers of the slap with high noise, which has the NIST fingerprint image quality (NFIQ) scores 3, 5, 4 and 5, respectively. NFIQ score ranges on the scale 1 to 5, where lesser quality score represents good quality and higher quality score represents poor quality. Fig 4.3(k) is the resultant image after binarization as well as foreground and background segmentation of the slap fingerprint image. Fig 4.4(a) shows the noise-free fingerprint image with recovered original data, and Figs 4.4(c), 4.4(d), 4.4(e) and 4.4(f) are the corresponding segmented fingers with NFIQ scores 1, 1, 1 and 3, respectively. Similarly, for the Slap-Group-2, it is observed that the accuracy of the slap fingerprint segmentation is improved. These details are given in the Table 6.3, where seg-fin-1,

seg-fin-2, seg-fin-3 and seg-fin-4 are the four segmented fingers from left to right on the slap fingerprint image.

**Table 4.4:** NFIQ scores for segmented fingerprints

	Slap-Group-1		Slap-Group-2	
	Before	After	Before	After
Seg-Fin-1	3	1	5	3
Seg-Fin-2	5	1	4	2
Seg-Fin-3	4	1	4	2
Seg-Fin-4	5	3	5	1

The results shown in Figs 4.5 and 4.6 illustrate the levels of segmented fingerprint image NFIQ scores of *before noise removal process* and *after noise removal process* of the entire dataset respectively. The NFIQ scale values from 1 to 5 are represented as NFIQ-1, NFIQ-2, NFIQ-3, NFIQ-4 and NFIQ-5 respectively. The X-axis shows the finger positions in the sequence of right thumb (RT), right index (RI), right middle (RM), right ring (RR), right little (RL), left thumb (LT), left index (LI), left middle (LM), left ring (LR) and left little (LL). The Y-axis represents the percentage of segmented fingers with NFIQ scores. The correct segmentation is defined by fixing a threshold on NFIQ score as 4 for all the segmented fingers. It is observed that the segmentation failure in *before noise removal process* for the two thumbs is 4%, the failure for the left four fingers slap is 11%, and it is 7% for the right four fingers slap as shown in Fig 4.5. The correct segmentation rate for the entire dataset is significantly improved to 99% as shown in Fig 4.6.

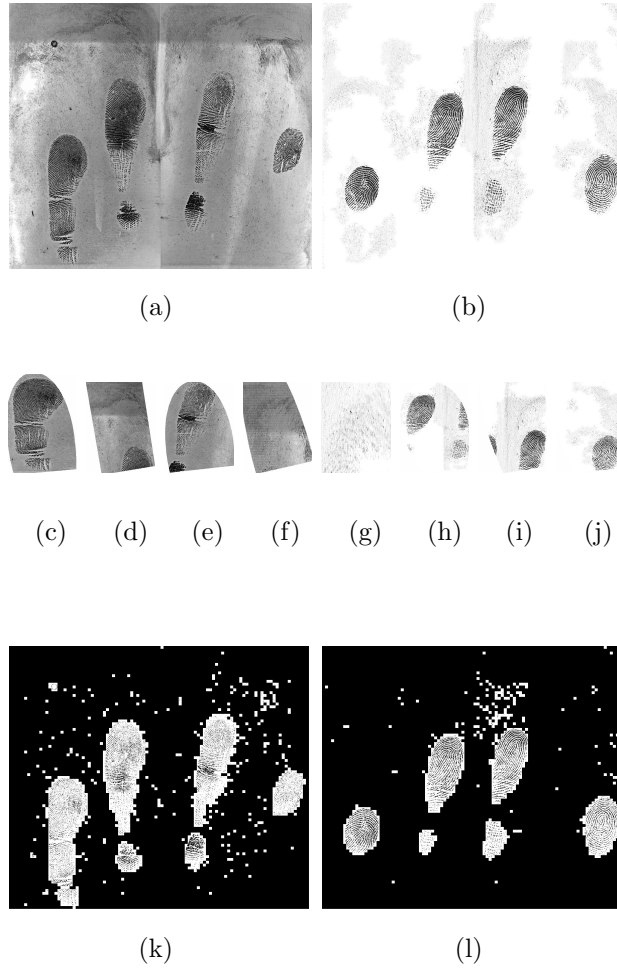


**Fig. 4.3:** Illustration of sequence of steps of de-noising slap fingerprints for accurate slap fingerprint segmentation: (a) slap with high noise, (b) slap with low noise, (c,d,e,f) are segmented fingers of the slap with high noise, (g,h,i,j) are segmented fingers of the slap with low noise, (k) foreground-background separation of high noisy slap, (l) foreground-background separation of low noisy slap.



**Fig. 4.4:** Illustration of sequence of steps of de-noising slap fingerprints for accurate slap fingerprint segmentation: (a) noise-free slap of high noise, (b) noise-free slap of low noise, (c,d,e,f) are segmented fingers of noise-free slap of high noise, and (g,h,i,j) are segmented fingers of noise-free slap of low noise.

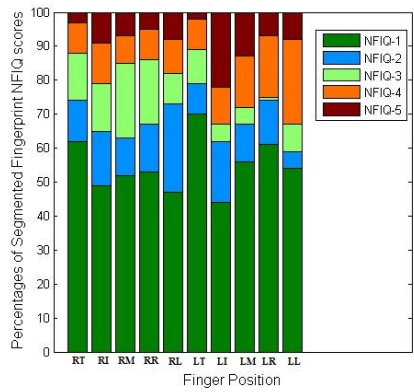


**Fig. 4.5:** Levels of fingerprint image NFIQ scores for the entire dataset - before noise removal process

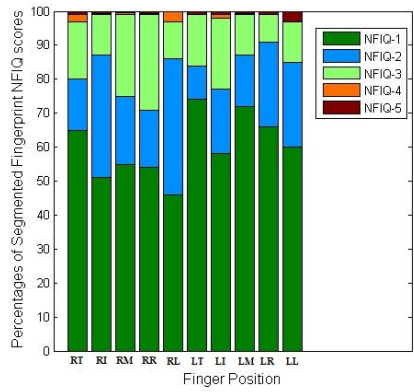


**Fig. 4.6:** Levels of fingerprint image NFIQ scores for the entire dataset - after noise removal process

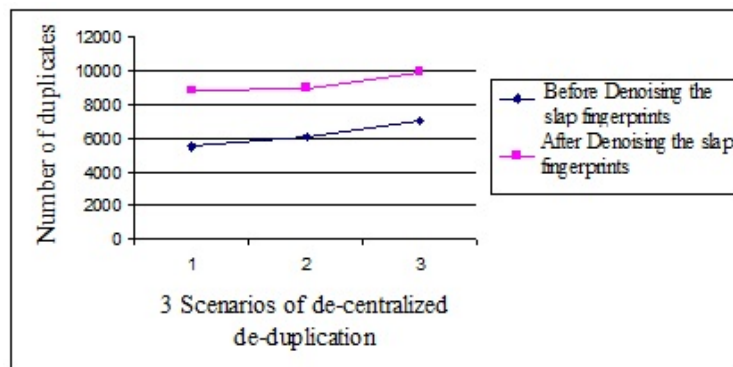


**Fig. 4.7:** De-duplication statistics of targeted public distribution system

Fig 4.7 shows the de-duplication statistics for the dataset of 0.6 million fingerprint data in the de-centralized architecture. The X-axis represents the 3 scenarios of de-centralized de-duplication, scenario-1 means "if 1 finger (say left thumb) is matched against all left thumbs of previously enrolled persons", scenario-2 means "if all 10 fingers are matched against the respective fingers of all the previously enrolled persons" and scenario-3 means "if all the 10 fingers are matched against all the fingers of all the previously enrolled persons". And the Y-axis represents the number of duplicates found in the entire dataset of 0.6 million fingerprint data. It is observed that the de-duplication accuracy is improved up to 0.5% after denoising the slap fingerprint data.

The cross-sensor fingerprint matching experiments are conducted using the database collected with three different live-scanners (Biomini, Cogent and Upek). The plain fingerprint data consists of all the 10 fingerprints of 30 subjects captured at 5 different instances. The proposed cross-sensor fingerprint matching algorithm is evaluated and compared with NIST Bozorth algorithm [41]. Table 4.5 shows that the performance of Bozorth algorithm and the proposed cross-sensor fingerprint matching algorithm. It can be observed that the proposed approach performance very well even with the fingerprint images captured using the cross-sensor fingerprint authentication devices. Experimental results show that the proposed technique achieves the equal error rate (EER) at 0.02 whereas the existing NIST open source Bozorth matching algorithm has the EER is at 0.15.

**Table 4.5:** Equal error rates (EER) of cross-sensor fingerprint recognition using kernel adaptation

Cross comparisons	NIST Bozorth EER (%)	(Proposed) Adapted EER (%)
BioMini vs. Rest	0.1	0.001
Cogent vs. Rest	0.2	0.005
Upek vs. Rest	0.9	0.001

## 4.6 SUMMARY

In this chapter, we addressed the issues related to fingerprint de-duplication accuracy in de-centralized architecture. Improper slap fingerprint segmentation often lead to reduced fingerprint matching performance. As a result the de-duplication accuracy will be decreased. In order to improve the slap fingerprint segmentation rate, a de-noising approach is proposed for slap fingerprint images using binarization of slap fingerprint image, and region labeling of desired regions with 8-adjacency neighborhood. The distinct feature of this technique is to remove the noise present in the data for accurate slap fingerprint segmentation as well as the improvement in the de-duplication accuracy. Also, due to the increasing demand for fingerprint biometrics, new fingerprint scanners are being deployed for scanning fingerprint images and the old fingerprint scanners are being frequently upgraded. The user enrollment is very expensive and time-consuming especially in large scale de-duplication applications. Upgrading with new fingerprint scanners for cross-sensor matching where the test fingerprint data is verified with the data enrolled with different fingerprint scanner often lead to reduced fingerprint matching performance. A new sensor adaptation algorithm is proposed for fingerprint biometrics using kernel transformation learning in order to improve the fingerprint matching performance.

## CHAPTER 5

# ENHANCEMENTS TO LATENT FINGERPRINT IDENTIFICATION USING ISO 19794-2 FINGERPRINT TEMPLATES

Latent fingerprint identification is a challenging task in criminal investigation due to the poor quality of ridge impressions and less region of interest on the fingerprint. In this chapter, we propose an automated latent fingerprint identification in lights-out mode using the global and local adaptive binarization, and global minutia features with ISO/IEC 19794-2 standard fingerprint templates. In the latent fingerprint identification, the fingerprints are matched with rolled fingerprint database from standard law enforcement database. Also, the latent fingerprints are matched with the plain fingerprints database from the data collected using live-scanners. The performance of minutiae-based rank-100 matching is improved with the proposed latent fingerprint identification system. Also, a semi-automated latent fingerprint identification is proposed to markup fingerprint landmarks manually using the image enhancement filters which will further improve the identification performance.

### 5.1 LATENT FINGERPRINT IDENTIFICATION IN FORENSICS

Fingerprints play an important role in forensic analysis for criminal identification using the clues collected from the crime scene. Fingerprint-based identification has been known and used for a very long time [109], [110], [111] and [112]. The fingerprint impressions which are left on the articles by the offenders at the crime scene are called



as chance prints. There are three ways of forming the chance prints, namely, visible prints, semi-visible prints and latent prints. The visible prints are the fingerprints which are collected and covered with ink, blood, dust, paint, etc. An example for the visible prints is shown in Fig. 5.1(a). Semi-visible prints, also known as plastic prints are the fingerprints which are collected by applying some pressure on the surface such as soap, wax, melted candle, etc. as shown in Fig. 5.1(b). The latent prints are the fingerprints which are collected by leaving the finger impressions formed with sweat from fingers as shown in Fig. 5.1(c). The latent prints have the poor quality of ridge impressions and partial fingerprint area. First two cases need no further development for analysis and identification of suspects as the ridge information is clear for identification, where as latent fingerprints need developments and enhancements to identify the suspects.

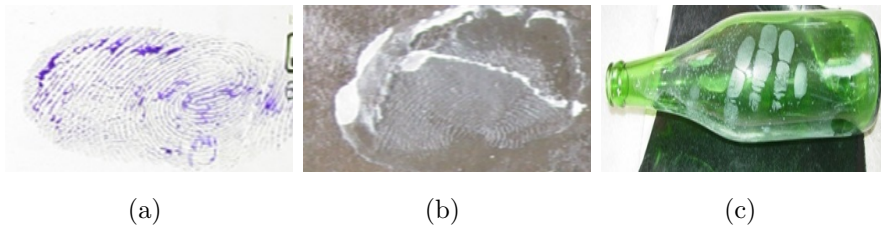


**Fig. 5.1:** Chance prints: (a) visible prints, (b) semi-visible prints or plastic prints, (c) latent prints

As shown in Fig. 5.2, there are three different types of finger acquisition, namely, rolled, plain and latent prints. The rolled fingerprints can be acquired by placing the fingerprint on the fingerprint sensor surface and moving it from nail to nail. The plain fingerprints can be captured by simply placing the fingerprint on the sensor surface. The latent fingerprints can be collected from the scene of crime as part of the forensic analysis. The automatic extraction of genuine minutia points from the latent fingerprints becomes difficult due to low fingerprint quality and less area of interest on the fingerprint image.

The manual latent identification process also known as ACE-V procedure [51]

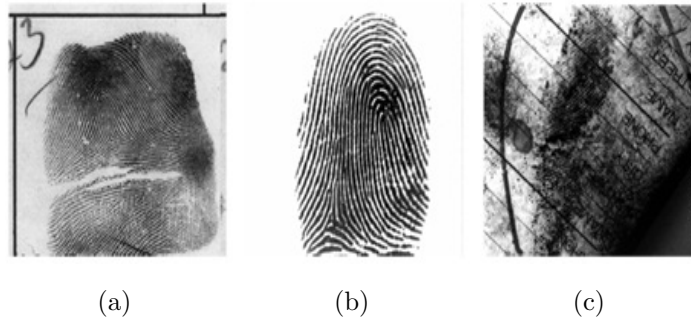


**Fig. 5.2:** Different fingerprint types: (a) rolled (b) plain and (c) latent prints

consists four steps, namely, analysis, comparison, evaluation, and verification.

1. Analysis: Assessment of quality of latent fingerprint and identification of the ridge and minutia information can be done by a human expert.
2. Comparison: Determine the similarity or dissimilarity of fingerprint landmarks using three levels of fingerprint features (level-1, level-2, and level-3) with a referent rolled/plain fingerprint.
3. Evaluation: Decide whether the fingerprint pair is a match or non-match.
4. Verification: Re-examination of the results by another human expert to verify the results of the first human expert.

The majority of the algorithms developed for automated fingerprint matching are based on minutiae [49], [50] and [51]. Several recent studies on fingerprint matching have focused on the use of local minutiae descriptors [52], [49], [53], [54]. Some algorithms combine ridge orientation with minutiae information either at feature level by including ridge orientation information in local minutiae descriptors [55], [56] or at score level by combining scores from minutiae matching and global orientation field matching [56], [57]. The latent fingerprint matching accuracy is improved by using the features which are marked manually from the latent fingerprints [58], [59], [60], [61]. However, marking extended features (orientation field, ridge skeleton, etc.) in poor quality latents' is very time-consuming. Thus, some studies have concentrated on

latent matching using a reduced amount of manual input, such as manually marked region of interest (ROI) and singular points [113], [114]. However, only a small portion of latents can be correctly identified using this approach. There have also been some studies on fusion of multiple matchers [62] or multiple latent prints [50]. NIST has been conducting a multi-phase project on evaluation of latent finger-print technologies (ELFT) to evaluate latent feature extraction and matching techniques [63]. Jain et. al. have proposed a latent matcher for automatic identification of suspects by using the extended features, namely, singularity, ridge quality map, and ridge flow map [47], [64]. The latent fingerprint image quality is measured by spectral image validation and verification (SIVV)-based metric [65] and the latent fingerprint image quality (LFIQ) metric based on triangulation of minutiae points [66].

In this chapter, we propose two approaches to automated latent fingerprint identification. The first approach uses the global and local adaptive binarization, and global minutia features with ISO 19794-2 standard fingerprint templates. And, the second approach is a semi-automated latent fingerprint identification system which uses different imaging filters to enhance the latent print. The semi-automated latent fingerprint identification system is more flexible for fingerprint forensics experts which would allow them to acquire fingerprint latents captured with various devices from crime scenes, falsified documents etc.

## **5.2 AUTOMATED LATENT FINGERPRINT IDENTIFICATION**

The proposed automated latent fingerprint identification consists of different phases: fingerprint enhancement, normalization of fingerprint image, feature extraction, spurious minutia removal and matching which are explained in the following sections.

### **5.2.1 Fingerprint enhancement**

A latent fingerprint image consists of more noise when compared to the plain fingerprints due to the acquisition and environmental conditions at the crime scene. The

image enhancement is introduced as a preprocessing step to reduce the noise [115] and to enhance visibility of ridge impressions. The steps involved in fingerprint enhancement are illustrated in Fig. 5.3. Each step is explained in detail in the following subsections.

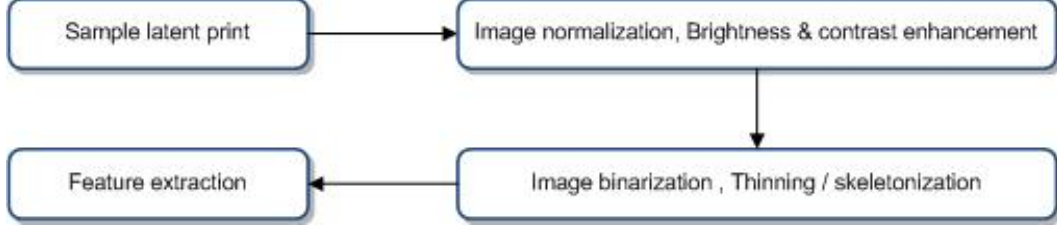


**Fig. 5.3:** Fingerprint image enhancement

### 5.2.2 Normalization, binarization and thinning

Normalization is a process of changing the range of pixel intensity values to enhance the contrast on image. Let us consider an image,

$$I : \{X \subset R^n\} \Rightarrow \{Min, \dots, Max\}, \quad (5.1)$$

with intensity values in the range  $(Min, Max)$  and  $X$  is a set of all intensity values in image  $I$ , and a new image

$$I_N : \{X \subset R^n\} \Rightarrow \{Min_{new}, \dots, Max_{new}\}, \quad (5.2)$$

with intensity values in the range  $(Min_{new}, Max_{new})$  where  $Min_{new}$  is the minimum intensity value and  $Max_{new}$  is the maximum intensity value in the new image. The linear normalization of a gray-scale image is computed using

$$I_N = (I - Min) \times \frac{Max_{new} - Min_{new}}{Max - Min} + Min_{new}. \quad (5.3)$$

In general, the latent fingerprint images have less contrast which are to be enhanced by adjusting the brightness and contrast of the image until the ridges are clear. The image is then submitted to the binarization followed by K3M thinning [116] as shown in

Fig. 5.4. The image binarization means changing the intensity levels from the original 256 (8-bit pixel) to 2 (1-bit pixel). Local adaptive thresholding [117] is applied instead of choosing a single intensity threshold value in the image binarization process as all the fingerprint images do not have the same contrast and brightness. The binarized image is shown in Fig. 5.4.

### 5.2.3 Feature extraction

Thinned image is useful for extracting the minutiae features like end point and bifurcation. The ISO template consists of three kinds of minutia, namely, end point, bifurcation and undetermined. The end point is the point where the ridge ends abruptly and the bifurcation is the point where the ridge bifurcates into two directions. From the thinned image the minutia points can be extracted using the crossing number (CN) concept. The ridge ending can be identified as the pixel point with only one neighbor and the bifurcation can be identified as a pixel point with three neighbors. Each minutia extracts the information like  $x - y$  coordinates, direction, type and quality. The fingerprint image is divided into  $16 \times 16$  blocks to compute the quality of each block depending on the variance of the pixels in that particular block. The fingerprint quality scale [41] is defined in the range from 1 to 5 depending on the variance difference. If the quality of the fingerprint information in a particular block is 1, then the block has good fingerprint area and if the quality of fingerprint is 5 means the block is in background area. The quality of fingerprint image is illustrated in Fig. 5.5.

### 5.2.4 Spurious minutia removal

The last stage in the feature extraction is the removal of spurious minutiae points. There are different types of spurious minutiae, namely, minutia near the borders, minutiae on short ridges, minutia due to bridges and minutia related to spurs. Minutiae near to the border can be eliminated using the quality image, where the minutia surrounding blocks are very poor. Spurs can be eliminated using a certain threshold on

the thinned image where the ridge is having both bifurcation and end point. Finally, the minutiae details can be packed into the ISO/IEC 19794-2 format [118] which is an international standard for fingerprint template to achieve the interoperability among different vendor specific automated fingerprint identification systems. Table 5.2.4 illustrates essential fields defined in the template.

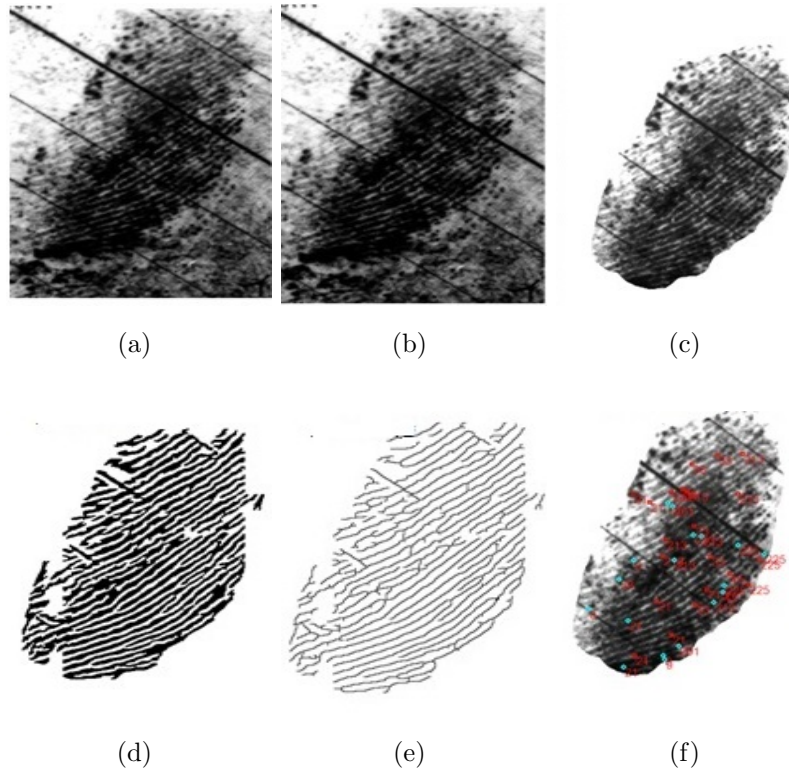


**Fig. 5.4:** Steps in latent fingerprint image enhancement and feature extraction: (a) sample latent print, (b) image normalization, (c) de-noising image, (d) image binarization, (e) image thinning, (f) feature extraction.

### 5.2.5 Matching

The proposed fingerprint matching algorithm uses ISO/IEC (International Organization for Standards/International Electro-technical Commission) [118] templates. The feature vector consists of the information;  $x-y$  coordinates, direction, type and quality

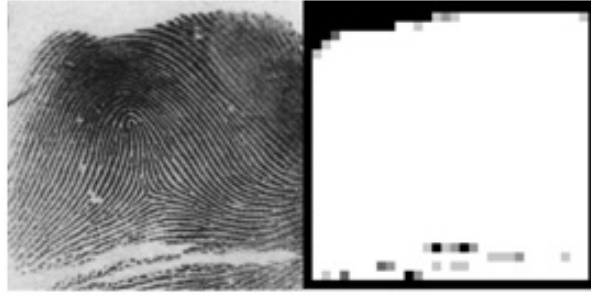


**Fig. 5.5:** Rolled fingerprint image with the corresponding quality image

**Table 5.1:** ISO/IEC 19794-2 template data information

Field	Size	Information
Image height	2 bytes	in pixels
Image width	2 bytes	in pixels
Finger position	1 byte	0 to 10
Number of Minutiae n	1 byte	0 to 255
Type	2 bits	00=other, 01=termination, 10=bifurcation
Position x	14 bits	in pixels
Position y	14 bits	in pixels
$\theta$ : Direction	1 byte	0 to 255 (resolution 1.40625 degrees)
Quality	1 byte	1 to 100 (0=quality not reported)

of each minutia. Each edge consists of the information like the edge distance and directional difference between minutiae. The proposed algorithm is of rotation invariant since it uses relative distances and angles between minutia points. The steps involved in the global and local minutia matching algorithm are summarized in Algorithm 1.

### 5.3 SEMI-AUTOMATED LATENT FINGERPRINT IDENTIFICATION

The proposed semi-automated latent fingerprint identification system consists of different phases, namely, fingerprint acquisition, finger markup & matching, results review and evidence exhibits. The phases involved in the latent fingerprint recognition system

---

**Algorithm 1** : Latent fingerprint matching algorithm

---

**Inputs:** Query and reference ISO/IEC fingerprint templates.

**Step 1.** Get the details of each minutia from the template information, namely, x-y coordinates, direction, type and quality.

**Step 2.** Compute the edge pair information for each minutia to all other minutia in order to form quadruplets.

**Step 3.** Sort the edge pair information using distance.

**Step 4.** Compute the edge pair information for each minutia to all other minutia based on quadruplets.

**Step 5.** Validate the matched minutia points to remove the falsely matched minutia pairs.

**Step 6.** Compute the matching score.

---

are explained in the following sections.

### 5.3.1 Image acquisition

Images can be acquired through a control capture device such as a scanner or a fixed focus camera. The image acquisition provides a perceived *dpi* (dots per inch) measurement to adjust the image resolution. The image *dpi* captured using a live-scanner is different from the image which is collected from the scene of crime. Typically, latent fingerprint examiners tend to follow a practice of placing a physical scale next to the latent fingerprint being photographed to give an idea to the user as well as systems to relate to the actual size of the real latent. The *dpi* measurement tool allows the system to determine the perceived *dpi* of the image using the ridge count or the distance between each fingerprint ridge. The latent fingerprint can be scaled up/down to the default fingerprint resolution, i.e.,  $500dpi$ , which improves the matching accuracy at later stage.



### **5.3.2 Image markup and matching**

Image markup allows to analyze and markup fingerprint landmarks. The markup provides image processing filters to enhance the image and to compose the desired effect by layering various directional filters like Sobel filter [119], emboss filter [120], lighting filter [119] and fingerprint skeletonization [116]. Basic image manipulations such as rotation and flipping are useful to trace the landmarks on the image. A set of tools to specify fingerprint landmarks are implemented which uses the proposed latent fingerprint recognition algorithm to automatically generate markup points which can be accepted by the user as valid points. The fingerprint matching algorithm used in this identification system which is similar to the matching algorithm proposed in automated identification system, i.e., Algorithm 1.

### **5.3.3 Result review/adjudication**

The biometric recognition system allows few errors in the identification process. In order to reduce the errors, fingerprint experts look for possible fingerprint matches and enhance the fingerprints to compare the minutia features manually using fingerprint adjudication process. Fingerprint adjudication means, comparison of two fingerprints side-by-side to analyze the matched minutia features. The search results allow to view the probe as well as the encounter candidate, side by side, with a template overlay. There is a match point highlight capability to view the actual matching landmarks in the system. A set of filters allow the user to enhance the images. The end objective is to allow the user to make the decision and call one or multiple encounters as a 'hit' for a particular case. The hit cases may be subjected to a peer review depending on the deployment scenario.

### **5.3.4 Evidence exhibit/reporting**

Once a set of encounters are marked as hit, the system generates an evidence exhibit, detailing image matching regions. Fig. 5.6 illustrates the sample of evidence reporting

for a particular matched fingerprint pair. The left side image is known as probe fingerprint or latent print and the right side image is known as candidate fingerprint or plain/rolled fingerprint. The matched regions are illustrated in circles.

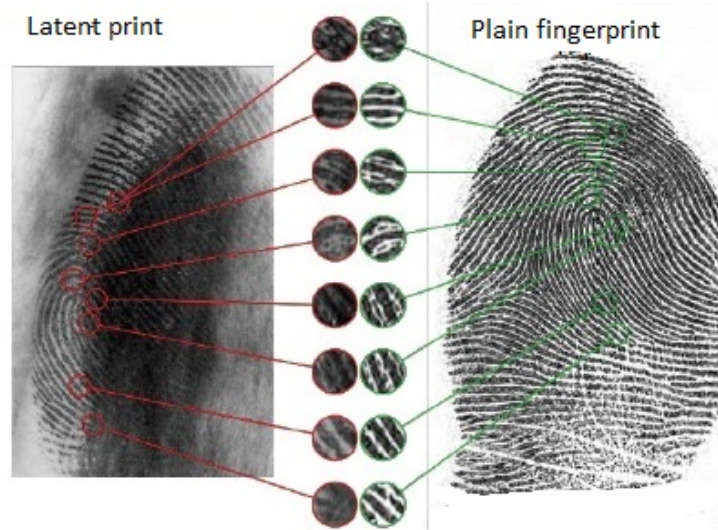


**Fig. 5.6:** Evidence exhibit of a particular matched fingerprint pair

#### 5.4 EXPERIMENTAL RESULTS

The experimental results of latent fingerprint recognition are presented in lights out mode. The standard NIST special database-27 [121] is used for the experiments which contains latent fingerprints from crime scenes and their corresponding rolled fingerprint mates. There are 258 latent cases, each case includes the latent image and the corresponding ten print image. The database is divided into three groups LF-1, LF-2 and LF-3, where the fingerprint qualities are good, bad and ugly, respectively. There are 88 latent prints in LF-1 group, 85 latent prints in LF-2 group and 85 latent prints in LF-3 group in SD27 database. Each image is of size  $800 \times 768$  pixels and scanned at 19.69 pixels per millimeter (ppmm)/ (500 pixels per inch (ppi)), quantized to 256 levels of gray, and stored in an uncompressed format. All data files are formatted according to the ANSI/NIST-ITL 1-2000 standard [36] using Type-1, 13, & 14 records.

The ISO/IEC 19794-2 templates are generated from latent and rolled fingerprints

and then submitted for matching. The latent prints were matched against the plain prints of 2258 images which are collected using live-scanner and the existing rolled fingerprints from the SD27 database. As shown in table 5.4, the matching accuracy is better in the group of LF-1 latent fingerprints where 60% of the cases are identified in top 10 of search results, 30% of the cases are identified in top 100 search results and around 10% are not identified. Similarly, in LF-2, latent fingerprints are identified around 40% in top 10 search results, 30% in top 100 search results and the remaining cases are not identified. LF-3 latent fingerprints around 70% are not identified. Figure 5.7 shows the CMC curves of the automated latent fingerprint identification for LF-1 (Good), LF-2 (Bad), and LF-3 (Ugly) quality latent prints. It is observed that the matching performance for LF-1 group latent fingerprint quality is significantly improved when compared with the latent fingerprints belonging to the other two groups LF-2 and LF-3. The results are compared with the existing method proposed by Anil K Jain et. al. [47] and observed the improvement in rank-1 identification rate as shown in Table 6.3 with the assumption that it will not be a big difference in the identification rate even if we add 1758 images to SD27 dataset.

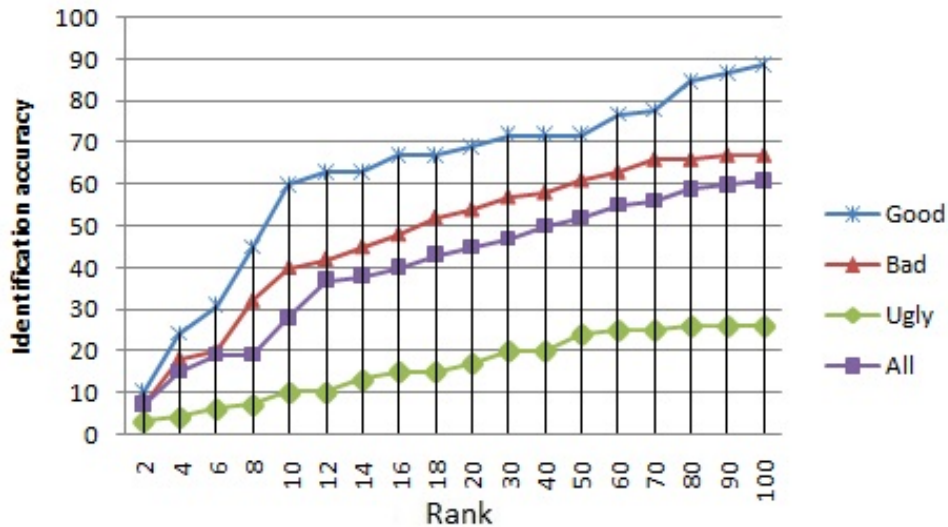
**Table 5.2:** Results of latent fingerprint matching

Latent-Group	Top 10 (%)	Top 100 (%)	Not in Top 100 (%)
LF-1 (Good)	60	30	10
LF-2 (Bad)	40	30	30
LF-3 (Ugly)	10	20	70

The unsolved latent fingerprints need an experts' manual intervention with semi-automated latent fingerprint identification system. As shown in Figs. 5.8 & 5.9, the latent fingerprints are enhanced to further submit in semi-automated identification system using the image processing filters, namely, Sobel, lighting, emboss and color filters. Fig. 5.8(a) is the portion of a sample latent print. The region of interest on latent print is located as illustrated in Fig. 5.8(b). Figs. 5.8(c) and 5.8(d) illustrate

**Table 5.3:** Comparison of rank-1 identification rate

Latent-Group	Anil K Jain et. al. [47] (%)	Proposed method (%)
LF-1 (Good)	83	87
LF-2 (Bad)	74	78
LF-3 (Ugly)	65	72

**Fig. 5.7:** CMC curves for different quality latent prints (good, bad, and ugly)

the image enhancements using color, brightness and contrast adjustments. The Sobel filter applied on the image with gradient directions  $0^0$ ,  $90^0$ ,  $180^0$  and  $270^0$  are shown in the Figs. 5.8(e), 5.8(f), 5.8(g) and 5.8(h), respectively. The emboss filter applied on the image with gradient directions  $0^0$ ,  $90^0$ ,  $180^0$  and  $270^0$  are shown in the Figs. 5.9(a), 5.9(b), 5.9(c) and 5.9(d), respectively. Similarly, the Sobel filter applied on the image with gradient directions  $0^0$ ,  $90^0$ ,  $180^0$  and  $270^0$  are shown in the Figs. 5.9(a), 5.9(b), 5.9(c) and 5.9(d), respectively. After these enhancements, the ridge information is highlighted to easily distinguish the hidden minutia points on the latent fingerprint image. It is observed that the matching accuracy improved to around 79% after the latent fingerprint enhancements using the semi-automated latent fingerprint

identification system.

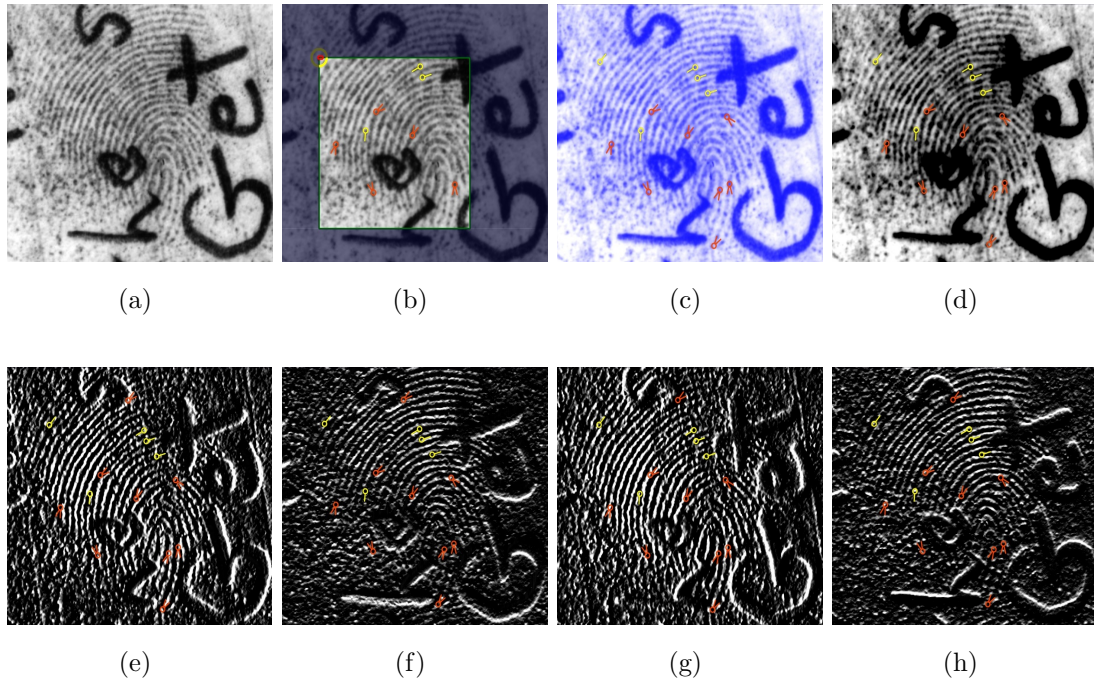


**Fig. 5.8:** Finger markup filters: (a) sample latent print from NIST SD-27, (b) region of interest marking, (c) enhance image with color filters, (d) brightness and contrast enhancements, (e) Sobel filter applied with gradient direction  $0^{\circ}$ , (f) Sobel filter applied with gradient direction  $90^{\circ}$ , (g) Sobel filter applied with gradient direction  $180^{\circ}$ , (h) Sobel filter applied with gradient direction  $270^{\circ}$ .

## 5.5 SUMMARY

In this work, two methods of latent fingerprint identification systems are proposed, namely, automated and semi-automated latent fingerprint identification systems. The automated latent fingerprint identification algorithm is proposed in lights-out mode where the standard ISO/IEC 19794-2 templates are considered. The proposed algorithm reduces the manual intervention of the fingerprint experts in identifying the suspects. The semi-automated latent fingerprint identification system have the image enhancement filters, namely, Sobel, emboss, and lighting. The matching performance for LF-1 group latent prints is significantly better than those for the latent prints

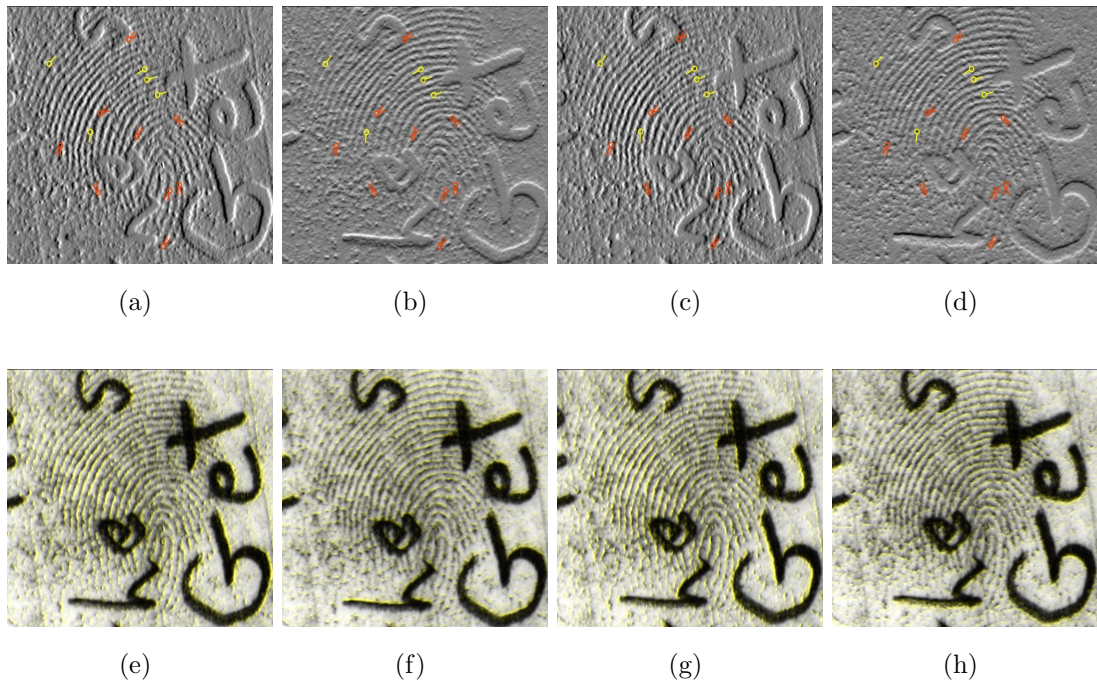


**Fig. 5.9:** Finger markup filters: (a) emboss filter applied with gradient direction  $0^{\circ}$ , (b) emboss filter applied with gradient direction  $90^{\circ}$ , (c) emboss filter applied with gradient direction  $180^{\circ}$ , (d) emboss filter applied with gradient direction  $270^{\circ}$ , (e) lighting filter applied with gradient direction  $0^{\circ}$ , (f) lighting filter applied with gradient direction  $90^{\circ}$ , (g) lighting filter applied with gradient direction  $180^{\circ}$ , (h) lighting filter applied with gradient direction  $270^{\circ}$ .

belonging to the other two groups LF-2 and LF-3. The matching performance is improved to around 79% after the latent fingerprint enhancements using the semi-automated latent fingerprint identification system.

## CHAPTER 6

# DEDUPLICATION USING PHOTOGRAPH AND FACE IMAGES

This chapter presents the de-duplication process using face biometrics. Face is one of the most widely used biometric in security systems. Despite its wide usage, face recognition is not a fully solved problem due to the challenges associated with varying illumination conditions. The illumination while capturing the face photographs plays an important role especially in out-door environment in the process of unique identity creation using de-duplication process. The thesis addresses the effect of illumination in face photographs as well as face images for de-duplication applications.

First we propose a method for de-duplication process of photographs is implemented using content based image retrieval (CBIR). The CBIR technique uses color histogram refinement feature. The photograph data is divided into different clusters using  $k$ -means clustering algorithm. The clusters count depends on the number of photographs in each district of the state. The photo de-duplication exercise was carried out in a large photograph database which contains 22 million (approximately) photograph images. Second, a new approach for illumination invariant face recognition using convolutional neural networks (CNN) [77]. The ability of a CNN to learn local patterns from data is exploited for facial recognition. The symmetry of facial information is exploited to improve the performance of the system by considering the horizontal reflections of the facial images.

## 6.1 PHOTOGRAPH DE-DUPLICATION FOR PUBLIC DISTRIBUTION SYSTEM

The targeted public distribution system (TPDS) is a mechanism for ensuring access and availability of food grains and other essential commodities at subsidized prices to the households. Identification of eligible beneficiaries and ensuring delivery of commodities to them effectively and efficiently is the main challenge for TPDS. As part of this, one department of civil supplies in India has issued around 22 million ration cards covering around 80 million citizens and this process was decentralized. The department noticed that there are some bogus ration cards and decided to execute the de-duplication process on entire data. De-duplication is carried out in two different ways, one is biometric-based and the other is photo-based. The reason to go for photo-based de-duplication is that there are some ration cards without biometrics. An attempt is made to explain the de-duplication process of photograph images.

Photo-based de-duplication means finding the duplicate ration cards based on the family photograph in the large scale database. The operators generated some duplicate ration cards using the family photographs of the already existing ration cards. They manipulated the photographs in such a way that they edit the photograph in an image editor tool, crop the corners of the photograph in rectangular shape, erase the corners image data and finally zoom the photograph image into the actual photograph image size.

The methods described in [122–124] are based on color histogram refinement technique using color coherent vectors, color and texture for content-based image retrieval. An algorithm is proposed to de-duplicate photographs using histogram refinement for content-based image retrieval (CBIR). Histogram refinement splits the pixels in a given bucket into several classes based on some local property. Within the given bucket, only pixels in the same class are compared. The equal error rate is fixed empirically at the threshold of 1500 by observing the false accept rates and false reject rates on sample training dataset which is created from the database of 22 million photographs.



The entire photographic data were divided into different groups in two levels, one is district-level grouping and the other level uses  $k$ -means clustering. District-level grouping means dividing the data into different clusters based on district names. There may be chances that a family can have two or more ration cards in different districts. The reason for not considering the state as single unit for the de-duplication process is to speed up the process. There are 23 groups formed based on district name. The next level of grouping is  $k$ -means clustering of district-level data which uses the color and texture features of the photograph.

### 6.1.1 CBIR technique using color histogram refinement

The proposed CBIR method uses the family photograph images. Fig. 6.1 represents the sample color photograph image which has the dimensions of  $320 \times 240$  image size. Generally, images are two-dimensional arrays of bytes which represent pixels. Each pixel has a gray-scale value which is ranging from 0 to 255.



**Fig. 6.1:** Family photograph of a household ration card

The steps in de-duplication of photographs using CBIR are given below:

1. Extraction of color features from photograph image.
2. Clustering of photographs using  $k$ -means algorithm.
3. De-duplication of photographs.

In the following subsections, each of the above steps is explained below in detail.

### 6.1.2 Extraction of features from photograph images

The color and texture features are extracted from the photograph images. Color histograms are more popular to compare images. They are more suitable against small changes in camera viewpoint. For example, Swain and Bellard [125] use color histograms for analyzing the data. A color histogram is represented by a vector  $H = \langle c_0, c_1, \dots, c_{n-1} \rangle$  where  $n = 256$  and  $c_j$  contains the number of pixels of color  $j$  in the image. Color images are represented in RGB color space. Each image consists of three color histograms, namely,  $R_h$  histogram,  $G_h$  histogram and  $B_h$  histogram. The color histogram  $H$  is an average of  $R_h$ ,  $G_h$  and  $B_h$  histograms. Images with same histograms may have entirely different appearances which can be overcome by histogram refinement [126] technique which divides the color histogram into two different histograms based on local features. The local feature (with diagonal line as the reference) is used to split the color histogram into two histograms, namely, left diagonal histogram  $H_L$  and right diagonal histogram  $H_R$ . The resulting split histograms can be compared using the Manhattan distance ( $L_1$ -distance) measure. The left diagonal color histogram is  $H_L = \langle cL_0, cL_1, \dots, cL_{n-1} \rangle$  and the right diagonal color histogram is  $H_R = \langle cR_0, cR_1, \dots, cR_{n-1} \rangle$ . The number of pixels of color  $j$  in the image becomes  $c_j = cL_j + cR_j$  where  $L_j$  and  $R_j$  represent the  $j^{th}$  bin of left diagonal histogram  $H_L$  and right diagonal histogram  $H_R$ , respectively.

$$H = H_L + H_R = \langle cL_0 + cR_0, cL_1 + cR_1, \dots, cL_{n-1} + cR_{n-1} \rangle \quad (6.1)$$

The photograph images have pixels data of 2-D array of  $320 \times 240$  which is in RGB (red, green, blue) color space. The image is partitioned into  $4 \times 4$  blocks. Each block is represented with one feature vector, consisting of six features [127]. Three of them are the average color components in a  $4 \times 4$  block. The other three represent energy in high frequency bands of wavelet transforms [128], that is, the square root of the second order moment of wavelet coefficients in high frequency bands.

The RGB color space is only rarely used for querying as it does not correspond

well to the human color perception. It seems reasonable to be used for photograph images taken under almost identical conditions each time. Although the duplicate photographs have the same capturing conditions as the original photograph, it may be altered while editing by the operators. The photograph image is transformed from *RGB* space to CIE *Luv* space [129], and then the features of the three color components are calculated. The CIE *Luv* color space is a perpetually uniform. To obtain the other three features, the Daubechies-4 wavelet transform is applied to the *L* component of the image. After a one-level wavelet transform, a  $4 \times 4$  block is decomposed into four frequency bands as shown in Fig 6.2.

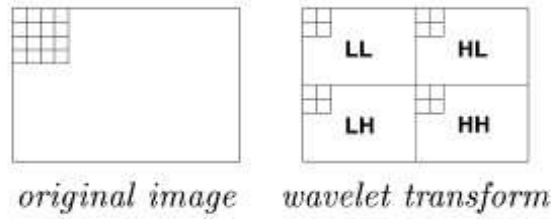


**Fig. 6.2:** Decomposition of images into frequency bands by wavelet transforms

Each band contains  $2 \times 2$  coefficients. Without loss of generality, suppose the coefficients in the *HL* band are  $(C_{k,l}, C_{k,l+1}, C_{k+1,l}, C_{k+1,l+1})$ . Then, one feature is

$$f = \left[ \frac{1}{4} \sum_{i=0}^1 \sum_{j=0}^1 C_{k+i,l+j}^2 \right]^{\frac{1}{2}}, \quad (6.2)$$

and the other two features are computed similarly from the *LH* and *HH* bands. Finally, compute the feature vector by taking the average of all the corresponding feature vectors of 4800 blocks.

### 6.1.3 *k*-means clustering algorithm

The standard *k*-means algorithm [130] is in the family of prototype based clustering algorithms. The general steps of the prototype based clustering are:

1. Let  $x$  be the feature vector consisting of 6 features. Initialize the centers  $c_i$  arbitrarily where  $i = 1$  to  $n$  where  $n$  is number of clusters.
2. For each feature vector  $x$ , compute its minimum distance with each center  $c_i$  and assign the data point to  $i^{th}$  cluster.
3. For each center  $c_i$ , recompute the new cluster center from all feature vectors  $x$  belong to this cluster.
4. Repeat steps 2 and 3 until convergence.

The input for the  $k$ -means clustering algorithm is the feature vectors and the number of clusters. Each vector has the length 6 (3-color components, 3-texture components). The cluster count depends on the numbers of ration cards in the district. Once the clustering is over, each cluster undergoes the de-duplication process which is explained in section 6.1.4.

#### **6.1.4 De-duplication process of photographs**

There are two phases involved in the process of photograph de-duplication. In Phase-I, the pre-processing steps for the de-duplication process is explained. In Phase-II, the actual de-duplication process is explained.

##### **Phase-I**

- Step 1. Resize the photograph images to  $320 \times 240$  to reduce the computational complexity.
- Step 2. For each photograph image, apply the histogram refinement technique and compute the histogram pair  $(H_L, H_R)$  where  $H_L$  is the left diagonal histogram and  $H_R$  is the right diagonal histogram.
- Step 3. For each photograph image, compute the feature vector of length 6, consisting of 3 color and 3 texture components.
- Step 4. Divide the entire data into 23 clusters based on district name.

Step 5. Each district-level cluster is further clustered using the k-means clustering algorithm. The input data for this algorithm is feature vector which is computed in Step 3. Number of clusters depend on the total number of photographs in each district.

Step 6. Apply de-duplication process for each cluster.

### Phase-II (De-duplication for each cluster)

Step 1. Pick one histogram pair from the set of histograms pairs  $\{(H_L, H_R)\}$ , say query histogram pair  $(HQ_L, HQ_R)$  which is not yet participated as a query histogram pair.

Step 2. The similarity score ( $L_1$ -distance) is calculated between the query histogram pair and the set of all the histogram pairs which are not participated as query histogram pair. The  $L_1$ -distance between the pairs  $(HQ_L, HQ_R)$  and  $(H_L, H_R)$  is defined as follows:

$$score = \sum_{i=0}^{n-1} (|HQ_L^i - H_L^i| + |HQ_R^i - H_R^i|), \quad (6.3)$$

where  $n$  is number of histogram bins.

Step 3. List the top 20 matches which have similarity scores less than or equal to 1500 (empirical threshold).

Step 4. The results are verified manually whether the results are correct or not. This is required because there is no guarantee that all the results are true matches.

## 6.2 FACE RECOGNITION IN DE-DUPLICATION PROCESS

Face recognition [67] has gained much attention from the research groups of pattern recognition and machine learning since the early 1990s. Face recognition is a difficult task due to the issues with illumination variance which affects the identification rate [68]. The illumination varies while capturing the face photographs, especially

in outdoor environment while creating person's identity using de-duplication process of face images. A fuzzy Fisher-face approach was proposed for face recognition [69] using Fisher discriminant analysis and principle component analysis. Face recognition is used in applications like access control and surveillance [2]. A new framework for face recognition and feature extraction is proposed with kernel Fisher discriminant analysis and fisher linear discriminant analysis [70]. Wiskott et. al. [71] proposed face recognition algorithm by using labeled elastic bunch graphs matching based on Gabor wavelet transform. A face verification algorithm was proposed [72] for training a very large and unknown data of different categories.

Variations in ambient lighting produces significant degradation in face recognition performance [2]. Thermal infrared (thermal IR) has been used in facial recognition systems with some success against the ambient illumination. Near infrared (NIR) has the potential to overcome the problems associated with visible [73] and thermal IR face recognition which is more robust against illumination variations and face detection [74]. NIR is useful for face detection as the bright eye effect [75] allows the eyes to be localized and skin reflectance properties at just above and below 1.4 microns which highlights the face regions clearly [74]. Over the last decade, convolutional neural networks [76] is widely used for various computer vision tasks [77].

### **6.2.1 Illumination invariant facial recognition using convolutional neural network**

A convolutional neural network, capable of learning local features from input data is used to discriminate facial images. A typical CNN classifier [131] consists of a CNN with alternating sequence of convolution and sub-sampling layers for feature extraction and a neural network in the last layer for classification. The architecture of CNN classifier considered in this work is shown in Fig. 6.2.1.

The template size considered in convolution layers ( $C1, C2$ ) and sub-sampling layers ( $S1, S2$ ) are  $5 \times 5$  and  $2 \times 2$ , respectively. The facial images are down-sampled

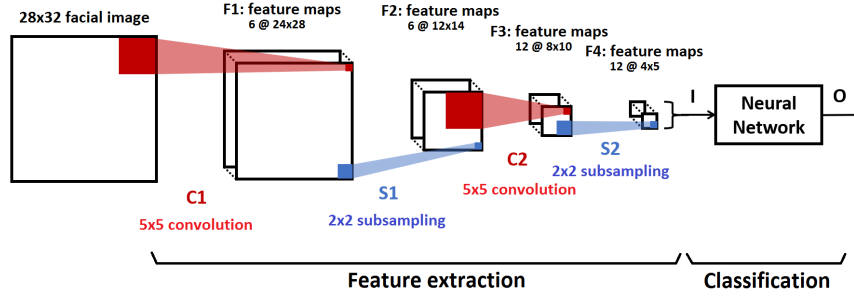


**Fig. 6.3:** Architecture of convolutional neural network

to images of size  $28 \times 32$  and given as input to the CNN. The number of feature maps considered in the first feature map set ( $F1$ ) and the third feature map set ( $F3$ ) are 6 and 12, respectively. The second feature map set ( $F2$ ) and the fourth feature map set ( $F4$ ) will have the same number of feature maps as  $F1$  and  $F3$ , respectively. The output of the CNN is traversed in a row major order to obtain a column vector ( $I$ ) of dimension  $240 \times 1$  which is used by the neural network to classify the input facial images into one of the 30 output classes ( $O$ ). The last two layers of the CNN classifier i.e.,  $F4$  and the neural network shown in Fig. 6.2.1 are fully-connected. The CNN classifier is trained using back-propagation algorithm in batch mode, to learn the convolution masks used in  $C1, C2$  and the connection weights between last two layers of the classifier. The following section explains the experimental setup used to evaluate the performance of the proposed approach.

### 6.3 EXPERIMENTAL RESULTS

**Photograph de-duplication** Table 6.3 shows the de-duplication results for face photograph images in the targeted public distribution system of the household information of 23 districts of Andhra Pradesh. The number of household cards in each district is given with the corresponding duplicate household cards and the number of clusters used in each district. The variation in number of classes depends on the number of household cards in each district. The de-duplication process used two 64-

bit windows 2000 servers having quadcore processor. Three 32-bit windows systems were used to extract features and for clustering. For each server, two de-duplication instances run, one instance is top-to-bottom de-duplication instance and the other is bottom-to-top de-duplication instance. Each instance used 25 threads to compute the similarity score using  $L_1$ -distance. The photo de-duplication process was carried out in a large scale photograph database having 22,916,243 images. The experimental results show that there were 353,650 duplicate photographs. Fig 6.4(a), 6.4(c), 6.4(e), and 6.4(g) are the original photographs. Fig 6.4(b), 6.4(d), 6.4(f), and 6.4(h) are the duplicate photographs.



**Table 6.1:** De-duplication results of photograph images

	Household cards or family photographs		
District	# of Images	Duplicates	# of Classes
D-1	774074	12685	3
D-2	646537	10044	3
D-3	1226020	18616	5
D-4	1358529	22736	5
D-5	1041159	13658	4
D-6	1208362	22333	5
D-7	1390698	20251	5
D-8	858607	12737	3
D-9	833137	9330	3
D-10	1067074	29073	4
D-11	811924	10990	3
D-12	1116510	17864	4
D-13	1027658	13442	4
D-14	1066708	15067	4
D-15	1300346	14805	5
D-16	1262954	18207	5
D-17	725254	10604	3
D-18	627405	11038	3
D-19	704406	8270	3
D-20	1087370	18397	4
D-21	1037474	16599	4
D-22	756072	12097	3
D-23	987965	14807	4



(a)

(b)



(c)

(d)



(e)

(f)



(g)

(h)

**Fig. 6.4:** Duplicate household ration cards

**Face recognition using CNN** The experiments were conducted on Extended Yale Face Database B [78], [132] which consists of  $168 \times 192$  gray scale facial images of 38 subjects under 9 poses and 64 illumination conditions. Five-fold cross validation is used to evaluate the performance of the proposed approach on facial images captured under varying illumination conditions. Similar to other existing approaches, the angle between the direction of light source and the camera axis are considered in grouping the facial images into 5 sets as shown in Table 6.3. We consider 62 illumination images of 30 subjects (a total 1860 frontal face images) from Extended Yale B database, for experimental evaluation of the proposed approaches. The typical distribution of facial images across the five sets are shown in Fig. 6.5, where facial images in one row correspond to one subset.

**Table 6.2:** Five sets of Extended Yale Database B

Set #	1	2	3	4	5
Lighting angle (deg)	0-12	13-25	26-50	51-77	>77



**Fig. 6.5:** Typical distribution of Extended Yale Face dataset B facial images across the five sets (only 6 instances per subset are shown)

The CNN is trained using back-propagation algorithm in batch mode with a batch size of 2 for 500 epochs and evaluated using 5-fold cross validation. The variation of

classification error with the number of training epochs is given in Table 6.3. The plot of classification performance against number of training epochs is shown Fig. 6.6. An average classification performance of 89.05% is obtained for the proposed approach. The recognition performance of sets #1 and #2 is better when compared to the other sets and relatively low for #3, #4 and #5, which could be due to the inadequacy of training data to capture the necessary discriminative information to recognize the faces in test dataset.

**Table 6.3:** Misclassification error (%) of the proposed approach for the five sets

Set #	5 epochs	50 epochs	250 epochs	500 epochs
1	81.1	0.88	0.4	0.35
2	64.1	3.33	1.96	1.21
3	84.4	18.8	14.72	12.93
4	95	23.8	18.05	17.2
5	88.05	28.3	25.5	23.05

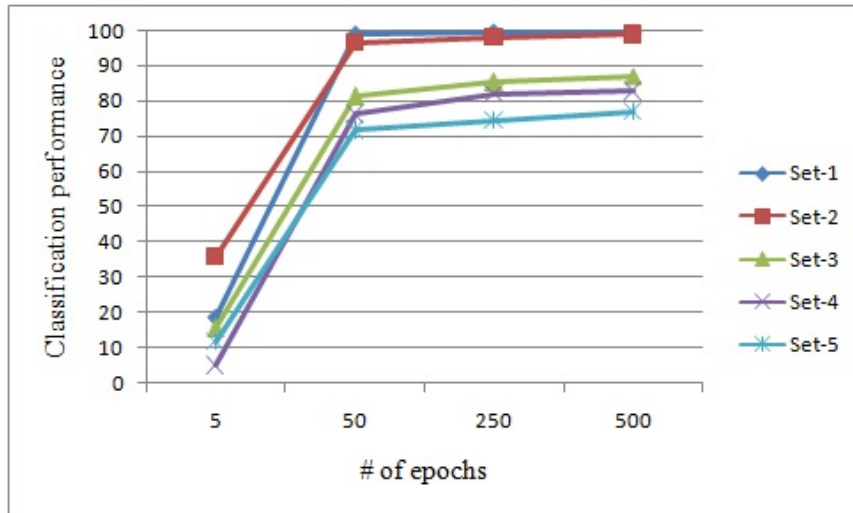


**Fig. 6.6:** Classification performance (%) on five sets of Extended Yale Face dataset B

The symmetry of facial information is considered along the vertical line passing through the center of the face image in order to address the issue. The training dataset

is enhanced by including the horizontal reflection of facial images. This enhancement will provide additional information to the classifier especially when there is a shadow on one side of the face. During testing, for a given facial image, the maximum value is considered among the evidences generated for each class to determine the output class. The misclassification error of the proposed approach with this enhancement is given in Table 6.3. Plot of classification performance against training epoch is shown in Fig. 6.7.

**Table 6.4:** Classification performance (%) of the proposed approach on the enhanced facial data

Set #	5 epochs	50 epochs	250 epochs	500 epochs
1	41.01	0.88	0.4	0.35
2	96.43	5.21	4.38	0.76
3	64.96	4.08	2.11	1
4	53.16	12.89	5.73	4.89
5	70.11	34.43	24.28	22.95

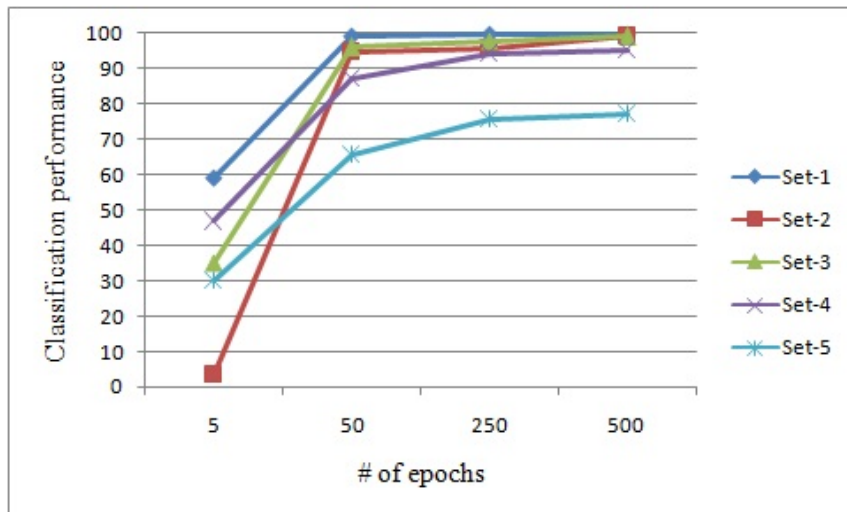


**Fig. 6.7:** Classification performance (%) including the horizontally reflected facial images on five sets of Extended Yale Face dataset B

An average classification accuracy of 94.01% is obtained by the proposed approach

on the enhanced facial data. It can be observed that the performance of the proposed approach improves by 4.96% when horizontal reflections of the facial data are considered in training.

The performances of existing approaches DT-CWT (dual-tree complex wavelet transform) [133]- [134], LBP (local binary patterns) [135], SQI (self quotient image) [136], LTV (logarithmic total variation) [137], LWT (logarithmic wavelet transform) [138], LNSCT (logarithmic nonsubsampled contourlet transform) [139] along with the two proposed approaches for facial recognition are given in Table 6.3. The classification performance of the existing methods and the proposed approach are shown in Fig. 6.8.

**Table 6.5:** Comparison of classification (%) performance with existing approaches

	Set 1	Set 2	Set 3	Set 4	Set 5	Avg.
LBP	100	100	62.28	10.34	6.65	55.85
Curvelet	91.66	100	55.92	14.85	5.95	53.67
Contourlet	76.31	98.68	52.19	22.36	9.83	51.87
DT-CWT	98.68	99.34	76.75	38.91	13.85	65.49
SQI	100	98.68	71.27	69.37	63.98	80.66
LTV	100	99.78	78.51	75.75	82.41	87.29
LWT	100	100	82.01	81.95	70.77	86.95
LNSCT	100	100	83.33	87.96	84.34	91.126
Proposed CNN	99.65	98.79	87.07	82.81	76.95	89.05
<b>Proposed CNN (reflection)</b>	<b>99.65</b>	<b>99.24</b>	<b>99</b>	<b>95.11</b>	<b>77.05</b>	<b>94.01</b>

The low classification accuracy for facial images in set-5 is due to the extreme illumination conditions as shown in the last row of Fig. 6.5. It is assumed that the performance of the proposed facial recognition approaches is unaffected by the inclusion of additional subjects, due to the uniform distribution of subjects facial images across

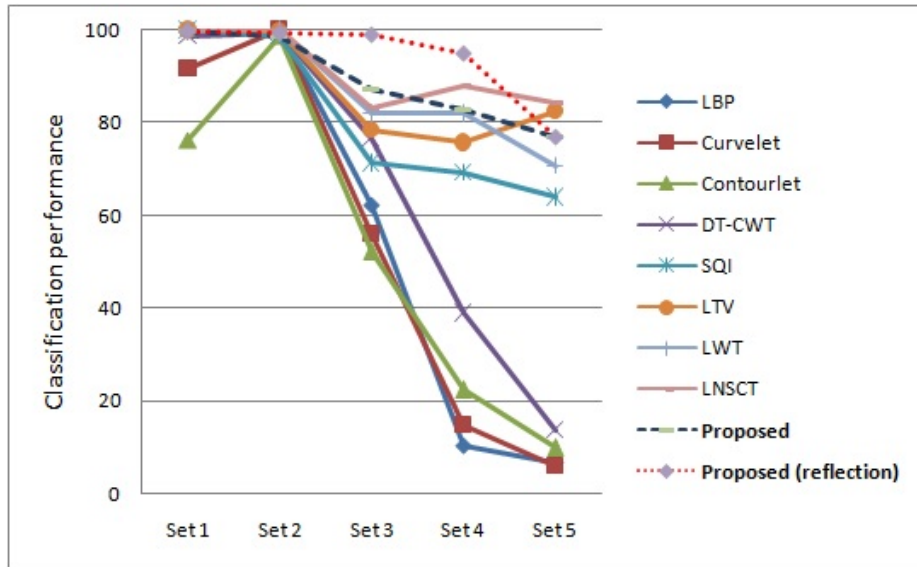


**Fig. 6.8:** Comparison of classification (%) performance with existing methods

all the five sets, thereby enabling the comparability of the proposed approach with the existing approaches as shown in Table 6.3. Table 6.3 shows the effectiveness of the proposed approaches for facial recognition. It is time consuming to train the convolutional neural network as the input image size increases.

#### 6.4 SUMMARY

In this chapter, a de-duplication process is implemented in large scale database of photographs. In the proposed method, an attempt is made to eliminate the duplicate ration cards from the database using histogram refinement technique. The proposed method eliminated nearly 0.35 million (approximately) duplicate ration cards. Also, an approach for illumination invariant facial recognition is proposed using convolutional neural networks (CNN) especially in the context of de-duplication process on the face images collected in out-door environment. CNN is used to learn the discriminative local patterns to recognize subjects from their facial images. Experiments conducted on Extended Yale Face Database B demonstrate the effectiveness of the proposed approach.

## CHAPTER 7

### UNIQUE IDENTITY CREATION USING MULTIMODAL BIOMETRICS FOR E-SOCIETY APPLICATIONS

In this chapter, some issues related with biometric data acquisition and storage are addressed while creating a persons' identity in the e-Society. The best practices for biometric data acquisition and identity creation is presented using multi-modal biometrics (fingerprints, iris, face and signature). Assigning a permanent identification number for every person in the E-Society would remove the need for a person to produce multiple documentary proofs of his identity for availing any government or private services. Multi-modal biometrics play an important role in creating unique identity for every person. Multimodal biometrics means combining two or more biometric modalities in the development of a single biometric identification system. Biometric recognition systems based solely on uni-modal biometrics will not meet the desired biometric performance requirements in large-scale biometric applications due to the problems such as noisy biometric information, failure to enroll rate, spoof attacks, unacceptable error rates and environmental conditions.

A fingerprint authentication approach is proposed for public distribution system (PDS) using point of sale (PoS) device. The public distribution system finds the genuine beneficiaries with the help of electronic fingerprint authentication system, and aadhaar central identification repository (CIDR). However, due to the smartcard storage constraints and cost-effectiveness, the utilization of data should be minimal. So, there is a need for compression of the biometric data without loss of important information or essential features of biometrics which are useful for identification. In order to store the signature biometric on a smart card, a novel algorithm is proposed



for reducing the size of data.

This chapter is organized as follows: Unique identity creation using compressed biometric data is explained in Section 7.1. Section 7.2 presents an application of biometrics in e-Governance using hand-held fingerprint units.

## **7.1 UNIQUE IDENTITY CREATION USING COMPRESSED BIOMETRIC DATA**

Data compression [140] can be divided into lossy and lossless compression techniques. Loss-less compression means the exact data can be reconstructed same as in original image, whereas the lossy compression techniques allows some image quality degradation with high compression ratio [141], [142]. BMP is a bitmap image format which has the image files of uncompressed raster graphics. JPEG (joint photographic experts group) image format allows the adjustable compression which balances both the size and quality of the image. In JPEG2000, the quality and adjustable compression ratio is improved. WSQ (wavelet scalar quantization) is a compression algorithm implemented for 8-bit grey-scale fingerprint images. GIF (graphics interchange format) is a bitmap image format limited to 256 colors or 8-bit palette and it is ineffective for detailed images. PNG (portable network graphics) is a lossless format, created to improve upon and to be a replacement for GIF format. TIFF (tagged image file Format) image format uses a lossless compression algorithm where the compression ratio is improved with bi-level images. The comparison between these image formats are already done in the context of biometric systems where the lossy compression techniques do not give much degradation in the quality of biometric image data. The impact of JPEG, JPEG2000, SPIHT (set partitioning in hierarchical trees), PRVQ (predictive residual vector quantization), and fractal image compression on recognition accuracy of selected fingerprint and face recognition systems is explained in [143]. Similarly, [144] also relates JPEG, JPEG2000, and WSQ compression rates to recognition performance of some fingerprint and face recognition systems. Few compression techniques

are analyzed on standard iris databases [145]. A drawback of lossy techniques as compared to lossless ones is their often significantly higher computational demand.

The lossless compression algorithms exploit the directional features in fingerprint images caused by ridges and valleys. A scanning procedure and the direction of dominant ridges are added to improve the lossless coding results as compared to JPEG-LS and PNG [146]. Few lossless compression algorithms [147] are compared when applied to multi-modal biometrics image data like fingerprints, hand data, face imagery, retina, and iris. Based on several evaluations and the most relevant compression algorithms for iris, fingerprints and face biometrics are Jp2 (JPEG2000), WSQ and JPEG image formats, respectively. The compression algorithms are more optimal and reliable. A new algorithm is proposed to compress the signature biometrics. And also, for better compression ratio, the quality of biometrics is always important while capturing the biometrics using biometric sensors. The best practices for acquiring the biometric data are presented in this work.

### 7.1.1 Best practices for biometric enrollments

Enrollment of each person can be registered by capturing the 10 fingerprints (in 4-4-2 manner) using L1 TP-AGILE device, 2 Iris images using L1 Mobile Eyes, face image using Canon digital camera and signature using Topaz signature pad as shown in Fig. 7.1. Quality assessment takes place while the capture process going on since there is an inbuilt quality checks based on some international standards. Apart from these quality checks, the operator at the enrollment station should take care some of the best practices to get the quality biometric data captured.

**Fingerprints:** One way of acquiring fingerprints is to capture the slap fingerprint. Slap fingerprints [115] are taken by pressing four fingers simultaneously onto a slap fingerprint scanner. In general, the capturing process will take place in the fashion of 4-4-2 fingers (as shown in Fig. 7.2), means capture left four fingers at one time, followed by all right four fingers and then followed by two thumb fingers. The fingerprints



**Fig. 7.1:** Enrollment station with biometric sensors

captured in this fashion reduces the time taken for capturing process. The captured slap fingerprints go for the slap fingerprint segmentation which splits the individual fingers from the slap image. The left four fingers slap can be segmented as in the sequence of left little (LL), left ring (LR), left middle (LM) and left index (LI). The right four fingers slap can be segmented as in the sequence of right index (RI), right middle (RM), right ring (RR) and right little (RL). The two thumb fingers can be segmented as left thumb (LT) and right thumb (RT). The quality of fingerprints can be assessed by NFIQ (NIST Fingerprint Image Quality) score. NFIQ score ranges on the scale 1 to 5, where lesser quality score represents good quality and higher quality score represents poor quality.

The enrollment application should provide the feedback if captured images are of bad quality. The application should have the capability of performing a sequence check and also have the capability of indicating any wrong hand placement. The application should also indicate mismatch between expected fingers based on amputation status versus actual segmented finger count. Apart from these practices, the following are the few things to take care while capturing fingerprints:

- Before capturing process initiates, if the finger is wet then make sure it is dry by cleaning the fingers with a smooth cloth. Also, it should not be too dry.

- Place the finger flat on the scanner.
- Place the bulb area of fingerprint on the sensor surface and apply smooth pressure.
- Operator need to be well trained to capture the fingers in proper sequence.
- The scanner need to be cleaned to avoid ghost fingers present on sensor surface which are placed while capturing the previous fingers.
- For old age people, the finger might be in dry and/or shivering nature, then the operator need to assist those people.



**Fig. 7.2:** 4-4-2 Fingerprints

**Iris:** The iris image can be captured both at a time using Mobile Eyes device. Apart from the quality checks in device-level, operator should assist the user to open the eyes properly in order to capture the iris image. The distance between the camera and iris images should not be too long or too short. The sample images are shown in Fig. 7.3.

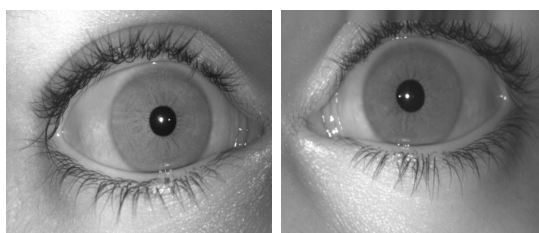


**Fig. 7.3:** Iris images

**Face:** The face photograph should meet the international civil aviation organization (ICAO) [148] standard. The enrollment station should allow at-least three attempts in order to select best face image among the captured attempts. The quality of the face image can be assessed based on the following parameters: *no hair covering front of face, eyes open, no portrait style images, eyes on same horizontal line, single color background, face centered, no single flash or flash artifacts, no red-eye, no shadows on background, no shadows on face, no sunglasses, no glare on glasses, remove hats, no shadows on face from religious head gear, lower veil to expose center of face from roughly crown to chin and ear to ear, no other face or partial face in image and no toys or other objects in image.* The sample photograph that meets all these parameters is shown in Fig. 7.4.



**Fig. 7.4:** Face photograph

**Signature:** The image captured using Topaz signature pad is of size 500×150. It is re-sampled to 168×44 image size in order to reduce the image size without loss of essential information. In case of physically challenged people/illiterates, a default single horizontal line should be assigned as the persons' signature by the application.



**Fig. 7.5:** Signature

### 7.1.2 Proposed compression algorithm for signature biometrics

The proposed compression algorithm is named as SIGN (signature data format). The following are the steps involved in the proposed signature image compression algorithm:

1. Input for the compression algorithm is the signature image with size  $500 \times 150$ .
2. Re-sample the image to a smaller image whose dimensions are multiples of 4, for example, the re-sampled image size is  $168 \times 44$ .
3. Extract the raw bytes from the image where each byte is the representation of pixels in the image. Typically, each pixel has gray scale variations from 0 to 255.
4. Binarize the re-sampled image in the fashion of assigning the values 0 or 1 for each raw byte with a threshold of 200.
5. Select all the consecutive 7 bytes from the binary array and represent the byte values as a single byte which have the most significant bit (MSB) is one followed by the 7 bytes, if the byte values contains at least one black pixel as shown in Fig. 7.6.
6. If more white pixels, fill MSB=0 and consecutive number of white byte groups as a single byte as shown in Fig. 7.6.
7. Output: Signature image of size  $500 \times 150$  is compressed to 30 bytes.

## 7.2 BIOMETRICS IN E-GOVERNANCE USING HAND-HELD FINGERPRINT UNITS

The fingerprints are mostly used in civilian applications due to its uniqueness and reliability. There are several fingerprint-based applications in the fields of forensics, border security, e-governance, academia and so on. Two different applications are presented using hand-held fingerprint terminals in the fields of e-governance and academia. One application is fingerprint-based on-line authentication approach for public distribution

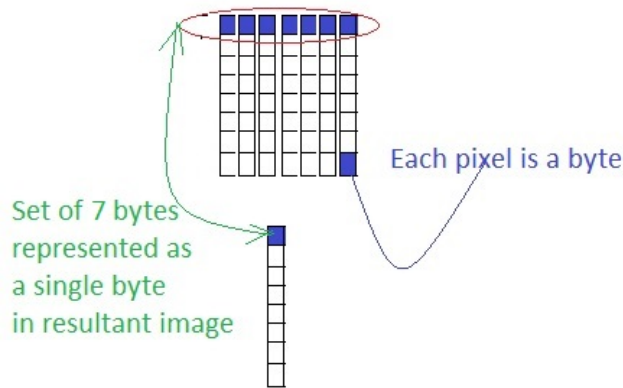


**Fig. 7.6:** Signature image compression

system (PDS) [149] using point of sale (PoS) device. After the implementation of India's large-scale aadhaar project, there is a growing demand for biometrics in public distribution systems (PDS). The goal of aadhaar project is to provide a Unique IDentity (UID) number for all the residents in India. A Unique IDentity number assigned for every person would obviate the need for a person to produce multiple documentary proofs of his/her identity for availing any government service. The unique identity number would remain a permanent identifier right from birth to death of every person in the country. UID would enable government to ensure that benefits under various welfare programs such as PDS reach the intended beneficiaries, prevent cornering of benefits by a few sections of people and minimize frauds. The main objective of the PDS is to find the genuine beneficiaries with the help of electronic fingerprint authentication system.

### 7.2.1 Aadhaar authentication

Aadhaar authentication is an on-line process of submitting aadhaar number along with other attributes, including biometrics to the central identification repository. Aadhaar authentication provides several ways in which a resident can authenticate themselves using the system. At a high level, authentication can be demographic authentication

and/or biometric authentication. During the authentication transaction, the resident's record is first selected using the aadhaar number and then the demographic/biometric inputs are matched against the stored data provided by the resident during enrollment/update process.

The point of sale (PoS) device is used in the proposed methods of fingerprint authentication or verification which consists of the display module, communication module, biometric module and printer. The communication modules are GPRS modem and ethernet connection. The PoS device consists of the UID compatible application interface for generating the request which is compatible with UID/Aadhaar authentication. The device will be placed at the fair-price-shop (FP shop) with the dealer. The device is locked with the particular FP shop dealer to make sure the device is operated by dealer only with his UID authentication. The PoS based on-line authentication systems have lot of advantages over traditional smart card authentication systems [150].

### **7.2.2 Fingerprint authentication approach using PoS units**

The fingerprint authentication workflow for the public distribution system is explained as follows:

1. The residents provide aadhaar number, necessary demographic and biometric details at PoS terminals to an operator.
2. Each device is installed with the aadhaar authentication-enabled software which packages the input parameters. The package will be encrypted and transmitted to the authentication server using a broadband/mobile network.
3. Authentication server validates the package and adds necessary headers (license key, transaction id, etc.), and passes the request to the central server (UIDAI CIDR).
4. Aadhaar authentication server returns a yes/no based on the match-ability of the input parameters.



5. The operator proceeds with the transaction based on the response at the PoS device.

The advantages of using PoS based biometric authentication system are:

1. Fast and efficient services are provided to the beneficiaries.
2. The commodities will be allocated to the FP shop based on the real time closing balances.
3. The accountability and transparency is increased at FP-shop level.
4. Eligible beneficiaries can get the commodities without wastage.

The program requires UID number as primary authentication for distribution of commodities. There is a secondary authentication method using mobile numbers for the residents who are not having the aadhaar numbers. The PoS terminal generates a one time password (OTP) and will be verified using the SMS received in the mobile. If the user does not have UID as well as mobile number, a government supervisor will authenticate on behalf of the beneficiary.

It is observed that the failure-to-capture rate exists for the people who works hard, old aged, people with leprosy, very dry fingers, very wet fingers, people with shivering hands. Nearly 60% of the people are able to authenticate in the first attempt, 30% to 35 % people are able to authenticate with in 4 attempts and 0.5% are not able to authenticate, mainly due to old age or leprosy.

### **7.3 EXPERIMENTAL RESULTS**

**Compressed biometric data** The experiments are conducted using the sample multi-modal biometric data collected in such a way that the 10 fingerprints (in 4-4-2 manner) using L1 TP-AGILE device, 2 iris images using L1 mobile eyes, face image using canon digital camera and signature using topaz signature pad. Table 7.3 shows different image sizes of raw biometric data.

**Table 7.1:** The standard biometric image dimensions

Biometric Image	Image dimension	Size (raw)	Size (compressed)
Iris	640×480	301KB	80-120KB
Slap (4-4-2)	1600×1500	2.3MB	NA
Two Finger	900×900	792KB	NA
Single Finger	Variable	200-800KB	10-20KB
Face	480×600	288KB	20-40KB
Signature	168×44	7.392KB	924 bytes

For creating a biometric-based identity, it should at least have the biometric information of 2 iris images, 2 fingerprints, 1 face photograph and 1 signature. The space required to store all these information in a smart card is around 1.365MB (minimum) to 2.565MB (maximum). It is a huge memory to store in a smart card which should be cost-effective. After compressing the biometric data using the relevant compression algorithms like WSQ (for fingerprints), JPEG2000 (for iris), JPEG (for face) and SIGN (for signature), the space required to store the compressed biometric information in smart card is around 111-181KB.

**PDS fingerprint authentication and its proof of concept** The proof of concept was implemented in 100 fair price (FP) shops in Andhra Pradesh, India. As part of this analysis, rural, urban and hamlet areas are chosen. Nearly 85 percent of the beneficiaries have the UID numbers and remaining 15 percent beneficiaries have enrollment Id (EID) numbers. The beneficiaries who have UID numbers are authenticated using fingerprints captured from PoS unit. The beneficiaries with EID numbers are authenticated using one time password (OTP) or authorized village servants' UID on behalf of the beneficiary. Initially, in the first month of implementation, 97 percent of the beneficiaries are authenticated with their fingerprints and the remaining 3 percent of the beneficiaries are mis-mapped their UIDs at the central server. In the second

month, 99 percent of the beneficiaries are authenticated with their fingerprints and rest of the beneficiaries were not able to authenticate due to the bad quality fingerprints. The authentication accuracy is improved by fusing the matching scores of two fingerprints.

Initially, the average number of authentications for each person was around two attempts. Later, it is reduced to 1.3 attempts using the method of 'best finger detection'. The 'best finger detection' method captures ten fingerprints of the beneficiary and sends the data in the form of UID compliant packet to the central server. It processes the request and gives the response of best fingers of the beneficiary on the rank scale of 1 to 10. If the fingerprints are not matched with the existing fingerprints data in the central server, the 'best finger detection' method prompts the message "recapture fingerprints again'. The implementation check out nearly 5 percent of the bogus cards and showed nearly 20 percent of savings to Government. The tests have been conducted on nearly 70000 families. Each family consists of approximately 4 persons and 85 percent of these families are having valid UID numbers.

#### **7.4 SUMMARY**

A unique identity (UID) creation for every person in the e-Society would obviate the need for a person to produce multiple documentary proofs of his identity. A novel algorithm for signature compression is proposed in order to compress the biometric data in an efficient manner. Each pixel byte value in the proposed algorithm is transformed as a single bit in the compressed signature data based on some empirical threshold. Experimental results shows that the proposed compression algorithm is more optimal and reliable. A fingerprint-based authentication approach is proposed for the applications in the field of e-Governance. The aadhaar authentication has been implemented in the 100 fair price (FP)-shops in Andhra Pradesh, India. It is observed that the process is faster than the traditional method of smart-card based authentication.

## CHAPTER 8

### CONCLUSIONS AND FUTURE WORK

In this thesis, we have proposed the methods to address two important issues in the large-scale de-duplication applications, namely, the speed of the matching and the accuracy of the matching. An iris classification approach was proposed based on sparse representation of Gabor features using dictionary learning for large-scale de-duplication applications. Also, an iris adjudication process was explained by comparing the matched iris-pair images side-by-side to make the decision on the identification score using color coding. The proposed iris de-duplication architecture did improve the speed of identification process and reduce the identification errors in large-scale de-duplication applications. A de-noising approach was proposed for accurate slap fingerprint segmentation which improves the performance of de-duplication process. A new cross-sensor adaptation algorithm is proposed for fingerprint biometrics using kernel transformation learning in order to improve the fingerprint matching performance while upgrading with new fingerprint scanners in large-scale applications which often lead to reduced fingerprint matching performance. The facial enrollments under different illumination conditions in outside environment produces degraded performance of face recognition. A new method for face recognition was proposed using convolutional neural networks in order to improve the identification performance in different illumination conditions. A new approach for photograph de-duplication was proposed using color histograms to eliminate the duplicate ration cards in targeted public distribution system. The best practices for biometric data acquisition and identity creation were presented using multi-modal biometrics (fingerprints, iris, face and signature) in order to minimize the data storage on a smart card.

## 8.1 CONTRIBUTIONS OF THE WORK

In the first de-duplication case study, Government of Andhrapradesh undertook the de-duplication of ration cards using 52 million people iris codes. The number of iris comparisons are performed over 6.26 quadrillion times to remove duplicate enrollments in 61 days which is not a scalable solution. In this thesis, we propose an approach for classification of iris images based on sparse representation of Gabor features using dictionary learning for large-scale de-duplication applications. Sparse coding involves the representation of an image as a linear combination of some atoms in a dictionary. The signals and images of interest tend to enjoy the property of being sparse in some dictionary. These dictionaries are often learned directly from the training data. Iris classification and adjudication framework is proposed in iris de-duplication architecture to speed-up the identification process and to reduce the identification errors.

In the second de-duplication application, Government of Orissa collected a total of 1.8 million slap fingerprint images of 0.6 million citizens as part of targeted public distribution system (TPDS) process. The slap fingerprint images had some noisy data due to some external factors which affect the calibration process of the fingerprint device. While doing the segmentation of these slap fingerprints, some of the fingerprint images are improperly segmented because of the noise present in the data and as a result, there is a reduction in the performance of de-duplication process. A de-noising approach is proposed to remove the noise present in the data using binarization of slap fingerprint image and region labeling of desired regions with 8-adjacency neighborhood. A framework is proposed to improve the fingerprint matching performance for cross-sensor adaptation in two different phases. In the first phase, few training samples were selected from three different fingerprint scanners. These samples are used to learn the adaptation parameters from optimized kernel matrix using the initial kernel matrix calculated with similarity measures of all selected samples. A convex optimization problem was formulated to minimize the logDet divergence between the initial kernel matrix and adapted kernel matrix. The sensor adaptation parameters were

calculated by imposing the distance preserving constraints and application-specific constraints. These constraints reduces the sensor mismatch problem when the matching performed for cross-sensor in the transformed domain. In the second phase, these parameters are incorporated while fingerprint matching in transformed domain. Also, a semi-automated latent fingerprint identification is proposed to markup fingerprint landmarks manually using the image enhancement filters which will further improve the identification performance.

In the third de-duplication scenario, Government of Andhra Pradesh has issued around 22 million ration cards in which there are few duplicate ration cards created in an unauthorized manner in order to mislead the benefits of beneficiaries. We propose a method for de-duplication of face photographs based on color histograms. Also, the issue of degraded face recognition rate with non-uniform illumination conditions is addressed in face photograph de-duplication, especially in outdoor environment. A new method is proposed for face recognition to address the issue of non-uniform illumination using convolutional neural networks (CNN). The symmetry of facial information is exploited to improve the performance of the face recognition system by considering the horizontal reflections of facial images.

Also, the thesis addresses some issues related with biometric data acquisition and storage while creating a persons' identity in the e-Society. The best practices for biometric data acquisition and identity creation is presented using multi-modal biometrics (fingerprints, iris, face and signature). In order to store the signature biometric on a smart card, a novel algorithm is proposed for reducing the size of data.

## **8.2 DIRECTIONS FOR FUTURE RESEARCH**

In this thesis, we have proposed the methods to address two important issues in the large-scale de-duplication applications, namely, the speed of the matching and the accuracy of the matching. An iris classification approach was proposed based on sparse representation of Gabor features using on-line dictionary learning (ODL) for large-

scale de-duplication applications. Also, an iris adjudication process was illustrated by comparing the matched iris-pair images side-by-side to make the decision on the identification score using color coding. The proposed iris de-duplication architecture did improve the speed of identification process and reduce the identification errors in large-scale de-duplication applications. The data used for iris classification was collected under visible illumination. Most of the iris recognition systems use the data acquired at near infra-red (NIR) wavelengths. These systems are more accurate among all the existing biometric recognition systems. It is very hard to label the iris classes in the available standard near infra-red databases. The same experimental setup should be executed for the near infra-red iris database which have more texture information to distinguish the iris labels.

A de-noising approach was proposed for accurate slap fingerprint segmentation which improved the performance of de-duplication process. Even though there exists different fingerprint classification approaches to speed up the identification process, integrating both proposed denoising approach and existing fingerprint classification with fingerprint de-duplication architecture might further improve the de-duplication performance. A new sensor adaptation algorithm was proposed for fingerprint biometrics using kernel transformation learning in order to improve the fingerprint matching performance in the context of large-scale fingerprint de-duplication system. The kernel dimensionality reduction may be explored for the fingerprint biometrics using the proposed framework and also different domain adaptation algorithms should be explored. Similar cross-sensor adaptation algorithms for multi-modal biometric recognition systems will also be considered in the future.

The face enrollments under different illumination conditions in the outside environment degrade the performance of face recognition. A new method was proposed for face recognition under non-uniform illumination using convolutional neural networks. The experiments were conducted using the standard face dataset. In order to study this illumination invariant face recognition especially in surveillance applications, the data should be collected at-a-distance and execute the experiments using CNN.

## APPENDIX A

### SPARSE REPRESENTATIONS

Suppose that there are  $K$  iris classes, and each iris class has a set of  $N$  iris images. Let a  $d$ -dimensional feature vector be extracted from each iris image. Let  $A_k$  be a  $d \times N$  matrix of feature vectors of the  $k^{th}$  class, where the column  $a_{kn} = [a_{kn1} a_{kn2} \dots a_{knd}]^T$  denotes the  $d$ -dimensional feature vector of the  $n^{th}$  iris image belonging to the  $k^{th}$  class.

$$A_k = [a_{k1} a_{k2} \dots a_{kn} \dots a_{kN}] \in R^{d \times N} \quad (\text{A.1})$$

An iris dictionary  $A$  can be dened as follows:

$$A = [A_1 A_2 \dots A_k \dots A_K] \in R^{d \times KN} \quad (\text{A.2})$$

where  $K$  represents some of the feature vectors from three different iris classes. Let  $y \in R^d$  be an observed feature vector extracted from a test iris image. The  $y$  can be expressed as a linear weighted sum of columns of iris dictionary  $A$  as

$$y = \sum_{k=1}^K \sum_{n=1}^N x_{kn} a_{kn} \quad (\text{A.3})$$

where the scalar  $x_{kn}$  is the weight associated with the column  $a_{kn}$ . The above equation can also be written in the matrix form as

$$\mathbf{y} = \mathbf{A}\mathbf{x} \quad (\text{A.4})$$

and the residual can be written as

$$r(y) = y - Ax \quad (\text{A.5})$$



The observation vector  $y$  belongs to a particular class meaning that it is approximately comes in the linear span of the training vectors of that iris class. In other words, the coefficients of the weight vector  $x$  that does not belong to that particular iris class are very close to zero and also  $x$  gives more sparsity with very few nonzero coefficients. The given system of linear equations in (A.4) is underdetermined, since the size of the feature vector ( $d$ ) is much greater than the number of feature vectors concatenated in the iris dictionary. The sparsest solution can be obtained from the infinitely many solutions by solving the following optimization problem

$$\min_x \|x\|_0 \text{ subject to } y = Ax, \quad (\text{A.6})$$

where  $\|x\|_0$  is zero norm of weight vector  $x$  which mean the number of nonzero coefficients in weight vector  $x$ . There were many iterative algorithms proposed like matching pursuit (MP), and orthogonal matching pursuit (OMP) to address the above optimization problem [10]. In the proposed iris classification methodology, OMP algorithm is chosen to calculate the approximate sparse weight vector  $x$  [3]. The main goal of the algorithm is to identify sparse weight vector  $x$  which gives a few nonzero coefficients. These coefficients will determine the few columns of  $A$  that participate in the representation of observation vector  $y$ . The algorithm chooses those columns in a greedy fashion. The following are the steps involved in OMP algorithm [3].

1. The sparse weight vector  $x$  is initialized with zero, ( $x^0 = 0$ ). The initial residual is,  $r^0(y) = y - Ax^0 = y$ . The solution support is initialized with  $S^0 = \text{Support}\{x^0\} = \phi$
2. Since the residual error depends on  $\|y\|_2$ , a fraction of  $\|y\|_2$  can be used as error threshold, i.e.,  $\theta_0 = \lambda\|y\|_2$ , where  $0 < \lambda < 1$ . The value should not be very high or very low. If the value is very high, it may not capture the iris class-specific characteristics. On the other hand, a low value of  $\lambda$  may spoil the sparsity of the weight vector  $x$  while minimizing the residual error.
3. The first iteration of the algorithm starts with  $k = 1$ .

4. The errors are computed for all columns of  $A$  using  $\theta(c) = \min_{z_c} \|a_c z_c - r^{k-1}\|_2^2$ , where  $c$  represents the column index and  $z_c = a_c^T r^{k-1} / \|a_c\|_2^2$ .
5. Among all the column errors, find a minimizer  $c_0$  from  $\theta(c)$  in such a way that the column should not be an element in previous solution support and  $\theta(c_0) \leq (c)$ . Update the solution support  $S^k$  by adding the minimizer  $c_0$  to previous solution support  $S^{k-1}$ .
6. Based on the updated solution support  $S^k$ , compute the sparse weight vector  $x^k$  by solving the  $\min \|y - Ax\|_2^2$ .
7. The residual is again computed for the current iteration using  $r^k = b - Ax^k$ .
8. If the  $l_2$  norm for the updated residual is below the predefined error threshold  $\theta_0$ , then  $x^k$  becomes the solution. Otherwise, repeat the steps from 4, by incrementing  $k$  by 1.

## APPENDIX B

### SUPPORT VECTOR MACHINES

The support vector machine (SVM) is a linear machine pioneered by Vapnik. The main idea of an SVM is to construct a hyperplane as the decision surface in such a way that the margin of separation between positive and negative examples is maximized. The notion that is central to the construction of the support vector learning algorithm is the innerproduct kernel between a support vector  $\mathbf{x}_i$  and a vector  $\mathbf{x}$  drawn from the input space. The support vectors constitute a small subset of the training data extracted by the support vector learning algorithm. The separation between the hyperplane and the closest data point is called the margin of separation, denoted by  $\rho$ . The goal of a support vector machine is to find a particular hyperplane for which the margin of separation  $\rho$  is maximized. Under this condition, the decision surface is referred to as the optimal hyperplane. Fig. B.1 illustrates the geometric construction of a hyperplane for two dimensional input space. The support vectors play a prominent role in the operation of this class of learning machines. In conceptual terms, the support vectors are those data points that lie closest to the decision surface, and therefore the most difficult to classify. They have a direct bearing on the optimum location of the decision surface.

The idea of an SVM is based on the following two mathematical operations:

1. Nonlinear mapping of an input pattern vector onto a higher dimensional feature space that is hidden from both the input and output.
2. Construction of an optimal hyperplane for separating the patterns in the higher dimensional space obtained from operation 1.

Operation 1 is performed in accordance with Cover's theorem on the separability of patterns. Consider an input space made up of nonlinearly separable patterns.

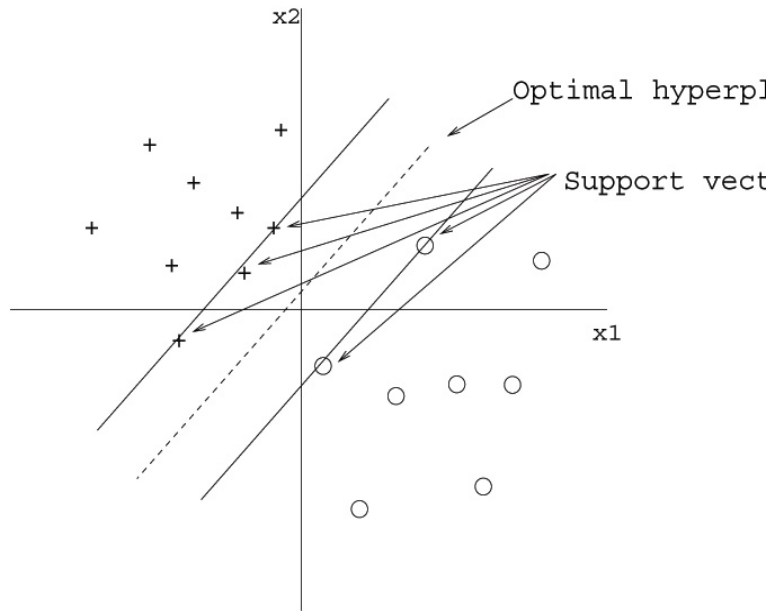


**Fig. B.1:** Illustration of the idea of support vectors and an optimal hyperplane for linearly separable patterns.

Cover's theorem states that such a multidimensional space may be transformed into a new feature space where the patterns are linearly separable with a high probability, provided the transformation is nonlinear, and the dimension of the feature space is high enough. These two conditions are embedded in operation 1. The separating hyperplane is defined as a linear function of the vectors drawn from the feature space. Construction of this hyperplane is performed in accordance with the principle of structural risk minimization that is rooted in Vapnik-Chervonenkis (VC) dimension theory [151]. By using an optimal separating hyperplane the VC dimension is minimized and generalization is achieved. The number of examples needed to learn a class of interest reliably is proportional to the VC dimension of that class. Thus, in order to have a less complex classification system, it is preferable to have those features which lead to lesser number of support vectors.

The optimal hyperplane is defined by:

$$\sum_{i=1}^{N_L} \alpha_i d_i K(\mathbf{x}, \mathbf{x}_i) = 0 \quad (\text{B.7})$$

where  $\{\alpha_i\}_{i=1}^{N_L}$  is the set of Lagrange multipliers,  $\{d_i\}_{i=1}^{N_L}$  is the set of desired classes and  $K(\mathbf{x}, \mathbf{x}_i)$  is the innerproduct kernel, and is defined by:

$$\begin{aligned} K(\mathbf{x}, \mathbf{x}_i) &= \varphi^T(\mathbf{x})\varphi(\mathbf{x}_i) \\ &= \sum_{j=0}^{m_1} \varphi_j(\mathbf{x})\varphi_j(\mathbf{x}_i), \quad i = 1, 2, \dots, N_L \end{aligned} \quad (\text{B.8})$$

where  $\mathbf{x}$  is a vector of dimension  $m$  drawn from the input space, and  $\{\varphi_j(\mathbf{x})\}_{j=1}^{m_1}$  denotes a set of nonlinear transformations from the input space to the feature space.  $\varphi_0(\mathbf{x}) = 1$ , for all  $\mathbf{x}$ .  $m_1$  is the dimension of the feature space. From (B.7) it is seen that the construction of the optimal hyperplane is based on the evaluation of an innerproduct kernel. The innerproduct kernel  $K(\mathbf{x}, \mathbf{x}_i)$  is used to construct the optimal hyperplane in the feature space without having to consider the feature space itself in explicit form.

The design of a support vector machine involves finding an optimal hyperplane. In order to find an optimal hyperplane, it is necessary to find the optimal Lagrange multipliers which are obtained from the given training samples  $\{(\mathbf{x}_i, d_i)\}_{i=1}^{N_L}$ . Dimension of the feature space is determined by the number of support vectors extracted from the training data by the solution to the optimization problem (B.7).

## REFERENCES

- [1] T. Mansfield, G. Kelly, D. Chandler, and J. Kane, “Biometric product testing final report,” *Computing, National Physical Laboratory, Crown Copyright, UK*, 2001.
- [2] W. Zhao, R. Chellappa, P. J. Phillips, and A. Rosenfeld, “Face recognition: A literature survey,” *Acm Computing Surveys (CSUR)*, vol. 35, no. 4, pp. 399–458, 2003.
- [3] K. Delac and M. Grgic, “A survey of biometric recognition methods,” in *Electronics in Marine. 46th International Symposium*, pp. 184–193, IEEE, 2004.
- [4] C. W. Oyster, *The human eye*. Sinauer Associates, 1999.
- [5] J. Daugman and C. Downing, “Epigenetic randomness, complexity and singularity of human iris patterns,” *Proceedings of the Royal Society of London. Series B: Biological Sciences*, vol. 268, no. 1477, pp. 1737–1740, 2001.
- [6] L. Flom and A. Safir, “Iris recognition system,” Feb. 3 1987. US Patent 4,641,349.
- [7] R. Johnson, “Can iris patterns be used to identify people,” *Los Alamos National Laboratory, CA, Chemical and Laser Sciences Division, Rep. LA-12331-PR*, 1991.
- [8] J. Daugman, “How iris recognition works,” *Circuits and Systems for Video Technology, IEEE Transactions on*, vol. 14, no. 1, pp. 21–30, 2004.
- [9] J. G. Daugman, “High confidence visual recognition of persons by a test of statistical independence,” *Pattern Analysis and Machine Intelligence, IEEE Transactions on*, vol. 15, no. 11, pp. 1148–1161, 1993.
- [10] J. G. Daugman, “Biometric personal identification system based on iris analysis,” Mar. 1 1994. US Patent 5,291,560.
- [11] A. L. Yuille, P. W. Hallinan, and D. S. Cohen, “Feature extraction from faces using deformable templates,” *International journal of computer vision*, vol. 8, no. 2, pp. 99–111, 1992.
- [12] L. Masek *et al.*, “Recognition of human iris patterns for biometric identification,” *Masters thesis, University of Western Australia*, 2003.
- [13] J. Daugman, “New methods in iris recognition,” *Systems, Man, and Cybernetics, Part B: Cybernetics, IEEE Transactions on*, vol. 37, no. 5, pp. 1167–1175, 2007.
- [14] R. P. Wildes, “Iris recognition: an emerging biometric technology,” *Proceedings of the IEEE*, vol. 85, no. 9, pp. 1348–1363, 1997.
- [15] Y.-P. Huang, S.-W. Luo, and E.-Y. Chen, “An efficient iris recognition system,” in *Machine Learning and Cybernetics, Proceedings. 2002 International Conference on*, vol. 1, pp. 450–454, 2002.

- [16] Y. Liu, S. Yuan, X. Zhu, and Q. Cui, "A practical iris acquisition system and a fast edges locating algorithm in iris recognition," in *Instrumentation and Measurement Technology, Proceedings of IEEE International Conference on*, vol. 1, pp. 166–169, 2003.
- [17] H. Sung, J. Lim, J.-h. Park, and Y. Lee, "Iris recognition using collarette boundary localization," in *Pattern Recognition (ICPR), Proceedings of the 17th International Conference on*, vol. 4, pp. 857–860, 2004.
- [18] Z. Sun, T. Tan, and Y. Wang, "Robust encoding of local ordinal measures: A general framework of iris recognition," in *Biometric Authentication*, pp. 270–282, Springer, 2004.
- [19] Z. Sun, Y. Wang, T. Tan, and J. Cu, "Robust direction estimation of gradient vector field for iris recognition," in *Pattern Recognition (ICPR), Proceedings of the 17th International Conference on*, vol. 2, pp. 783–786, 2004.
- [20] L. Ma, T. Tan, Y. Wang, and D. Zhang, "Efficient iris recognition by characterizing key local variations," *Image Processing, IEEE Transactions on*, vol. 13, no. 6, pp. 739–750, 2004.
- [21] L. Ma, T. Tan, Y. Wang, and D. Zhang, "Local intensity variation analysis for iris recognition," *Pattern Recognition*, vol. 37, no. 6, pp. 1287–1298, 2004.
- [22] L. Chenhong and L. Zhaoyang, "Efficient iris recognition by computing discriminable textons," in *Neural Networks and Brain (ICNN&B), International Conference on*, vol. 2, pp. 1164–1167, 2005.
- [23] C.-T. Chou, S.-W. Shih, W.-S. Chen, and V. W. Cheng, "Iris recognition with multi-scale edge-type matching," in *Pattern Recognition (ICPR), 18th International Conference on*, vol. 4, pp. 545–548, 2006.
- [24] P. Yao, J. Li, X. Ye, Z. Zhuang, and B. Li, "Iris recognition algorithm using modified log-gabor filters," in *Pattern Recognition (ICPR), 18th International Conference on*, vol. 4, pp. 461–464, 2006.
- [25] D. M. Monro, S. Rakshit, and D. Zhang, "Dct-based iris recognition," *Pattern Analysis and Machine Intelligence, IEEE Transactions on*, vol. 29, no. 4, pp. 586–595, 2007.
- [26] K. W. Bowyer, K. I. Chang, P. Yan, P. J. Flynn, E. Hansley, and S. Sarkar, "Multi-modal biometrics: an overview," in *Second Workshop on Multi-Modal User Authentication*, 2006.
- [27] K. I. Chang, K. W. Bowyer, and P. J. Flynn, "An evaluation of multimodal 2d+ 3d face biometrics," *Pattern Analysis and Machine Intelligence, IEEE Transactions on*, vol. 27, no. 4, pp. 619–624, 2005.
- [28] P. J. Phillips, P. J. Flynn, T. Scruggs, K. W. Bowyer, and W. Worek, "Preliminary face recognition grand challenge results," in *Automatic Face and Gesture Recognition (FGR), 7th International Conference on*, pp. 15–24, 2006.

- [29] Y. Du, "Using 2d log-gabor spatial filters for iris recognition," in *Defense and Security Symposium, International Society for Optics and Photonics*, pp. 62020F–62020F, 2006.
- [30] C. Liu and M. Xie, "Iris recognition based on dlda," in *Pattern Recognition (ICPR), 18th International Conference on*, vol. 4, pp. 489–492, 2006.
- [31] L. Ma, T. Tan, Y. Wang, and D. Zhang, "Personal identification based on iris texture analysis," *Pattern Analysis and Machine Intelligence, IEEE Transactions on*, vol. 25, no. 12, pp. 1519–1533, 2003.
- [32] E. Krichen, L. Allano, S. Garcia-Salicetti, and B. Dorizzi, "Specific texture analysis for iris recognition," in *Audio-and Video-Based Biometric Person Authentication*, pp. 23–30, Springer, 2005.
- [33] G. of Andhra Pradesh, "Civil supplies department," <http://www.apcivilsupplies.gov.in/>.
- [34] F. B. O. INVESTIGATION, "The science of fingerprints," *Washington, D. C.: U. S. Government Printing Office*, 1963.
- [35] U. Bradfor, H. Austin, W. Craig, I. Michael, and K. Kayee, "Slap fingerprint segmentation evaluation 2004 analysis report," tech. rep., Technical report, National Institute of Standards and Technology, 2005.
- [36] R. McCabe, "Ansi/nist-itl 1-2000 data format for the interchange of fingerprint, facial, and scar mark & tattoo (smt) information," 2000.
- [37] M. U. Akram, S. Nasir, A. Tariq, I. Zafar, and W. S. Khan, "Improved fingerprint image segmentation using new modified gradient based technique," in *Electrical and Computer Engineering (CCECE), IEEE Canadian Conference on*, pp. 001967–001972, 2008.
- [38] L. Hong, Y. Wan, and A. Jain, "Fingerprint image enhancement: algorithm and performance evaluation," *Pattern Analysis and Machine Intelligence, IEEE Transactions on*, vol. 20, no. 8, pp. 777–789, 1998.
- [39] D. Maltoni, D. Maio, A. K. Jain, and S. Prabhakar, *Handbook of fingerprint recognition*. springer, 2009.
- [40] P. Z.-P. Lo and P. V. Sankar, "Slap print segmentation system and method," July 4 2006. US Patent 7,072,496.
- [41] "Nist biometric image software," <http://biometrics.nist.gov/nigos/>.
- [42] B. Ulery, A. Hicklin, C. Watson, M. Indovina, and K. Kwong, "Slap fingerprint segmentation evaluation 2004," *Slapseg04 analysis report*, 2005.
- [43] M. Kaur, M. Singh, A. Girdhar, and P. S. Sandhu, "Fingerprint verification system using minutiae extraction technique.," *Proceedings of World Academy of Science: Engineering & Technology*, vol. 48, 2008.



- [44] M. Tarjoman and S. Zarei, "Automatic fingerprint classification using graph theory," in *Proceedings of World Academy of Science, Engineering and Technology*, vol. 30, pp. 831–835, 2008.
- [45] L. Wei, "Fingerprint classification using singularities detection," *international journal of mathematics and computers in simulation*, vol. 2, no. 2, pp. 158–162, 2008.
- [46] A. Lumini and L. Nanni, "Advanced methods for two-class pattern recognition problem formulation for minutiae-based fingerprint verification," *Pattern Recognition Letters*, vol. 29, no. 2, pp. 142–148, 2008.
- [47] A. K. Jain and J. Feng, "Latent fingerprint matching," *Pattern Analysis and Machine Intelligence, IEEE Transactions on*, vol. 33, no. 1, pp. 88–100, 2011.
- [48] L. Li, K. Lv, and N. He, "An improved cross-matching algorithm for fingerprint images from multi-type sensors," in *Image and Signal Processing (CISP), 2011 4th International Congress on*, vol. 3, pp. 1472–1475, 2011.
- [49] A. M. Bazen and S. H. Gerez, "Fingerprint matching by thin-plate spline modelling of elastic deformations," *Pattern Recognition*, vol. 36, no. 8, pp. 1859–1867, 2003.
- [50] A. Wahab, S. Chin, and E. Tan, "Novel approach to automated fingerprint recognition," in *Vision, Image and Signal Processing, IEE Proceedings-*, vol. 145, pp. 160–166, 1998.
- [51] D. R. Ashbaugh and C. Press, *Quantitative-qualitative friction ridge analysis: an introduction to basic and advanced ridgeology*. CRC press Boca Raton, 1999.
- [52] J. Qi and Y. Wang, "A robust fingerprint matching method," *Pattern Recognition*, vol. 38, no. 10, pp. 1665–1671, 2005.
- [53] N. K. Ratha, K. Karu, S. Chen, and A. K. Jain, "A real-time matching system for large fingerprint databases," *Pattern Analysis and Machine Intelligence, IEEE Transactions on*, vol. 18, no. 8, pp. 799–813, 1996.
- [54] A. Ross, A. Jain, and J. Reisman, "A hybrid fingerprint matcher," *Pattern Recognition*, vol. 36, no. 7, pp. 1661–1673, 2003.
- [55] X. Chen, J. Tian, and X. Yang, "A new algorithm for distorted fingerprints matching based on normalized fuzzy similarity measure," *Image Processing, IEEE Transactions on*, vol. 15, no. 3, pp. 767–776, 2006.
- [56] X. Luo, J. Tian, and Y. Wu, "A minutiae matching algorithm in fingerprint verification," in *Pattern Recognition, 15th IEEE International Conference on*, vol. 4, pp. 833–836, 2000.
- [57] N. K. Ratha, R. M. Bolle, V. D. Pandit, and V. Vaish, "Robust fingerprint authentication using local structural similarity," in *Applications of Computer Vision, Fifth IEEE Workshop on.*, pp. 29–34, 2000.

- [58] T.-Y. Jea and V. Govindaraju, “A minutia-based partial fingerprint recognition system,” *Pattern Recognition*, vol. 38, no. 10, pp. 1672–1684, 2005.
- [59] D. Maio, D. Maltoni, R. Cappelli, J. L. Wayman, and A. K. Jain, “Fvc2002: Second fingerprint verification competition,” in *Pattern Recognition, 16th IEEE International Conference on*, vol. 3, pp. 811–814, 2002.
- [60] L. O’Gorman and J. V. Nickerson, “An approach to fingerprint filter design,” *Pattern Recognition*, vol. 22, no. 1, pp. 29–38, 1989.
- [61] Z. Guo and R. W. Hall, “Parallel thinning with two-subiteration algorithms,” *Communications of the ACM*, vol. 32, no. 3, pp. 359–373, 1989.
- [62] Z. Bian, D. Zhang, and W. Shu, “Knowledge-based fingerprint post-processing,” *International Journal of Pattern Recognition and Artificial Intelligence*, vol. 16, no. 01, pp. 53–67, 2002.
- [63] A. K. Hrechak and J. A. McHugh, “Automated fingerprint recognition using structural matching,” *Pattern Recognition*, vol. 23, no. 8, pp. 893–904, 1990.
- [64] A. K. Jain, J. Feng, A. Nagar, and K. Nandakumar, “On matching latent fingerprints,” in *Computer Vision and Pattern Recognition Workshops (CVPRW), IEEE Computer Society Conference on*, pp. 1–8, 2008.
- [65] H. Guan, A. M. Dienstfrey, and M. F. Theofanos, “A new metric for latent fingerprint image preprocessing,” in *Computer Vision and Pattern Recognition Workshops (CVPRW), IEEE Conference on*, pp. 84–91, 2013.
- [66] S. Yoon, K. Cao, E. Liu, and A. K. Jain, “Lfiq: Latent fingerprint image quality,” in *Biometrics: Theory, Applications and Systems (BTAS), IEEE Sixth International Conference on*, pp. 1–8, 2013.
- [67] C. Garcia and M. Delakis, “Convolutional face finder: A neural architecture for fast and robust face detection,” *Pattern Analysis and Machine Intelligence, IEEE Transactions on*, vol. 26, no. 11, pp. 1408–1423, 2004.
- [68] A. S. Georghiades, P. N. Belhumeur, and D. Kriegman, “From few to many: Illumination cone models for face recognition under variable lighting and pose,” *Pattern Analysis and Machine Intelligence, IEEE Transactions on*, vol. 23, no. 6, pp. 643–660, 2001.
- [69] K.-C. Kwak and W. Pedrycz, “Face recognition using a fuzzy fisherface classifier,” *Pattern Recognition*, vol. 38, no. 10, pp. 1717–1732, 2005.
- [70] J. Yang, A. F. Frangi, J.-y. Yang, D. Zhang, and Z. Jin, “Kpca plus lda: a complete kernel fisher discriminant framework for feature extraction and recognition,” *Pattern Analysis and Machine Intelligence, IEEE Transactions on*, vol. 27, no. 2, pp. 230–244, 2005.

- [71] L. Wiskott, J.-M. Fellous, N. Kuiger, and C. Von Der Malsburg, “Face recognition by elastic bunch graph matching,” *Pattern Analysis and Machine Intelligence, IEEE Transactions on*, vol. 19, no. 7, pp. 775–779, 1997.
- [72] S. Chopra, R. Hadsell, and Y. LeCun, “Learning a similarity metric discriminatively, with application to face verification,” in *Computer Vision and Pattern Recognition (CVPR), IEEE Computer Society Conference on*, vol. 1, pp. 539–546, 2005.
- [73] D. A. Socolinsky, A. Selinger, and J. D. Neuheisel, “Face recognition with visible and thermal infrared imagery,” *Computer Vision and Image Understanding*, vol. 91, no. 1, pp. 72–114, 2003.
- [74] J. Dowdall, I. Pavlidis, and G. Bebis, “Face detection in the near-ir spectrum,” *Image and Vision Computing*, vol. 21, no. 7, pp. 565–578, 2003.
- [75] C. H. Morimoto, D. Koons, A. Amir, and M. Flickner, “Pupil detection and tracking using multiple light sources,” *Image and vision computing*, vol. 18, no. 4, pp. 331–335, 2000.
- [76] A. Syafeeza, M. Khalil-Hani, S. Liew, and R. Bakhteri, “Convolutional neural network for face recognition with pose and illumination variation.,” *International Journal of Engineering & Technology (0975-4024)*, vol. 6, no. 1, 2014.
- [77] Y. LeCun, K. Kavukcuoglu, and C. Farabet, “Convolutional networks and applications in vision,” in *IEEE International Symposium on Circuits and Systems (ISCAS 2010)*, pp. 253–256, 2010.
- [78] P. N. Belhumeur, J. P. Hespanha, and D. Kriegman, “Eigenfaces vs. fisherfaces: Recognition using class specific linear projection,” *Pattern Analysis and Machine Intelligence, IEEE Transactions on*, vol. 19, no. 7, pp. 711–720, 1997.
- [79] P. N. Belhumeur and D. J. Kriegman, “What is the set of images of an object under all possible illumination conditions?,” *International Journal of Computer Vision*, vol. 28, no. 3, pp. 245–260, 1998.
- [80] Z. Pan, G. Healey, M. Prasad, and B. Tromberg, “Face recognition in hyperspectral images,” *Pattern Analysis and Machine Intelligence, IEEE Transactions on*, vol. 25, no. 12, pp. 1552–1560, 2003.
- [81] Y. Gao and M. K. Leung, “Face recognition using line edge map,” *Pattern Analysis and Machine Intelligence, IEEE Transactions on*, vol. 24, no. 6, pp. 764–779, 2002.
- [82] K.-C. Lee, J. Ho, and D. Kriegman, “Nine points of light: Acquiring subspaces for face recognition under variable lighting,” in *Computer Vision and Pattern Recognition (CVPR), IEEE Proceedings of Computer Society Conference on*, vol. 1, pp. I–519, 2001.
- [83] H. F. Chen, P. N. Belhumeur, and D. W. Jacobs, “In search of illumination invariants,” in *Computer Vision and Pattern Recognition, IEEE Proceedings of International Conference on*, vol. 1, pp. 254–261, 2000.

- [84] W. Zhao and R. Chellappa, "Illumination-insensitive face recognition using symmetric shape-from-shading," in *Computer Vision and Pattern Recognition, IEEE Proceedings of International Conference on*, vol. 1, pp. 286–293, 2000.
- [85] Z. Sun, H. Zhang, T. Tan, and J. Wang, "Iris image classification based on hierarchical visual codebook," *Pattern Analysis and Machine Intelligence, IEEE Transactions on*, vol. 36, no. 6, pp. 1120–1133, 2014.
- [86] A. Ross and M. S. Sunder, "Block based texture analysis for iris classification and matching," *Computer Vision and Pattern Recognition Workshops (CVPRW), IEEE Computer Society Conference on*, pp. 30–37, 2010.
- [87] H. Zhang, Z. Sun, T. Tan, and J. Wang, "Iris image classification based on color information," *Pattern Recognition (ICPR), 21st International Conference on*, pp. 3427–3430, 2012.
- [88] I. Ramirez, P. Sprechmann, and G. Sapiro, "Classification and clustering via dictionary learning with structured incoherence and shared features," *Computer Vision and Pattern Recognition (CVPR), IEEE Conference on*, pp. 3501–3508, 2010.
- [89] J. Mairal, F. Bach, J. Ponce, and G. Sapiro, "Online dictionary learning for sparse coding," *Machine Learning, 2009 ACM Conference on*, pp. 689–696, 2009.
- [90] M. Aharon, M. Elad, and A. Bruckstein, "The k-svd: An algorithm for designing over-complete dictionaries for sparse representation," *Signal Processing, IEEE Transactions on*, vol. 54, no. 11, pp. 4311–4322, 2006.
- [91] K. Engan, S. O. Aase, and J. Hakon Husoy, "Method of optimal directions for frame design," *Acoustics, Speech, and Signal Processing, IEEE International Conference on*, vol. 5, pp. 2443–2446, 1999.
- [92] K. Etemad and R. Chellappa, "Separability-based multiscale basis selection and feature extraction for signal and image classification," *Image Processing, IEEE Transactions on*, vol. 7, no. 10, pp. 1453–1465, 1998.
- [93] P. Sprechmann and G. Sapiro, "Dictionary learning and sparse coding for unsupervised clustering," *Acoustics Speech and Signal Processing (ICASSP), IEEE International Conference on*, pp. 2042–2045, 2010.
- [94] F. Rodriguez and G. Sapiro, "Sparse representations for image classification: Learning discriminative and reconstructive non-parametric dictionaries," 2008.
- [95] K. Huang and S. Aviyente, "Sparse representation for signal classification," *NIPS*, pp. 609–616, 2006.
- [96] H. Lee, A. Battle, R. Raina, and A. Y. Ng, "Efficient sparse coding algorithms," *Advances in neural information processing systems, MIT Transactions on*, vol. 19, p. 801, 2007.
- [97] S. G. Mallat and Z. Zhang, "Matching pursuits with time-frequency dictionaries," *Signal Processing, IEEE Transactions on*, vol. 41, no. 12, pp. 3397–3415, 1993.

- [98] U. Foundation, “The rayid model of iris interpretation,” <http://rayid.com/main/structures.asp>, 2009.
- [99] CASIA-IrisV1, “Chinese academy of sciencesinstitute of automation iris database,” <http://biometrics.idealtest.org/>.
- [100] A. Kumar and A. Passi, “Comparison and combination of iris matchers for reliable personal authentication,” *Pattern Recognition*, vol. 43, no. 3, pp. 1016–1026, 2010.
- [101] A. Kumar and A. Passi, “Indian institute of technology delhi (iitd) iris database,” [http://www4.comp.polyu.edu.hk/~csajaykr/IITD/Database\\_Iris.htm](http://www4.comp.polyu.edu.hk/~csajaykr/IITD/Database_Iris.htm).
- [102] M. Dobeš, J. Martinek, D. Skoupil, Z. Dobešová, and J. Pospíšil, “Human eye localization using the modified hough transform,” *Optik-International Journal for Light and Electron Optics, Elsevier journal on*, vol. 117, no. 10, pp. 468–473, 2006.
- [103] M. Dobeš, L. Machala, P. Tichavský, and J. Pospíšil, “Human eye iris recognition using the mutual information,” *Optik-International Journal for Light and Electron Optics, Elsevier journal on*, vol. 115, no. 9, pp. 399–404, 2004.
- [104] M. Dobe and L. Machala, “Upol iris database,” <http://www.inf.upol.cz/iris/>, 2004.
- [105] R. C. Gonzalez and R. E. Woods, “Digital image processing,” *Prentice Hall*, 2002.
- [106] J. K. Pillai, M. Puertas, and R. Chellappa, “Cross-sensor iris recognition through kernel learning,” *Pattern Analysis and Machine Intelligence, IEEE Transactions on*, vol. 36, no. 1, pp. 73–85, 2014.
- [107] B. Kulis, M. Sustik, and I. Dhillon, “Learning low-rank kernel matrices,” in *Proceedings of the 23rd international conference on Machine learning*, pp. 505–512, ACM, 2006.
- [108] J. V. Davis, B. Kulis, P. Jain, S. Sra, and I. S. Dhillon, “Information-theoretic metric learning,” in *Proceedings of the 24th international conference on Machine learning*, pp. 209–216, 2007.
- [109] C. E. Chapel, *Fingerprinting: a manual of identification*. Coward-McCann, 1941.
- [110] F. Galton, *Finger prints*. Macmillan and Company, 1892.
- [111] C. Lin, J. Liu, J. Osterburg, and J. Nicol, “Fingerprint comparison. i: Similarity of fingerprints,” *Journal of forensic sciences*, vol. 27, no. 2, pp. 290–304, 1982.
- [112] J. Hollingum, “Automated fingerprint analysis offers fast verification,” *Sensor Review*, vol. 12, no. 3, pp. 12–15, 1992.
- [113] A. K. Jain, S. Prabhakar, and L. Hong, “A multichannel approach to fingerprint classification,” *Pattern Analysis and Machine Intelligence, IEEE Transactions on*, vol. 21, no. 4, pp. 348–359, 1999.
- [114] Q. Xiao and H. Raafat, “Fingerprint image postprocessing: a combined statistical and structural approach,” *Pattern Recognition*, vol. 24, no. 10, pp. 985–992, 1991.

- [115] N. P. Ramaiah and C. K. Mohan, “De-noising slap fingerprint images for accurate slap fingerprint segmentation,” in *Machine Learning and Applications and Workshops (ICMLA), 10th International Conference on*, vol. 1, pp. 208–211, 2011.
- [116] K. Saeed, M. Tabedzki, M. Rybnik, and M. Adamski, “K3m: A universal algorithm for image skeletonization and a review of thinning techniques,” *International Journal of Applied Mathematics and Computer Science*, vol. 20, no. 2, pp. 317–335, 2010.
- [117] J.-j. Gao and M. Xie, “The layered segmentation, gabor filtering and binarization based on orientation for fingerprint preprocessing,” in *Signal Processing, IEEE International Conference on*, vol. 4, 2006.
- [118] “Iso/iec 19794-2:2005,” *Information Technology Biometric Data Interchange Formats Part 2: Finger Minutiae Data*, 2005.
- [119] R. C. Gonzalez, R. E. Woods, and S. L. Eddins, *Digital image processing using MATLAB*. Pearson Education India, 2004.
- [120] “<http://lodev.org/cgtutor/filtering.html>,” *Image Filtering - Emboss filter, Lode’s Computer Graphics Tutorial*.
- [121] M. D. Garris and R. M. McCabe, “Nist special database 27: Fingerprint minutiae from latent and matching tenprint images,” *Disponivel emj [http://www. itl. nist. gov/iaui/894.03/databases/](http://www.itl.nist.gov/iaui/894.03/databases/). Acesso em: June, 2000.*
- [122] J. R. Smith and S.-F. Chang, “Tools and techniques for color image retrieval,” in *Electronic Imaging: Science & Technology, SPIE Conference Proceedings on*, pp. 426–437, 1996.
- [123] J. Puzicha, T. Hofmann, and J. M. Buhmann, “Histogram clustering for unsupervised segmentation and image retrieval,” *Pattern Recognition Letters*, vol. 20, no. 9, pp. 899–909, 1999.
- [124] M. A. Stricker and M. Orengo, “Similarity of color images,” in *IS&T/SPIE’s Symposium on Electronic Imaging: Science & Technology*, pp. 381–392, 1995.
- [125] M. J. Swain and D. H. Ballard, “Color indexing,” *International journal of computer vision*, vol. 7, no. 1, pp. 11–32, 1991.
- [126] G. Pass and R. Zabih, “Histogram refinement for content-based image retrieval,” in *Applications of Computer Vision (WACV), IEEE International Workshop on*, pp. 96–102, 1996.
- [127] Y. Chen and J. Z. Wang, “A region-based fuzzy feature matching approach to content-based image retrieval,” *Pattern Analysis and Machine Intelligence, IEEE Transactions on*, vol. 24, no. 9, pp. 1252–1267, 2002.
- [128] I. Daubechies *et al.*, *Ten lectures on wavelets*, vol. 61. SIAM, 1992.
- [129] A. K. Jain, *Fundamentals of digital image processing*, vol. 3. Prentice-Hall Englewood Cliffs, 1989.

- [130] D. Malyszko and S. T. Wierzchon, "Standard and genetic k-means clustering techniques in image segmentation," in *Computer Information Systems and Industrial Management Applications (CISIM), IEEE International Conference on*, pp. 299–304, 2007.
- [131] R. B. Palm, "Prediction as a candidate for learning deep hierarchical models of data," Master's thesis, Technical University of Denmark, Asmussens Alle, Denmark, 2012.
- [132] K.-C. Lee, J. Ho, and D. Kriegman, "Acquiring linear subspaces for face recognition under variable lighting," *Pattern Analysis and Machine Intelligence, IEEE Transactions on*, vol. 27, no. 5, pp. 684–698, 2005.
- [133] N. Kingsbury, "Complex wavelets for shift invariant analysis and filtering of signals," *Applied and computational harmonic analysis*, vol. 10, no. 3, pp. 234–253, 2001.
- [134] A. Baradarani, Q. M. J. Wu, and M. Ahmadi, "An efficient illumination invariant face recognition framework via illumination enhancement and dd-dtwt filtering," *Pattern Recognition*, vol. 1, pp. 57–72, 2013.
- [135] T. Ahonen, A. Hadid, and M. Pietikainen, "Face description with local binary patterns: Application to face recognition," *Pattern Analysis and Machine Intelligence, IEEE Transactions on*, vol. 28, no. 12, pp. 2037–2041, 2006.
- [136] H. Wang, S. Z. Li, and Y. Wang, "Generalized quotient image," in *Computer Vision and Pattern Recognition (CVPR) Proceedings of the 2004 IEEE Computer Society Conference on*, vol. 2, pp. II–498, 2004.
- [137] T. Chen, W. Yin, X. S. Zhou, D. Comaniciu, and T. S. Huang, "Total variation models for variable lighting face recognition," *Pattern Analysis and Machine Intelligence, IEEE Transactions on*, vol. 28, no. 9, pp. 1519–1524, 2006.
- [138] T. Zhang, B. Fang, Y. Yuan, Y. Yan Tang, Z. Shang, D. Li, and F. Lang, "Multiscale facial structure representation for face recognition under varying illumination," *Pattern Recognition*, vol. 42, no. 2, pp. 251–258, 2009.
- [139] X. Xie, J. Lai, and W.-S. Zheng, "Extraction of illumination invariant facial features from a single image using nonsubsampling contourlet transform," *Pattern Recognition*, vol. 43, no. 12, pp. 4177–4189, 2010.
- [140] M. Gostencnik, D. Gacnik, and I. Kramberger, "Survey of image compression algorithms for esmo mission," in *Systems, Signals and Image Processing (IWSSIP), 18th International Conference on*, pp. 1–4, 2011.
- [141] V. Mosorov and A. Patyk, "Method coding for lossless greyscale image compression," in *The Experience of Designing and Application of CAD Systems in Microelectronics (CADSM), Proceedings of the 6th International Conference*, pp. 212–213, 2001.
- [142] B. G. Haskell and A. N. Netravali, "Digital pictures: representation, compression, and standards," 1997.

- [143] A. Mascher-Kampfer, H. Stögner, and A. Uhl, “Comparison of compression algorithms’ impact on fingerprint and face recognition accuracy,” in *Electronic Imaging 2007*, vol. 1, pp. 650810–650810, 2007.
- [144] W. Funk, M. Arnold, C. Busch, and A. Munde, “Evaluation of image compression algorithms for fingerprint and face recognition systems,” in *Information Assurance Workshop, 2005. IAW’05. Proceedings from the Sixth Annual IEEE SMC*, pp. 72–78, 2005.
- [145] K. Horvath, H. Stogner, G. Weinhandel, and A. Uhl, “Experimental study on lossless compression of biometric iris data,” in *Image and Signal Processing and Analysis (ISPA), 7th International Symposium on*, pp. 379–384, 2011.
- [146] J. Thärnå, K. Nilsson, and J. Bigun, “Orientation scanning to improve lossless compression of fingerprint images,” in *Audio-and Video-Based Biometric Person Authentication*, pp. 343–350, Springer, 2003.
- [147] G. Weinhandel, H. Stogner, and A. Uhl, “Experimental study on lossless compression of biometric sample data,” in *Image and Signal Processing and Analysis (ISPA), Proceedings of 6th International Symposium on*, pp. 517–522, 2009.
- [148] I. Secretariat, “Icao environmental report 2010: Aviation outlook,” 2010.
- [149] A. Tritah, “The public distribution system in india: Counting the poor from making the poor count,” *Toulouse, France: Universite des Sciences Sociales, Groupe de Recherche en Economie Mathématique et Quantitative*, 2003.
- [150] A. Krishnan, K. Raju, and A. Vedamoorthy, “Unique identification (uid) based model for the indian public distribution system (pds) implemented in windows embedded ce,” in *Advanced Communication Technology (ICACT), 2011 13th International Conference on*, pp. 1441–1445, 2011.
- [151] S. Haykin, *Neural Networks: A Comprehensive Foundation*. New Jersey: Prentice-Hall International, 1999.



# List of Publications

## CONFERENCES

1. N. Pattabhi Ramaiah, M. Srinivas and C. Krishna Mohan, "Iris Classification & Adjudication Using Online Dictionary Learning," Communicated to *IEEE Int. Joint Conf. on Neural Networks (IJCNN)*, to be held in Killarney, Ireland, Jul. 2015.
2. N. Pattabhi Ramaiah, A. Tirupathirao and C. Krishna Mohan, "Best Practices for Biometric-based Identity Creation in the E-Society," in *IDES Int. Conf. on Computational Intelligence and Information Technology (ICCIIT)*, to be held in Bhopal, India, Jul. 2015.
3. N. Pattabhi Ramaiah, Earnest Paul and C. Krishna Mohan, "Illumination Invariant Face Recognition Using Convolutional Neural Networks," in *IEEE Int. Conf. on Signal Processing, Informatics, Communication and Energy Systems (SPICES)*, Calicut, India, Feb. 2015.
4. N. Pattabhi Ramaiah, A. Tirupathirao and C. Krishna Mohan, "Enhancements to Latent Fingerprints in Forensic Applications," in *19<sup>th</sup> IEEE Int. Conf. on Digital Signal Processing (DSP2014)*, Hong Kong, pp. 439-443, Aug. 2014.
5. A. Tirupathi Rao, N. Pattabhi Ramaiah and C. Krishna Mohan, "Latent Fingerprint Recognition using ISO 19794-2 Fingerprint Templates," in *Proc. Elsevier S&T Int. Conf. on Advances in Information Technology and Mobile Communication (ICAIM)*, Kolkatta, India, pp. 1-4, Jun. 2014

6. A. Tirupathi Rao, N. Pattabhi Ramaiah and C. Krishna Mohan, "Biometrics in e-Governance & Academia using Hand-held fingerprint terminals," in *Proc. Elsevier S&T Int. Conf. on Advances in Communication Network and Computing (ICCNC)*, Chennai, India, pp. 653-658, Feb. 2014.
7. N. Pattabhi Ramaiah and C. Krishna Mohan, "De-noising Slap Fingerprint Images For Accurate Slap Fingerprint Segmentation," in *Proc. IEEE Int. Conf. on Machine Learning and Applications (ICMLA)*, Honolulu, Hawaii, USA, pp. 1-4, Dec. 2011.
8. N. Pattabhi Ramaiah and C. Krishna Mohan, "ROI-based Tissue Type Extraction and Volume Estimation in 3D Brain Anatomy," in *Proc. IEEE Int. Conf. on Image Information Processing (ICIIP)*, Shimla, India, pp. 391-395, Nov. 2011.
9. N. Pattabhi Ramaiah and C. Krishna Mohan, "De-duplication of Photograph Images Using Histogram Refinement," in *Proc. IEEE Int. Conf. on Recent Advances in Intelligent Computational Systems (ICRAICS)*, Trivandrum, India, pp. 1-5, Sep. 2011.

## JOURNALS

1. N. Pattabhi Ramaiah and C. Krishna Mohan, "Iris Classification based on Sparse Representations using ODL for Large-scale De-duplication Applications," Communicated to *Journal of Circuit Systems and Signal Processing (Springer)*.

2. N. Pattabhi Ramaiah and C. Krishna Mohan, “De-duplication Complexity of Fingerprint Data in Large-scale Applications,” in *Journal of Electronic Science and Technology*, vol.12, no. 2, pp. 1-5, Jun. 2014.
  
3. A. Tirupathi Rao, N. Pattabhi Ramaiah and C. Krishna Mohan, “Fingerprint Recognition on Various Authentication Sensors,” in *Journal of Electronic Science and Technology*, vol.12, no. 1, pp. 139-143, Mar. 2014.

# CURRICULUM VITAE

1. **Name:** N. Pattabhi Ramaiah

2. **Date of Birth:** 21<sup>st</sup> July 1981

3. **Permanent Address:**

S/o. N VV Satyanarayana

D.No: 1-142, Vanapallipalem

P.O. Uppalaguptam - 533222

East Godavari Dist., Andhra Pradesh, India

4. **Educational Qualifications:**

- May 2015: Doctor of Philosophy in Computer Science and Engineering (Ph.D., Dept. of CSE, IIT Hyderabad, A.P., India)
- May 2007: Master of Technology in Artificial Intelligence (M.Tech., University of Hyderabad, A.P., India)
- May 2004: Bachelor of Technology in Computer Science and Information Technology (B.Tech., JNTU, Hyderabad, A.P., India)

5. **Employment History:**

- Jul 2007 - Feb 2008: Software Engineer in SEEC Technologies Asia Pvt. Ltd., Hyderabad, A.P., India.
- Mar 2008 - Sep 2010: Senior Programmer in 4G Identity Solutions Pvt. Ltd., Hyderabad, A.P., India.

## DOCTORAL COMMITTEE

1. **Chairperson:** Dr. M. V. Pandurangarao

2. **Guide:** Dr. C. Krishna Mohan

3. **Members:**

- Dr. Naveen. Sivadasan (Dept. of CSE)
- Dr. Ch. Sobhan Babu (Dept. of CSE)
- Dr. K. Sri Rama Murthy (Dept. of EE)
- Dr. J. Bala Subramaniam (Dept. of Mathematics)